

**CENTRAL NERVOUS SYSTEM EXTRACELLULAR MATRIX AS A THERAPEUTIC
BIOSCAFFOLD FOR CENTRAL NERVOUS SYSTEM INJURY**

by

Christopher Joseph Medberry

Bachelor of Science, The Pennsylvania State University, 2008

Submitted to the Graduate Faculty of
Swanson School of Engineering in partial fulfillment
of the requirements for the degree of
Doctor of Philosophy

University of Pittsburgh

2013

UNIVERSITY OF PITTSBURGH
SWANSON SCHOOL OF ENGINEERING

This dissertation was presented

by

Christopher Joseph Medberry

It was defended on

September 11, 2013

and approved by

Patricia Hebda, PhD, Associate Professor, Department of Plastic Surgery

Kacey Marra, PhD, Associate Professor, Department of Plastic Surgery

Michel Modo, PhD, Associate Professor, Department of Radiology

Martin Oudega, PhD, Assistant Professor, Department of Physical Medicine and

Rehabilitation

Dissertation Director: Stephen F. Badylak, DVM, PhD, MD, Professor, Department of

Surgery

Copyright © by Christopher Joseph Medberry

2013

CENTRAL NERVOUS SYSTEM EXTRACELLULAR MATRIX AS A THERAPEUTIC BIOSCAFFOLD FOR CENTRAL NERVOUS SYSTEM INJURY

Christopher Joseph Medberry, PhD

University of Pittsburgh, 2013

Traumatic central nervous system (CNS) injuries lack effective treatment options and typically result in irrecoverable tissue damage and lifelong neurologic impairment. An ideal therapeutic would provide structural support for axonal regrowth as well as modulate the default secondary injury associated with CNS injuries. Extracellular matrix (ECM) bioscaffolds derived by decellularization promoted functional remodeling in numerous non-CNS applications; however, there has been minimal investigation of this technology in the CNS. The objectives of this work were to evaluate the tissue specific properties of CNS-ECM in terms of (1) hydrogel characteristics and biochemical composition, (2) neurotrophic potential, and (3) ability to alter the innate immune response.

Bioscaffolds composed of CNS-ECM were formed into injectable solutions that polymerize to form hydrogels at body temperature. Hydrogels derived from CNS-ECM were compared to a hydrogel form of a non-CNS ECM, urinary bladder matrix (UBM-ECM), using compositional analyses for retained ECM molecules, mechanical assessments for rheological and turbidimetric properties, and multiphoton microscopy to visualize in-vitro three-dimensional neurite outgrowth. ECM hydrogels from both tissue sources had mechanical properties similar to native CNS and supported three-dimensional neurite outgrowth.

CNS-ECM and UBM-ECM bioscaffold mediated alteration of the innate immune and neural stem cell response was interrogated in-vitro using macrophages and spinal cord stem cells

(SPCs). While all ECM scaffolds evaluated decreased astrocyte differentiation, only UBM-ECM increased SPC neuronal differentiation. Bioscaffolds derived from both CNS and non-CNS tissue sources promoted a pro-repair macrophage phenotype as demonstrated through immunofluorescent results. Finally, CNS-ECM bioscaffolds were compared to UBM-ECM in a rat model of contusion spinal cord injury. Macrophage polarization was evaluated over 4 weeks and a histologic evaluation of the lesion site completed. While the ECM bioscaffolds did not improve functional recovery, pro-repair macrophages were found closely associated with the ECM injection sites.

This body of work demonstrates CNS-ECM bioscaffolds can be isolated and are capable of minimally invasive injection, supporting neurite extension in-vitro, and modulating macrophage and stem cell responses. Future research is necessary to determine the added benefits that can be obtained when this technology is combined with others known to be beneficial for CNS tissue repair.

TABLE OF CONTENTS

PREFACE.....	XVIII
1.0 INTRODUCTION AND SPECIFIC AIMS.....	1
1.1 TRAUMATIC SPINAL CORD INJURIES	2
1.1.1 Primary and Secondary Injury	2
1.1.2 Macrophage and Microglia Response.....	3
1.1.2.1 Macrophage Origin.....	4
1.1.2.2 Microglia Origin.....	5
1.1.2.3 Macrophages and Microglia in SCI	7
1.1.2.4 Dichotomy of Macrophage and Microglia Response	9
1.2 CURRENT TREATMENT.....	12
1.3 EXTRACELLULAR MATRIX BIOSCAFFOLDS	13
1.3.1.1 ECM Mediated Constructive Remodeling Mechanisms	14
1.3.1.2 ECM Bioscaffolds Derived for Spinal Cord Repair	16
1.3.2 Organ Specific Bioscaffolds	17
1.4 SPECIFIC AIMS	18
2.0 BIOLOGIC SCAFFOLDS COMPOSED OF CENTRAL NERVOUS SYSTEM EXTRACELLULAR MATRIX	20
2.1 INTRODUCTION	20
2.2 MATERIALS AND METHODS.....	21

2.2.1	Preparation of CNS-ECM.....	21
2.2.2	Characterization of CNS-ECM constituents.....	23
2.2.2.1	Characterization of residual DNA in CNS-ECM.....	23
2.2.2.2	Protein content of CNS-ECM	24
2.2.3	In-vitro Characterization of CNS-ECM.....	25
2.2.4	Statistical Analysis.....	27
2.3	RESULTS	28
2.3.1	Efficacy of Decellularization Method	28
2.3.2	CNS-ECM Constituents	29
2.3.3	In-vitro Characterization of CNS-ECM.....	31
2.4	DISCUSSION.....	34
2.5	CONCLUSIONS	37
2.6	FUTURE WORK.....	37
3.0	HYDROGELS DERIVED FROM CENTRAL NERVOUS SYSTEM EXTRACELLULAR MATRIX	39
3.1	INTRODUCTION	39
3.2	MATERIALS AND METHODS	40
3.2.1	Overview of Experimental Design.....	40
3.2.2	ECM Biologic Scaffold Production	41
3.2.3	ECM Digestion and Solubilization.....	42
3.2.4	Collagen and sGAG Quantification	43
3.2.5	Scanning Electron Microscopy.....	43
3.2.6	Turbidity Gelation Kinetics	44

3.2.7	Rheological Measurements	45
3.2.8	N1E-115 ECM Cytocompatibility and Two Dimensional Neurite Extension.....	45
3.2.9	Neurite Extension in Three Dimensional Culture	46
3.2.10	Statistical Analysis.....	47
3.3	RESULTS	48
3.3.1	Collagen and sGAG Quantification	48
3.3.2	Qualitative Assessment.....	49
3.3.3	Turbidimetric Gelation Kinetics	50
3.3.4	Rheologic Measurements	52
3.3.5	N1E-115 ECM Cytocompatibility and Two Dimensional Neurite Extension.....	53
3.3.6	Neurite Extension in Three Dimensional Culture	55
3.4	DISCUSSION.....	57
3.5	CONCLUSIONS	59
3.6	FUTURE WORK.....	59
4.0	ALTERNATIVE MACROPHAGE POLARIZATION AND ENHANCED NEURAL STEM CELL REGENERATIVE POTENTIAL WITH BIOSCAFFOLDS DERIVED FROM CENTRAL NERVOUS SYSTEM EXTRACELLULAR MATRIX. 61	
4.1	INTRODUCTION	61
4.2	MATERIALS AND METHODS	63
4.2.1	UBM-ECM and CNS-ECM Scaffold Preparation	63
4.2.1.1	UBM-ECM.....	63
4.2.1.2	CNS-ECM.....	64
4.2.2	ECM Digestion and Solubilization.....	65

4.2.3	Human Macrophage Description	65
4.2.3.1	Human Macrophage Polarization with ECM Bioscaffolds.....	66
4.2.3.2	Human Macrophage Chemotaxis	66
4.2.4	Mouse Macrophage Description.....	66
4.2.4.1	Mouse Bone Isolation.....	67
4.2.4.2	Mouse Macrophage Culture	67
4.2.4.3	Mouse Macrophage Polarization and Treatment with ECM Conditioned Media.....	67
4.2.4.4	Mouse Macrophage Immunolabeling.....	68
4.2.5	Spinal Cord Stem Cell (SPC) Description.....	68
4.2.5.1	Spinal Cord Stem Cell Chemotaxis	69
4.2.5.2	Spinal Cord Stem Cell Proliferation.	69
4.2.5.3	Spinal Cord Stem Cell Differentiation	70
4.2.6	Cytocompatibility Analysis.....	71
4.2.7	Statistical Analysis.....	71
4.3	RESULTS	72
4.3.1	Cellular Cytocompatibility	72
4.3.2	Macrophage Chemotaxis	72
4.3.3	Macrophage Polarization.....	74
4.3.3.1	Human Macrophage Polarization	74
4.3.3.2	Human Monocyte Polarization	75
4.3.3.3	Mouse Macrophage Polarization.....	76
4.3.4	SPC Behavioral Response to ECM Bioscaffolds.....	79
4.3.4.1	Chemotaxis	79

4.3.4.2	Proliferation	80
4.3.4.3	Differentiation	81
4.4	DISCUSSION	83
4.5	CONCLUSION	86
4.6	LIMITATIONS AND FUTURE WORK	87
5.0	CONTUSION SPINAL CORD INJURY TREATMENT WITH INJECTABLE EXTRACELLULAR MATRIX BIOSCAFFOLDS	88
5.1	INTRODUCTION	88
5.2	MATERIALS AND METHODS	90
5.2.1	Overview and Experimental Design	90
5.2.2	UBM-ECM and CNS-ECM Scaffold Preparation	90
5.2.2.1	CNS-ECM	91
5.2.3	ECM Digestion and Solubilization	91
5.2.4	Spinal Cord Injury	92
5.2.4.1	Post-surgical Animal Care and Euthanasia	92
5.2.5	Immunofluorescence and Histochemistry	93
5.2.5.1	Macrophage Triple Immunolabeling	93
5.2.6	Behavioral Testing	94
5.2.6.1	BBB	94
5.2.6.2	Gridwalk	95
5.2.6.3	Digigait	95
5.2.7	Statistical Analysis	95
5.3	RESULTS	96
5.3.1	Masson’s Trichrome Lesion Assessment	96

5.3.2	Temporospatial Macrophage Evaluation.....	98
5.3.3	Locomotor and Sensorimotor Recovery.....	101
5.4	DISCUSSION.....	105
5.5	CONCLUSIONS.....	106
5.6	LIMITATIONS AND FUTURE WORK.....	107
6.0	DISSERTATION SYNOPSIS.....	109
6.1	MAJOR FINDINGS.....	109
6.2	OVERALL CONCLUSIONS.....	111
	APPENDIX.....	112
	BIBLIOGRAPHY.....	118

LIST OF TABLES

Table 1. Methods for Decellularization and Solubilizing B-ECM, SC-ECM, and UBM-ECM. .	42
Table 2. Summary of Rheologic and Turbidity Values for B-ECM, SC-ECM, and UBM-ECM. * Indicates statistical significance at $p < 0.05$ when one group is statistically different from the other two.	52
Table 3. Summary of data for macrophage chemotaxis in response to SC-ECM, B-ECM, and UBM-ECM. Only UBM-ECM significantly increase migration. Data expressed as fold change of cells migrated normalized to the pepsin digestion buffer.	74

LIST OF FIGURES

- Figure 1. Resting state microglia in a ramified morphology in healthy CNS tissue. Green = tomato lectin, 200x magnification. 8
- Figure 2. Markers, secreted products, and functionality of macrophages polarized towards a classic M1 or alternative M2 polarization state. Reprinted with permission from (63) with permission from Elsevier. 10
- Figure 3. Decellularized spinal cord, right, appears whiter in color than its lyophilized native counterpart (left). Ruler marks indicate 1mm. 22
- Figure 4. Decellularized whole brain, right, appears whiter in color and less dense than its lyophilized native counterpart (left). Ruler marks indicate 1mm. 23
- Figure 5. H&E and DAPI images of whole brain ECM and spinal cord ECM following decellularization. The decellularized scaffolds are compared to their native counterpart to demonstrate decellularization efficacy. All decellularized images have been over exposed to demonstrate the lack of nuclei found post decellularization. 28
- Figure 6. Spinal Cord ECM and Whole brain ECM contain less than 50ng DNA/ mg ECM as denoted by the red line. DNA remnants must less than 200bp to mitigate disease transmission 29
- Figure 7. Myelin was present in the native brain, native spinal cord, decellularized brain, and decellularized spinal cord as shown by luxol fast blue staining. Laminin was also present in brain ECM, spinal cord ECM, and their native counterparts as shown by immunohistochemistry with hematoxylin counterstain. Magnification is 100x. 30
- Figure 8. Growth factor content of CNS-ECM scaffolds. Spinal cord ECM, brain ECM, and urinary bladder ECM retained detectable concentrations of VEGF and bFGF, while only native tissues contain NGF. 31
- Figure 9. PC12 viability for CNS-ECMs and UBM-ECM is equivalent to the basal media control. 32

- Figure 10. Mitogenic effects of CNS-ECM scaffolds. Undifferentiated PC12 cell proliferation was modulated by spinal cord ECM, brain ECM, and urinary bladder ECM as determined by BrdU incorporation during PC12 cell mitosis. Increases in mitogenesis peaked at 53% (brain ECM, 25 mg protein per ml). * Indicates $p < 0.05$ by one-way ANOVA. 32
- Figure 11. Chemotactic effects of CNS ECM scaffolds. Undifferentiated PC12 cell migration was modulated by spinal cord ECM, brain ECM, and urinary bladder ECM as determined by trans-membrane PC12 cell migration. Changes in chemotaxis ranged from increases of 53% (brain ECM, 100 mg protein per ml) to decreases of 50% (urinary bladder ECM, 25 mg protein per ml). * Indicates $p < 0.05$ by one-way ANOVA. 33
- Figure 12. Differentiation effects of CNS-ECM scaffolds. PC12 neuronal differentiation induced by CNS and non-CNS ECM as indicated by neurite extension. Differentiation was compared using the following medium supplements: PBS as a negative control, spinal cord ECM at 100 $\mu\text{g/ml}$, brain ECM at 100 $\mu\text{g/ml}$, urinary bladder ECM at 100 $\mu\text{g/ml}$, or bFGF at 0.20 $\mu\text{g/ml}$ as a positive control. *Urinary bladder ECM at 100 μg protein per ml induced greater differentiation than any other condition including the positive control (bFGF, 0.20 $\mu\text{g/ml}$). ** Spinal cord ECM or brain ECM at 100 $\mu\text{g/ml}$ induced differentiation at rates comparable to the positive control which were greater than all other conditions except urinary bladder ECM at 100 μg protein per ml. ***Urinary bladder ECM at 10mg protein per ml induced differentiation at greater rates than the negative control (no ECM: 0mg/ml). # Differentiation rates increased with concentration for spinal cord ECM, brain ECM, and urinary bladder ECM (10 μg protein per ml vs. 100 μg protein per ml). Significant differences were determined between all groups shown by one-way ANOVA. 33
- Figure 13. Collagen and sGAG composition in B-ECM and SC-ECM scaffolds. (A) SC-ECM contains a significantly higher percentage of collagen than B-ECM. (B) B-ECM contains a significantly higher concentration of sGAGs than SC-ECM. 48
- Figure 14. B-ECM, SC-ECM, and UBM-ECM hydrogels and their respective Scanning Electron Micrographs (6mg/mL). (A) B-ECM hydrogel; (B) SC-ECM hydrogel; (C) UBM-ECM hydrogel; (D) B-ECM 1000x; (E) SC-ECM 1000x; (F) UBM-ECM 1000x; (G) B-ECM 10000x; (H) SC-ECM 10000x; (I) UBM-ECM 10000x. 49
- Figure 15. B-ECM and SC-ECM representative turbidimetric and normalized turbidimetric curves. (A) Example absorbance curve and the metrics analyzed. (B) Normalized absorbance for B-ECM (diamonds), SC-ECM (squares), and UBM-ECM (triangles). (C) Lag time comparison for B-ECM, SC-ECM, and UBM-ECM. (D) Time to 50% complete gelation for B-ECM, SC-ECM, and UBM-ECM. (E) Time to 95% complete gelation for B-ECM, SC-ECM, and UBM-ECM. (F) Velocity to complete gelation for B-ECM, SC-ECM, and UBM-ECM following the lag time. 51
- Figure 16. Representative rheologic gelation kinetics for B-ECM and SC-ECM hydrogels (4, 6, and 8 mg/mL). G' represents the storage modulus and G'' represents the loss modulus. SC-ECM is significantly stiffer than B-ECM at each hydrogel concentration. (A) Storage modulus time sweep for B-ECM, SC-ECM, and UBM-ECM at 8mg/mL. (C) Storage

modulus time sweep for B-ECM, SC-ECM, and UBM-ECM at 6mg/mL. (C) Storage modulus time sweep for B-ECM, SC-ECM, and UBM-ECM at 4mg/mL. (D) Final storage modulus for B-ECM, SC-ECM, and UBM-ECM at each concentration. * Indicates statistical significance of $p < 0.05$	53
Figure 17. Live/dead cytotoxicity analysis for B-ECM, SC-ECM, and UBM-ECM. (A) B-ECM, (B) SC-ECM, and (C) UBM-ECM pre-gel solutions are non-cytotoxic when added to culture medium of N1E-115 cells (10x; scale bar is approximately 200 μm).	54
Figure 18. B-ECM and SC-ECM pre-gel solutions increase the number of cells with neurite extensions. All Scaffolds show a dose dependent increase for the number of cells with neurite extension, while only B-ECM shows a dose dependent increase in neurite length with increasing concentrations of ECM. * Indicates statistical significance of $p < 0.05$. ..	55
Figure 19. Neurite Extension in B-ECM, SC-ECM, and UBM-ECM in 6mg/mL hydrogels in a 3-D cube or compressed Z-stack. (A) N1E-115 cell extension following 7 days culture in B-ECM in 3-D cube. (B) N1E-115 cell extension following 7 days culture in SC-ECM in 3-D cube. (C) N1E-115 cell extension following 7 days culture in UBM-ECM in 3-D cube. The compressed Z-stack shows B-ECM has short arborizing extensions at two days, while SC-ECM and UBM-ECM have uni- or bi-polar extensions. At 7 days all ECM hydrogels support uni- or bi-polar N1E-115 cell extensions. For 3-D cubes the major tick mark represents 50 μm and the minor tick mark represents 10 μm . For the Z-stacks the scale bar represents 50 μm	56
Figure 20. Prior to differentiation assays, SPCs were examined for their expression of neural stem cell markers Sox 2 and Nestin. Transcription factor Sox 2 colocalizes with the nuclei of the SPC cells, while Nestin can be seen as an intermediate filament.	70
Figure 21. ECM bioscaffolds are not cytotoxic to human monocyte derived macrophages.	72
Figure 22. Only M2 macrophages increase their chemotactic ability in response to UBM-ECM digestion products, suggesting an additional mechanism for how ECM scaffolds polarize macrophages at an injury site. * indicates a significant difference ($p < 0.05$) compared to pepsin digestion buffer control.	73
Figure 23. Moderate M1 responses to B-ECM and SC-ECM after 48 hours in polarization.	75
Figure 24. Human Monocytes show a decreased M1 response as anticipated with UBM-ECM, however high variability makes interpretation difficult.	76
Figure 25. Control plate for mouse macrophage staining shows positive M1 iNOS marker when macrophages are polarized with IFN γ /LPS and Fizz1 when polarized with IL-4.	77
Figure 26. All ECM scaffolds exhibit M2 macrophage activation (via Fizz1 expression), however expression appears to be higher in UBM-ECM and SC-ECM as compared to B-ECM. The digestion buffer does not show iNOS or Fizz1 expression.	78

Figure 27. Quantification of mouse macrophage polarization shows that all ECM bioscaffolds promote an M2 polarization through an increase in Fizz1 expression with minimal M1 (iNOS) activation. The digestion buffer control does not show an increase in either iNOS or Fizz 1. 79

Figure 28. SPCs respond to SC-ECM with an increase in migration, whereas to B-ECM and UBM-ECM, the SPCs exhibit a dose dependent decrease in migration. 80

Figure 29. SPCs exhibit differential effects in mitogenesis following exposure to ECM scaffolds. In response to high levels of SC-ECM, mitogenesis is maintained at basal levels, whereas in response to high levels of B-ECM, mitogenesis is increased. * indicates a significant increase in comparison to the pepsin and basal media controls. # indicates a significant decrease in comparison to the pepsin digestion buffer control. 81

Figure 30. Following 21 days in culture with media conditioned with 250ug ECM/mL SPCs were stained for B3-tubulin denoting neuronal differentiation or GFAP denoting astroglial differentiation. UBM-ECM had significantly increased neuronal differentiation (# = p <0.05) and significantly decreased astrocyte differentiation (* = p<0.05) when compared to all other groups. ECM conditioned media was at a concentration of 250 g ECM/mg..... 82

Figure 31. Pepsin and SC-ECM occasionally produced GFAP differentiated cells with morphology commonly expressed by reactive astrocytes. 83

Figure 32. Trichrome staining of UBM, B-ECM, SC-ECM treated spinal cords as compared to a pepsin buffer control. All ECM scaffolds maintain a fibrous structure throughout the volume of the lesion as compared to the pepsin control. 97

Figure 33. Pepsin buffer control macrophage response over 28 days following injury. The pepsin treated animals show CD206 expression, and a dense accumulation of CD86 positive cells at day 28..... 99

Figure 34. SCI repair with UBM-ECM over 28 days showed a dense accumulation of CD206 positive cells that maintained over 28 days. The CD86 positive cells were diffuse through the lesion area throughout the time points examined. 99

Figure 35. SCI repaired with B-ECM showed a moderate CD206 population that became more diffuse by 28 days. The CD86 cell population is present throughout the lesion site..... 100

Figure 36. SCI repaired with SC-ECM shows dense CD206 and CD86 cell populations throughout the lesion at days 7 and 14. By day 28, CD206 positive cells were found closer to cavity edges, whereas CD86 remained diffuse. 100

Figure 37. BBB open field locomotor assessment shows all animals recovering to approximately a 12 on the BBB scale. There are no differences between injury controls and treatment

groups. Additional controls were added to the graph that include laminectomy only, PBS injection, and contusion with no injection.	101
Figure 38. At 14 days post injury, there are no sensorimotor differences between treatment groups as shown through the gridwalk analysis.	102
Figure 39. At 28 days post injury, gridwalk slip analysis shows no differences between treatment groups and injection buffer control.	102
Figure 40. Digigait stride length assessment between CNS-ECM and a non-CNS ECM scaffold show no differences between treatment groups and controls.	103
Figure 41. Digigait paw angle assessment shows no difference between the uninjured control, pepsin, UBM-ECM, B-ECM, and SC-ECM.	103
Figure 42. Digigait fore and hind limb step angle assessment shows no difference between uninjured animals, pepsin control, or ECM treatment groups.	104
Figure 43. Digigait assessment of limb stance width shows a moderate increase in the hind limb stance width between uninjured and injured animals. There are no differences between injury controls and treatment groups.	104

PREFACE

My time here at the University of Pittsburgh has been one of growth and development, both professional and personal. I owe Dr. Badylak my sincerest gratitude for both taking me into his laboratory and providing me with his valuable time and mentorship. The time I have spent here has fostered my development into a researcher capable of asking pointed questions that lead to scientific answers and further our field of regenerative medicine. I would also like to thank my committee members: Dr. Patricia Hebda, Dr. Kacey Marra, Dr. Michel Modo, and Dr. Martin Oudega, as well as Dr. Lance Davidson for their support and guidance throughout my doctoral degree. Their insights have developed my capabilities as a researcher.

I would like to thank everyone in Dr. Badylak's research laboratory who has been there for guidance, experimental support, and anything else that I needed. I am truly grateful for everything you have done for me. Scott Johnson, Hongbin Jiang, Li Zhang, Alex Huber, Kerry Daly, Elizabeth Kollar, and John Freund who have been there to help with experiments and my development. Janet Reing and Neill Turner for molecular biology and microscope support. The members of the neural research group who worked side by side to better understand the interactions of the CNS and extracellular matrix as well as working through all of our animal work: Steve Tottey, Peter Crapo, Kristen Jones, Jeremy Kelly, Fanwei Meng, and Pete Slivka. I thank Chris Dearth for scientific strategy and experimental design, Deanna Rhoads and Jennifer

DeBarr for their help and hard work with histologic preparation of slides and staining, Jocelyn Runyon, Dawn Robertson, Eve Simpson, and Allison Lacovey for all of their assistance with schedule, manuscript support, guidance, and so many other things. I also acknowledge the undergraduate and summer students who helped support my research: Abby Stahl, Yolandi van der Merwe, Jenna Dziki, Tori Bain, Bernard Siu, Soni Nag, Mike Pezzone, Vince Russell, Ari Schuman, Philip Short, and Thu Nguyen, the graduate students who finished before me and provided all of the help I could have asked for in learning the lab culture and how to be successful: Vineet Agrawal, John Wainwright, Bryan Brown, Jolene Valentin, and Ellen Brennan-Pierce, and finally the graduate students who I work with currently: Chris Carruthers, Brian Sicari, Matt Wolf, Tim Keane, Denver Faulk, Ricardo Londono, and Lisa Carey; I don't think I would have made it this far without all of your help and support.

I would also like to thank my family. My beautiful and lovely wife, Beth, who has been there for me through everything and supported me when I needed it most; I owe everything to her. To my parents, Marge and Joe, whose love and constant support will always be there for me when I need them. To my grandparents, George and Grace Medberry, Irving and Dorothy Dark, who unfortunately won't be here for my graduation, but whose love will forever be in my memory. To my wife's parents, Liz and Jim Baldys, and her siblings, James, Kate, and Abigail for welcoming me into their family and treating me as one of their own.

Finally I would like to acknowledge my funding sources: NIH-NHLBI training grant (T32-EB001026) entitled "Cellular Approaches to Tissue Engineering and Regeneration" and the Armed Forces Institute for Regenerative Medicine. The Bioengineering Department here has also been a wonderful source of support: Dr. Borovetz, Joan Williamson, Lynette Spataro, Glenn

Peterson, Nick Mance, and Zack Strickler. To anyone else that I may have forgotten, thank you for your help throughout my graduate career, I would not have accomplished this without you.

1.0 INTRODUCTION AND SPECIFIC AIMS

Regenerative medicine therapies that actively harness innate healing mechanisms to promote tissue reconstruction are currently being implemented for the creation of non-traditional therapeutics that restore morphologically and functionally normal tissue. Tissue engineering, a subset of regenerative medicine that takes advantage of traditional engineering techniques, commonly uses material scaffolds, cells, and bioactive molecules in application specific combinations to promote healing and functional tissue restoration. While many techniques use synthetic and polymeric materials for tissue reconstruction, others take advantage of the natural extracellular matrix (ECM). Through the process of decellularization, the ECM of a tissue is harvested and transformed into a bioscaffold that acts as a bioactive template capable of promoting site specific constructive remodeling in numerous preclinical and clinical applications. The unique ECM structure and molecular composition maintained by resident cell types of an organ are continually modified by a process termed dynamic reciprocity. In this process, the cells that maintain the ECM alter their behavior in response to the current conditions of the ECM. This, in turn, causes the cells to modify the structural and molecular composition of the ECM in a continuous feedback loop that adjusts for the current microenvironment. It is logical then, that a bioscaffold derived from homeostatic tissue homologous to the site at which it will be applied may maintain structural and molecular components of the ECM that could influence the microenvironment and host response to promote reconstruction of functional tissue.

1.1 TRAUMATIC SPINAL CORD INJURIES

Traumatic CNS injuries result in irrecoverable severe neurologic impairments, paralysis, and even death. While the mechanisms following injury have similarities throughout the locations of the CNS, this dissertation will focus on injuries to the spinal cord. Currently, approximately 1.3 million people live with severe spinal cord injury (SCI) throughout the world (1) with an estimated additional 20,000 injuries occurring yearly (2). Neurologic impairment and extent of lesion is highly dependent upon the injury location. The spinal cord is segmented into four regions, cervical, thoracic, lumbar, and sacral, moving caudally along the rostrocaudal axis in accordance to the spinal cord nerves and the peripheral tissues they innervate. Injuries leading to tetraplegia occur in a cervical segment of the spinal cord, whereas those with paraplegia sustained injuries in the thoracic, lumbar, or sacral portions of the spinal cord. In the United States, tetraplegia accounts for 52.2% of injuries while incomplete or complete paraplegia result in 36.7% of injuries. For tetraplegia the estimated lifetime cost of care is between 2 and 4.6 million dollars, while the cost for paraplegics is between 1.4 and 2.2 million dollars (3), suggesting a strong clinical and economic need for a regenerative approach that can promote functional neurologic recovery. Traumatic injuries to the spinal cord occur in two injury phases, the primary insult, and the secondary injury.

1.1.1 Primary and Secondary Injury

The primary insult is most commonly a combination of the initial impact in conjunction with compression that results in cell death via hemorrhagic necrosis (4) and apoptosis (5, 6), disconnection of long fiber tracts and axons (7, 8), and demyelination (9-11). Secondary injury

commonly includes (8) an inflammatory response (12), calcium mediated damage (13), glutamate excitotoxicity (14), vascular disruption (15), and apoptosis (5). In the later phase of secondary degeneration, Wallerian degeneration occurs as neurons and their myelin sheaths degrade rostral to the lesion site (16). An astroglial scar is formed by tightly interwoven astrocytes attached by tight junctions and surrounded by proteoglycans (17). In human SCI, it is common to find relatively mild astroglial scars accompanied by mesenchymal scars composed primarily of collagen (16) that develop through the recruitment of meningeal fibroblasts (16). In addition to axonal degeneration and scar tissue deposition is the liquefractive tissue necrosis and formation of one of two forms of a lesion cavity. The first form is a cyst surrounded by a thin astrogliotic wall and can be considered the final stage of healing. The cyst commonly retains residual macrophages, small numbers of axons, bands of connective tissue, and blood vessels (16, 18). The other cavity form is a syrinx that consists of a dense gliotic wall under pressure. The pressure may result in syringomyelia, enlargement of the cavity and compression of the surrounding parenchyma (19). While numerous secondary injury mechanisms contribute to the liquefractive tissue necrosis and cavity formation, this dissertation will focus on the roles of macrophages and microglia in this process.

1.1.2 Macrophage and Microglia Response

Macrophages and microglia are important contributors and mediators of the inflammatory environment in both acute and chronic SCI. Although the cells have different developmental origins, their behavior following injury is classically considered similar and detrimental to the healing process. Therefore, to overcome their detrimental behavior previous therapeutics were aimed at reducing the immune response rather than harnessing its role in tissue repair. As both

macrophages and microglia play important roles in pro- and anti-inflammatory functions, it is logical that modulation of the cells towards a pro-remodeling phenotype could benefit wound resolution and constructive tissue remodeling. The following section provides a brief overview of macrophages and microglia, including their origins, roles, and a dichotomy of behavior following SCI.

1.1.2.1 Macrophage Origin

Macrophages, part of the mononuclear phagocyte system, are derived from monocytes that develop from a common myeloid progenitor cell (20) in the bone marrow (21). Progenitors originating in the bone marrow experience a cytokine cascade of granulocyte colony-forming unit and macrophage colony-forming unit that differentiate the cells to monoblasts, pro-monocytes, and finally monocytes. The monocytes then migrate from the bone marrow to the blood stream where they comprise of 5-10% of circulating blood cells. Monocytes are then recruited from the blood stream in response to immune, metabolic, and pro-inflammatory stimuli (22). In some tissues, monocyte recruitment also occurs to maintain sufficient populations of non-CNS tissue macrophages (23).

Peripheral blood monocytes are a heterogeneous population defined and categorized by Ly6C expression. Ly6C⁺ monocytes exit the bone marrow and adopt the Ly6C^{mid} phenotype characterized by expression of CC-chemokine receptor 7 (CCR7) and CCR8 (24). The Ly6C^{+/mid} populations migrate towards inflammatory signals, exit the blood stream, and become macrophages that respond to clearance of pathogens and become involved in inflammatory resolution. The Ly6C⁻ population plays a role in replenishing tissue macrophages (20). Many types of tissue macrophages have repopulation mechanisms to maintain independence from peripheral blood derived monocytes, however this is unique to each tissue and also can change in

a non-homeostatic state (23). In the case of CNS phagocytic cells, which include microglia, perivascular macrophages, meningeal macrophages, and choroid plexus macrophages, there is a unique repopulation mechanism for each cell type. Meningeal macrophages are rapidly repopulated, which suggests a bone marrow origin, while perivascular and choroid plexus macrophages repopulate in a slower fashion, indicating mechanisms independent of the peripheral blood system (25). While some CNS macrophages may be derived from the peripheral blood myeloid system, the origin of microglia and their homeostatic repopulation appear to be in a closed system.

1.1.2.2 Microglia Origin

While microglia origin was originally believed to be of the same myeloid as macrophages, it has now been demonstrated that microglia are derived from primitive erythromyeloid progenitors that invade the brain from the embryonic yolk sac (26). Microglia derive from macrophages in the yolk sac that have committed towards a macrophage lineage and have been described as participants of a second wave of primitive yolk sac hematopoiesis (27). Microglia again contrast other myeloid cell populations as the developmental transcription factors necessary for myeloid development are not required (28). This further stresses the notion that the microglial developmental program differs from peripheral tissue macrophages that microglia may have a behavioral skillset that diverges from peripheral monocytes and macrophages. Although there are several developmental differences between microglia and peripheral macrophages, the microglial repopulation mechanism has been a continued point of contention. While many studies in the early 1990s agreed that the adult brain microglia population was sustained via peripheral blood derived macrophages (29, 30), it has since been shown that microglia are an independent population during tissue homeostasis (26, 31).

Conventional thought processes place this as differing from non-CNS tissues however, it has been seen that organs such as the liver, skin, and spleen, and lung also (23, 32) have self-renewal mechanisms independent of the myeloid system. While during injury states, both traumatic and autoimmune, peripheral blood monocytes traverse the blood brain barrier become macrophages and strongly participate in the disease state, thus raising the question of how similar to a microglial cell a macrophage can become.

Transgenic animal models exist to analyze the ability of macrophages to become microglial cells following microglial ablation. Mouse models of microglia removal, such as the CD11b-HSVTK transgenic model of microglial ablation (33), effectively remove these tissue macrophages from the CNS. Following microglia ablation the brain macrophage population is repopulated with CCR2⁺ monocytes from the blood stream. While this suggests blood monocytes may have built in systems that can duplicate microglia behavior and phenotype, following 27 weeks in the CNS the monocytes cannot fully replicate microglia (33). This speaks to the nature of microglia as an independent cell type from the peripheral myeloid cells. The distinct behavior of microglia may be due to the complex milieu of signals in the CNS and the additional neurosignaling capacity microglia may have in comparison to their peripheral counterpart.

The early infiltration into the CNS provides primitive microglia with a continuous array of neural specific signals ranging from electrical stimulus to neurotrophic factors (34). Microglia interaction with neurons and astrocytes also supports their integral role in the maintenance of neural structures (35). During development, the close link between microglia and neurons allows microglia to interact with neuronal signals and, in part, mediate neuronal activity and function. In fact, microglia play a significant role in development by participating in synaptic

stripping, a process of removing presynaptic junctions receiving weaker inputs neuronal connections during development (36). This is partially completed using the CR3/C3 signaling complement components of the innate immune effector system in this process (37). As these examples, among others, illustrate, there is a unique difference in functionality between microglia and peripheral macrophages. As another example, microglia are actively suppressed during homeostasis through the CX3CL1 (38) receptor, which differs significantly from peripheral monocytes and macrophages that are recruited through this mechanism. Microglia may also secrete neurotrophic factors and play a role in CNS vascularization (39). The lack of histologic markers to distinguish the two cell types (other methods for distinguishing the roles of the two cell types include: cell sorting [CD45^{high}, indicating macrophage, or CD45^{low}, indicating microglia (40)], scanning electron microscopy [ruffled surface “rose aspect”, indicating macrophage, or spikey, indicating microglia (41)], transgenic models (42, 43)) limits the ability to perform spatial analyses that could detail the contributions of the two cells to inflammation, constructive remodeling, and wound resolution.

1.1.2.3 Macrophages and Microglia in SCI

In homeostatic conditions microglia maintain a resting state ramified morphology (Figure 1) that constantly monitor the environment (44) for serum proteins and abnormal neurotransmitter signaling such as damage signals (39). Upon sensing a perturbation in the environment, microglia alter their morphology towards an amoeboid shape (45). This morphology change can be classified as a shift towards a migratory phagocytic cell capable of engulfment and removal of injury debris, leaked blood parts, and micro-organisms (41, 46). Microglia can reach an injury site and begin to secrete pro-inflammatory cytokines such as IL-1 β (47) as early as 30 minutes post injury (46, 48). While it is assumed microglia play the

predominant role in the early pro-inflammatory secretions, without histologic markers capable of distinguishing between microglia and macrophages a non-transgenic model cannot make this assessment.

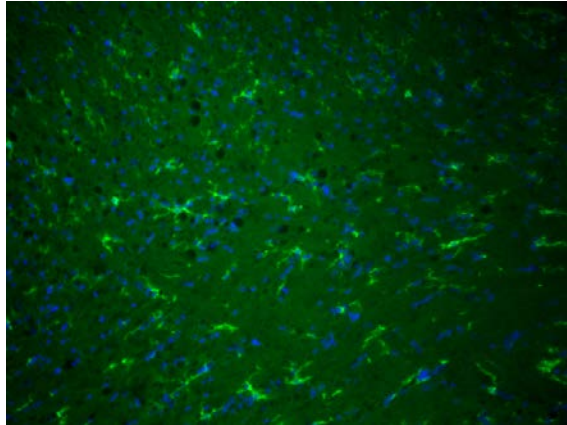


Figure 1. Resting state microglia in a ramified morphology in healthy CNS tissue. Green = tomato lectin, 200x magnification.

While microglia respond immediately to the traumatic injury, it is hypothesized that much of the macrophage infiltration begins approximately 3 – 7 days post injury. At this point, increased concentrations of OX41 and ED1 positive cells can be found at the immediate lesion area (49, 50). At this point, macrophages/microglia contribute to the pro-inflammatory milieu and are partially responsible for the secretion of TNF- α , IL-1 β , NO, Superoxide, and hydrogen peroxide (51). These pro-inflammatory molecules and reactions participate in cell death and ultimately lesion formation. While the common perception is to view the macrophage response in only a negative manner, other research suggests that the peripheral macrophage response may be necessary for inflammatory resolution and deposition of site appropriate new ECM (52).

The immune response plays an important role in pro-inflammatory resolution and tissue healing through secretion of trophic molecules and ability to scavenge toxic factors (53, 54). Following injury in peripheral nerves, macrophages contribute significantly to wound resolution and healing (55). While this macrophage contribution to SCI repair is not apparent, upon closer examination of the wound environment, it can be seen that monocyte derived macrophages participate in neurotrophic functions and neural repair (50, 56). Through a novel chimeric mouse model, Michal Schwartz's research group demonstrated an anti-inflammatory role provided by peripheral macrophages, but not microglia (42). This may suggest that microglia play a role in immediate debris clearance and bactericidal functions, while macrophages provide immunoregulatory signals via IL-10 to resolve harmful inflammation (57-59). A subset of the monocyte derived macrophage population, CD11c⁺ (42), participated in this effect, which further identifies a distinct macrophage population that can contribute to spinal cord repair (60, 61).

1.1.2.4 Dichotomy of Macrophage and Microglia Response

The dichotomy of the macrophage response is well described in non-CNS tissues (62-66). Following injury, macrophages polarize along a response continuum ranging from the classically activated M1 macrophages to the alternatively, or regulatory, activated M2 macrophages. In response to the immunologic microenvironment, M2 macrophages are further divided into three subsets as shown in Figure 2 (63). M1 macrophages are polarized via LPS/IFN γ (i.e. classically activated) and mediate tissue damage, initiate inflammatory (67-69) response, and are responsible for pathogen resistance (70, 71). M2 macrophages, polarized via IL-4, IL-10, IL-13/IL-1R, are broken down into a subset of 3 types based on the polarization mechanisms. M2a promotes Th2 responses and provides parasite resistance. M2b is involved in immunoregulatory functions and participates in IL-10 secretion (72). M2c is involved in immunoregulation, matrix

deposition, and tissue remodeling (20). The M2 phenotype has recently been shown to be strongly associated with skeletal muscle regeneration (62).

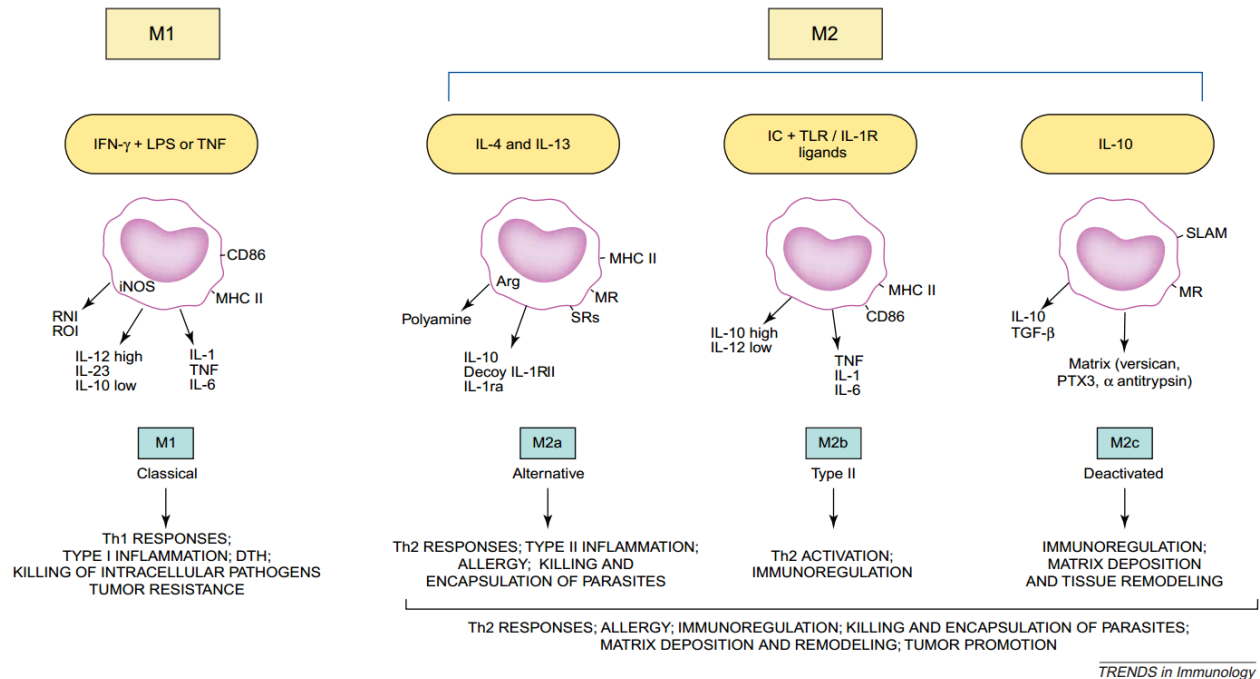


Figure 2. Markers, secreted products, and functionality of macrophages polarized towards a classic M1 or alternative M2 polarization state. Reprinted with permission from (63) with permission from Elsevier.

In response to implanted ECM bioscaffolds and their degradation products, approximately 50% macrophages polarize towards M2 side of the spectrum (73). This phenomenon has been shown to be an effective predictor for constructive tissue remodeling following injury (74). The implantation of M2 macrophages also promotes nerve tissue remodeling in a sciatic nerve pre-clinical model (66). Mokarram et. al. demonstrated that macrophages polarized to the M1 end of the continuum through IFN-γ stimulation and M2 through IL-4 stimulation produce opposite effects on sciatic nerve reconstruction. Nerve repair grafts implanted with IFN-γ to produce M1 macrophages with showed diminished nerve repair whereas those treated with IL-4 to produce

M2 macrophages increased axons orders of magnitude higher than the non-cytokine treated scaffold. While similar effects have been observed following spinal cord repair (75), the modulation of the immune system toward these beneficial effects has only recently been accepted as viable therapeutic options for treatment of CNS injury (76-78). While a similar polarization paradigm has been documented for microglia (79), no research has been completed to understand ECM bioscaffold mediated polarization on microglia.

Macrophage Polarization in the Spinal Cord

Following spinal cord injury, classic dogma dictated that the immune system played the predominant role only in pro-inflammatory secreting, secondary degeneration promoting, and multifaceted harmful invading cells that would be better removed than harnessed for any repair potential (80). This idea has since evolved and grown to the understanding that the immune system plays a dual role and is involved in both CNS repair and injury (60, 81). Implantation of macrophages, polarized with autologous skin (77) and peripheral nerve (78), promoted partial functional recovery following rat spinal cord injury. Phase I clinical trials with polarized macrophage implantation showed the treatment as safe for use as a human SCI therapeutic as well as promoted partial bladder recovery in two patients (82). Additionally, Kigerl et. al. demonstrated that following spinal cord injury, early macrophage and microglia infiltrate upregulated CD206 and arginase I (i.e. M2 phenotype markers) up to day 14 following injury simultaneously with their transcription of iNOS and CD86 (i.e. M1 phenotype markers). While this phenomenon is highly diminished by 7-14 days post injury, it shows the natural presence of M2 macrophages following SCI, and points to the pro-inflammatory microenvironment as the cause for diminishing their presence. Kigerl et. al. further stressed the importance of the microenvironment by implanting M2 macrophages into the center of the spinal cord lesion. As

hypothesized, M2 macrophages could not be found at the injury site several days post implantation, which may indicate the highly plastic cells (83, 84) were polarized into an M1 state, thus diminishing the pro-regenerative effects, and questioning the benefits of implanting pushed macrophages at the injury site. M2 macrophages and microglia have also been shown to promote remyelination (85), a critical factor in reconstructing the CNS. While these immune modulating therapies have reached clinical trials(82), their use has remained minimal and current treatments aim for patient stabilization and maintenance of tissue surviving injury.

1.2 CURRENT TREATMENT

Traumatic SCIs can produce injuries with irrecoverable neurologic outcomes and impairments. The current standard of care for new injuries is avoidance of hypotension and decompression of spinal cord impingements (86). Additionally, the acute management of such injuries revolves around the use of immobilization, airway management, and reduction of impingement to promote spinal cord blood re-perfusion (87). It was previously thought that pharmaceutical treatments designed to diminish the inflammatory response, such as systemic methylprednisolone (88), could reduce the chronic inflammation and secondary injury. While such therapies provided initial promise (89, 90), results have since been shown to be variable and limited (91, 92). Anti-immune therapeutics are now used sparingly by clinicians (93). Furthermore, it has since been demonstrated that the immune response is critical mediator in pre-clinical models of regeneration (94). A regenerative medicine treatment that both alters the inflammatory response and promotes reconstruction at the site of injury would be a therapeutic advancement for the treatment of SCI.

1.3 EXTRACELLULAR MATRIX BIOSCAFFOLDS

Bioscaffolds derived from naturally occurring extracellular matrix (ECM) scaffolds have been successful for tissue remodeling in a wide array of preclinical and clinical models. The bioscaffolds that have been most commonly used include those derived from the porcine small intestinal submucosa (SurgisisTM), bovine dermis (TissueMendTM), human dermis (AllodermTM), porcine dermis (AllomaxTM), and porcine urinary bladder (MatristemTM). Biologic scaffolds composed of ECM facilitated the constructive remodeling of numerous tissues including esophagus (95, 96), lower urinary tract (97, 98), muscle and tendon (99, 100), and myocardium (101, 102), among others. The successful use of these FDA-approved scaffolds to augment or replace injured tissues in clinical practice (103, 104) suggests that they may be a viable therapeutic for regenerative medicine approaches to SCI reconstruction.

Both the compatibility and host response to ECM bioscaffolds are highly dependent upon decellularization and post-processing procedures (i.e crosslinking and terminal sterilization) (105). Decellularization procedures can include a wide array agents and commonly include combinations of detergents, (i.e triton X-100, sodium dodecyl sulfate, sodium deoxycholate, and CHAPS), enzymes (i.e. trypsin, DNases, RNases), mechanical perturbation, acids (i.e. peracetic acid) , and bases (i.e. calcium hydroxide, sodium hydroxide), among others (106). Incomplete decellularization treatments do not remove all cellular debris and result in a pro-inflammatory immune response (73, 107). On the other end, while extreme procedures can effectively remove all cellular components, they often harm the ECM structure and decrease ECM scaffold efficacy. Thus decellularization protocols must be carefully optimized to understand in-vitro cellular and in-vivo host responses. ECM post-processing techniques also modify the scaffolds and alter host response. Crosslinked ECM bioscaffolds have been shown to be non-degradable and actively

promote a chronic inflammatory response that includes multinucleated giant cells (108). When comparing crosslinked versus non-crosslinked bioscaffolds decellularized using the same methodology, the non-crosslinked bioscaffold degrades releasing ECM degradation products and promotes constructive remodeling, while the crosslinked scaffold does not degrade. Beyond crosslinking, terminal sterilization techniques including ethylene oxide, gamma irradiation, and E-beam can alter the scaffold (109). These post-processing methods affect the structure of the ECM, and thus alter the constructive remodeling mechanisms.

1.3.1.1 ECM Mediated Constructive Remodeling Mechanisms

ECM mediated constructive remodeling occurs through multiple mechanisms that can alter the normal wound healing behavior to promote site appropriate tissue reconstruction. A well created decellularization procedure maintains the ECM composition, including collagens, growth factors, and glycosaminoglycans, among others, which as the scaffold degrades releases degradation products and bioactive peptides that influence cell behavior. The degradation and cryptic peptides enhanced perivascular stem cell regenerative potential through increasing proliferation and migration (110), influencing osteogenesis and bone remodeling (111), and recruiting endogenous stem cell populations in-vivo (99, 112). Cryptic peptides may also modulate vasculogenesis (113) and play a role in the deposition of new, site-appropriate ECM molecules (114). Also maintained in the ECM bioscaffold, and possibly released during degradation, are growth factors that include VEGF (115), bFGF (116), and TGF- β 1 (105). Molecules remaining in ECM bioscaffolds also promoting host tissue infiltration and participate in mechanotransduction. Mechanotransduction has been shown to be a requirement for constructive remodeling of functional tissue in the urinary bladder (117) and tendon (118). In these models, when physiologic loading was removed (i.e. through the use of a catheter or

immobilizing cast, respectively), ECM scaffolds degraded and were not developed into site appropriate tissue. Further mechanisms of ECM bioscaffold constructive remodeling include promoting innervation and modulation of the innate immune response.

Innervation is partially mediated by the ECM (119, 120) and is a crucial factor for regeneration (121). In several models of ECM bioscaffold-mediated constructive tissue remodeling, including the esophagus, skeletal muscle, and the abdominal body wall, innervation can be found in the reconstructed tissue along with functional smooth and skeletal muscle (122-124). Furthermore, ECM bioscaffold degradation products induced Schwann cell migration (122), which has the potential to recruit cells that play a major role in remyelination following injury. While the ability to support infiltrating axons and functional innervation are integral for constructive tissue reconstruction following SCI, axonal regrowth cannot occur successfully in a non-permissive pro-inflammatory environment found following CNS injury.

Macrophages are critical for constructive remodeling following ECM bioscaffold implantation, both through degradation and immunoregulatory functions. Using a rat model of ECM mediated constructive remodeling in the abdominal body wall, Valentin et. al. demonstrated that depletion of macrophages severely limited ECM scaffold degradation, and did not lead to tissue repair (125). Further investigation into the role of macrophages for tissue remodeling showed that properly produced ECM bioscaffolds promote a pro-regenerative M2, alternatively activated, macrophage phenotype (74). Thus, ECM bioscaffolds support cell infiltration and innervation, degrade to produce bioactive molecules that enhance stem cell regenerative potential, and alter the innate immune response towards functional tissue reconstruction. These mechanisms behind constructive remodeling suggest that bioscaffolds

derived by decellularization of tissues and organs could be viable therapeutics for spinal cord repair.

1.3.1.2 ECM Bioscaffolds Derived for Spinal Cord Repair

Recent tissue engineering strategies have combined the use of acellular ECM bioscaffolds with cells or pharmaceuticals for use in CNS repair. This dissertation focuses on the use of bioscaffolds derived from whole organs that maintain the complex mixture of ECM molecules found in the native ECM. Although the extent of ECM bioscaffolds in the CNS had been limited to dural repair (126, 127), recent experimental therapies have evaluated these bioscaffolds for SCI repair. Xue et. al. evaluated acellular skeletal muscle ECM bioscaffolds seeded with amniotic epithelial cells in a hemisection model of SCI (128). The bioscaffolds promoted moderate functional recovery, increased axonal sprouting, and remyelination. Li et. al. examined acellular sciatic nerve constructs in combination with brain-derived neurotrophic factor in a transection model of SCI (129). While functional recovery was not observed, retrograde axonal tracing indicated that the constructs created a permissive environment for axonal recovery. Liu et. al. implanted acellular spinal cord ECM constructs seeded with mesenchymal stem cells in a hemisection model of SCI (130). Both the acellular spinal cord constructs and those combined with mesenchymal stem cells showed moderate functional recovery, though there was no difference between the acellular and seeded scaffolds at 8 weeks. The results also showed an increase in remyelination. The experimental treatments detailed here were implanted in a highly invasive model (hemi- or transection spinal cord injury) that may not be as clinically applicable as delivering these scaffolds in a non-invasive manner. Although, while perhaps not as clinically relevant, these studies support the use of ECM bioscaffolds as therapeutics for CNS repair and begin to explore the use of organ specific ECM bioscaffolds as

enhancements that further increase the efficacy of ECM scaffolds to promote tissue reconstruction.

1.3.2 Organ Specific Bioscaffolds

ECM bioscaffold success has been augmented through the use of site specific scaffolds derived from homologous tissue sources. As cells interact with their ECM through reciprocal and dynamic interactions, cells shape ECM to be organ specific and tailored to the needs of the current physiologic state. Thus, it is logical, that the use of ECM scaffolds derived from homeostatic tissue, homologous to that which it will be repairing, may contain signals and molecules necessary for organ recapitulation. This topic has been demonstrated in several preclinical models, including, as previously discussed the spinal cord, but also the adrenal (131), lung (132, 133), and liver (134, 135). The use of an acellular spinal cord ECM bioscaffold promoted partial recovery in a rat model of hemisection spinal cord injury (130). Acellular ECM bioscaffolds derived from adrenal tissue supported adrenocortical cell proliferation and maintained cortisol secretion (131). Acellular scaffolds derived from the lung promoted differentiation of embryonic stem cells to lung specific cell phenotypes (136) and demonstrated in-vivo functionality (132). Hydrogels derived from liver ECM supported liver specific sinusoidal endothelial function, whereas non-site specific scaffolds could not (134). While these topics were cursorily evaluated by Liu et. al. (130) in some of the spinal cord ECM scaffolds for spinal cord injury, there has not been a systematic evaluation of the characterization and development of CNS-ECM bioscaffolds as therapeutics for CNS repair. Therefore the objective of the present dissertation is to evaluate the use of CNS-ECM bioscaffolds for the reconstruction

of CNS tissue. This objective will be accomplished through the completion of three specific aims designed to interrogate the reconstructive potential of CNS-ECM.

1.4 SPECIFIC AIMS

SPECIFIC AIM No. 1: To decellularize CNS tissue and characterize the resultant CNS-ECM.

SUB-AIM No. 1-1: To develop and characterize the biologic and material properties of a hydrogel form of CNS-ECM.

Rationale: ECM is deposited by resident cells of each tissue and organ and the composition and structure is optimized for the maintenance of each respective tissue. Therefore it is plausible that ECM derived from the CNS has a unique composition or structure that may facilitate constructive remodeling of CNS tissue following injury (132-134, 136-140).

Hypothesis₁: Decellularized CNS tissue yields ECM contains a neurotrophic composition that can enhance neurite and support neurite outgrowth in three-dimensions.

SPECIFIC AIM No. 2: To determine the effect of CNS-ECM upon human peripheral blood macrophage phenotype and spinal cord stem cell regenerative potential in-vitro.

Rationale: Macrophage polarization is predictor of downstream remodeling and associated function following SCI (60); therefore an in-vitro determination of macrophage phenotype may provide insight into the in-vivo macrophage response to CNS-ECM (73, 74, 125). ECM bioscaffolds enhance the regenerative potential of perivascular stem cells, and may aid in promoting a similar response to a human derived spinal cord stem cell.

Hypothesis2: Exposure to CNS-ECM induces an M2 regenerative phenotype in naïve macrophages and promotes human spinal cord stem cell mitogenesis, chemotaxis, and phenotypic maintenance.

SPECIFIC AIM No. 3: To evaluate regenerative potential of CNS-ECM in a rat model of contusion SCI.

Rationale: ECM scaffolds promote the recruitment of progenitor cells (99, 141), modulate the innate immune response (73, 74, 125), and degrade to generate bioactive molecular cues (142); all properties shown to be important for site-specific constructive tissue remodeling.

Hypothesis3: Following spinal cord contusion, local injection of CNS-ECM promotes M2 macrophage polarization and leads to tissue reconstruction.

2.0 BIOLOGIC SCAFFOLDS COMPOSED OF CENTRAL NERVOUS SYSTEM EXTRACELLULAR MATRIX

2.1 INTRODUCTION

The extracellular matrix (ECM) represents the secreted product of the resident cells of each tissue and organ and thus logically defines the ideal substrate or scaffold for maintenance of tissue specific cell phenotype. The ECM is a critical determinant of cell behavior and is known to affect intracellular signaling pathways, cell differentiation events, and cell proliferation among other important characteristics of tissue identity (132, 134, 136-139, 143, 144). These events are mediated through integrins and other cell surface receptors in response to ligands present within the ECM of every tissue (145-147). Subtle changes in ECM structure and mechanical properties can affect cell transcriptional events and associated cell phenotype and function (148, 149). Biologic scaffolds composed of ECM have been commonly used for the therapeutic reconstruction of many tissues including myocardium (150-152), kidney (153), lower urinary tract (154, 155), musculotendinous tissues (156-158), esophagus (96), and peripheral nerve (159), among others. There is clinical precedent for the application of ECM scaffolds in reconstruction of central nervous system (CNS) structures (127, 160), but the development of ECM scaffolds for CNS regenerative medicine strategies has received relatively scarce attention (161-163). It has been suggested that ECM harvested from specific tissues is the preferred

substrate for cells native to those respective tissues if maintenance of phenotypic characteristics is important (132, 134, 136-140). The methods by which ECM scaffolds are prepared vary greatly and such methods can markedly affect the composition, architecture, and material properties of the resulting construct (106, 164-166) as well as the host response following implantation (73, 107, 125, 167). Therefore, the methods of preparing ECM scaffolds intended for use in the repair and reconstruction of complex vital tissues such as heart, liver, kidney, and the CNS must be carefully considered as regenerative medicine strategies are developed for these tissues and organs.

The objectives of the present study were to (1) develop a method for decellularization of a brain and spinal cord, (2) characterize the resulting CNS-ECM scaffolds in terms of composition and in vitro cytocompatibility, and (3) investigate potential tissue-specific advantages of CNS-ECM scaffolds compared to non CNS-ECM scaffolds by evaluating in vitro modulation of PC12 cell line mitogenesis, chemotaxis, and differentiation.

2.2 MATERIALS AND METHODS

2.2.1 Preparation of CNS-ECM

Porcine brain and spinal cord tissues were obtained from animals (weight ~120 kg) at a local abattoir (Thoma's Meat Market, Saxonburg, PA). Tissues were frozen (>16 h at 80°C), thawed completely, and separated from all non-CNS tissue. Dura mater was removed, and spinal cord tissues were longitudinally quartered and cut into lengths (<3 cm). The decellularization process consisted of a series of agitated baths: water (type I reagent water per ASTM D1193; 16 h at

4°C; 60 rpm), 0.02% trypsin/0.05% EDTA (60 min at 37°C) (Invitrogen Corp., Carlsbad, CA, USA), 3.0% Triton X-100 (60 min) (Sigma-Aldrich Corp., St. Louis, MO, USA), 1.0 M sucrose (15 min) (Fisher Scientific, Pittsburgh, PA, USA), water (15 min), 4.0% deoxycholic acid (60 min) (Sigma), 0.1% peracetic acid (Rochester Midland Corp., Rochester, NY, USA) in 4.0% ethanol (120 min), PBS (15 min) (Fisher), water (15 min), water (15 min), and PBS (15 min). Agitation speed was 200 rpm for spinal cord tissues or 120 rpm for brain tissue with the exception of the initial step at 60 rpm. Decellularized spinal cord (Figure 3), and brain (Figure 4) were lyophilized and stored dry until use.



Figure 3. Decellularized spinal cord, right, appears whiter in color than its lyophilized native counterpart (left). Ruler marks indicate 1mm.



Figure 4. Decellularized whole brain, right, appears whiter in color and less dense than its lyophilized native counterpart (left). Ruler marks indicate 1mm.

2.2.2 Characterization of CNS-ECM constituents

2.2.2.1 Characterization of residual DNA in CNS-ECM

Qualitative assessment of residual DNA (106, 168) was conducted by fixation of non-lyophilized ECM scaffolds in 10% neutral buffered formalin, which was then embedded in paraffin, sectioned, and stained with hematoxylin and eosin (H&E) or with 4,6-diamidino-2-phenylindole (DAPI). Quantitative analysis of DNA content and base pair length in the remaining CNS ECM was conducted by digestion of comminuted ECM with 0.1 mg/ml proteinase K solution (48 - 144 h). Protein was removed by repeated phenol/chloroform extraction and centrifugation (10,000g) until no white precipitate (protein) was observed at the interface, and the aqueous phase extract was mixed with 3 M sodium acetate and 100% ethanol. The solution was centrifuged to pellet DNA, and the pellet was rinsed with 70% ethanol, centrifuged, and dried. Double-stranded DNA was quantified using PicoGreen (Invitrogen) per kit instructions. Base pair length of residual DNA in CNS-ECM scaffolds was determined by gel

electrophoresis of DNA extracts on 1.0% agarose gel with ethidium bromide (2 h at 60 V) followed by imaging with ultraviolet transillumination. Decellularization was evaluated against established criteria: (1) absence of visible nuclei in H&E and DAPI stained sections; (2) no DNA fragments exceeding 200 bp in length; and (3) <50 ng dsDNA per mg lyophilized ECM (106).

2.2.2.2 Protein content of CNS-ECM

Unstained sections of native (non-decellularized) spinal cord, and brain and their respective ECM were deparaffinized, rehydrated, and stained for myelin via luxol fast blue (169) or immunostained for laminin via citrate antigen retrieval, blocking with 2% normal goat serum, incubation with rabbit anti-human laminin primary antibody (diluted 1:25; Sigma, L9393), H₂O₂, goat anti-rabbit IgG peroxidase-conjugated secondary antibody (diluted 1:400; Sigma, A0545), and diaminobenzidine (ImmPACT DAB substrate; Vector Laboratories Inc., Burlingame, CA, USA), followed by hematoxylin counterstaining and ethylene-xylene dehydration.

Growth factors were extracted from 30 to 50 mg comminuted ECM per ml buffer by one of two methods. The first method used 50 mM Tris containing 2.0 M urea, 5.0 mg/ml heparin, and protease inhibitors, and the second method used 20 mM Tris containing 1.0% NP40, 10% glycerol, and protease inhibitors (105). Vascular endothelial growth factor (VEGF) and basic fibroblast growth factor (bFGF) were assayed in urea-heparin extracts, while nerve growth factor (NGF) was assayed in NP40-glycerol extracts. Growth factors were quantified via Quantikine Human VEGF Immunoassay (R&D Systems Inc., Minneapolis, MN, USA), Quantikine Human FGF basic Immunoassay (R&D Systems), and NGF Emax ImmunoAssay System (Promega Corp., Madison, WI, USA) per manufacturer instructions. Primary and secondary extracts were obtained and assayed separately, with results summated. Growth factor analysis was indicative of

concentration but not activity. Urinary bladder ECM was prepared as described previously (142) and used as a reference material.

2.2.3 In-vitro Characterization of CNS-ECM

The pheochromocytoma-derived PC12 cell line (CRL-1721; ATCC, Manassas, VA, USA), a neoplastic rat cell line arising from neural crest tissue (170), was used as a model neural-like cell to evaluate in-vitro modulation of mitogenesis, chemotaxis, and differentiation by ECM derived from decellularized CNS tissues. Urinary bladder ECM was again used as a reference material (i.e. non-CNS tissue source) to determine whether CNS-ECM scaffolds offered any tissue-specific advantages.

For in-vitro cell assays, individual ECM samples were comminuted into particles (<1.0 mm) and solubilized with 1.0 mg/ml pepsin in 0.01 N HCl (Fisher). Protein concentrations were assayed in multiple dilutes of solubilized ECM against a bovine serum albumin standard curve using bicinchoninic acid. Each pepsin-HCl ECM solution was neutralized to pH 7.4 with 0.1 N NaOH (Fisher), isotonicity balanced with 10X PBS (Fisher), and diluted to desired concentrations with 1X PBS. Mitogenic and chemotactic effects of ECM on PC12 cells were assayed for a range of concentrations (2.5, 10, 25, or 100 mg protein per ml), and PBS and/or neutralized pepsin lacking ECM served as controls in all assays. All in-vitro assays were conducted as three or more replicates in triplicate or quadruplicate per condition. Undifferentiated PC12 cells (P5-9) were passaged at 30-90% confluence on flasks coated with poly-L-lysine (PLL) in complete culture medium containing RPMI 1640 supplemented with 10% heat-inactivated horse serum (Sigma), 5.0% fetal bovine serum (FBS; Thermo Fisher Scientific Inc., Waltham MA, USA), and 100 U/ml penicillin/100 mg/ml streptomycin (pen/strep). To

determine potential cytotoxic effects of ECM scaffolds, PC12 cells were plated on PLL-coated sterile glass coverslips at 70,000 cells per well in 12-well plates. ECM or PBS was added to the medium at 100 µg/ml 2 h after plating and cells were cultured for an additional 24 h.

Cytocompatibility was determined using a Live/Dead Viability Kit (Invitrogen) per manufacturer instructions using 4.0 mM calcein AM and 4.0 mM ethidium homodimer-1. Viability of PC12 cells was quantified in fluorescence images using ImageJ (NIH) to split red and green channels, threshold, and count particles (cells), with binning to differentiate between cell clusters of various counts. The same ImageJ macro was used to analyze all images.

Mitogenic effects of CNS-ECM scaffolds were determined by plating undifferentiated PC12 cells on PLL-coated 96-well plates at 4000 cells per well. After 12 h, ECM or PBS was added to each well and cells were cultured for another 20 h, followed by culture for 4.0 h with 5-bromo-20-deoxyuridine (BrdU) and quantification of BrdU incorporation into PC12 DNA using a colorimetric BrdU cell proliferation ELISA (Roche Diagnostics Corp., Indianapolis, IN, USA) per manufacturer instructions.

Chemotactic effects of CNS-ECM scaffolds were determined by transmembrane migration using blind-well chambers and polycarbonate filters with 8.0 mm pore size (AP48; Neuro Probe Inc., Gaithersburg, MD, USA). Filters were coated in 30 mg/ml laminin (Sigma) for 30 min and allowed to dry completely. Undifferentiated PC12 cells were cultured to 70-90% confluence, starved overnight in RPMI 1640 supplemented with 1.0% FBS (Thermo Fisher) and pen/strep, trypsinized, and resuspended in unsupplemented 50:50 RPMI 1640:PBS. Each ECM was brought to concentration with PBS and diluted 50:50 with RPMI 1640, with 10% FBS in RPMI 1640 used to verify chemotaxis through each filter. Wells were loaded with 40,000 cells per well, and after 6 h each filter was removed, the upper (non-migratory) surface scraped, and

the lower (migratory) surface fixed with methanol, stained with DAPI, and imaged. Cells were quantified using ImageJ to threshold and count cells, with binning to differentiate between cell clusters of various counts. The same ImageJ macro was used to analyze all images.

Differentiation effects of CNS-ECM scaffolds were determined by plating PC12 cells at low density (1500 cells per well) in PLL-coated 48-well plates. After 6 h for attachment, cells were starved for 16 h in 1.0% heat-inactivated horse serum with pen/strep. bFGF (171), ECM, or PBS was added 50:50 to medium in each well to obtain desired final concentrations, and cells were cultured for another 48 h followed by fixation with paraformaldehyde, permeabilization with 0.1% Triton X-100, actin staining with Fluorescein-conjugated phalloidin, and imaging with a Zeiss AxioObserver Z1 microscope. The percentage of differentiated cells was determined by manually quantifying cells with at least one neurite-like process longer than the soma diameter, with a minimum of 300 cells counted per well (172, 173).

2.2.4 Statistical Analysis

Graphical representations of all data show mean +/- standard deviation of at least three replicates, each conducted in triplicate or quadruplicate. Experimental groups depicted graphically as a pair were compared using a Student's t-test. All other groupings were compared using one-way analysis of variance (ANOVA) with Tukey-Kramer post hoc analysis. Outliers greater than three standard deviations from the mean were excluded from data sets.

2.3 RESULTS

2.3.1 Efficacy of Decellularization Method

No residual nuclei were visible in H&E and DAPI images of ECM derived from spinal cord, or brain (Figure 5). Maximum fragment size of residual DNA in CNS-ECM scaffolds did not exceed 200 bp (Figure 6) (106). Quantification of dsDNA using PicoGreen showed that CNS-ECM scaffolds retained <50 ng dsDNA per mg dry ECM (Figure 6). Concentrations of dsDNA were 37.9 ± 7.7 ng/mg in spinal cord ECM and 40.2 ± 3.8 ng/mg in brain ECM.

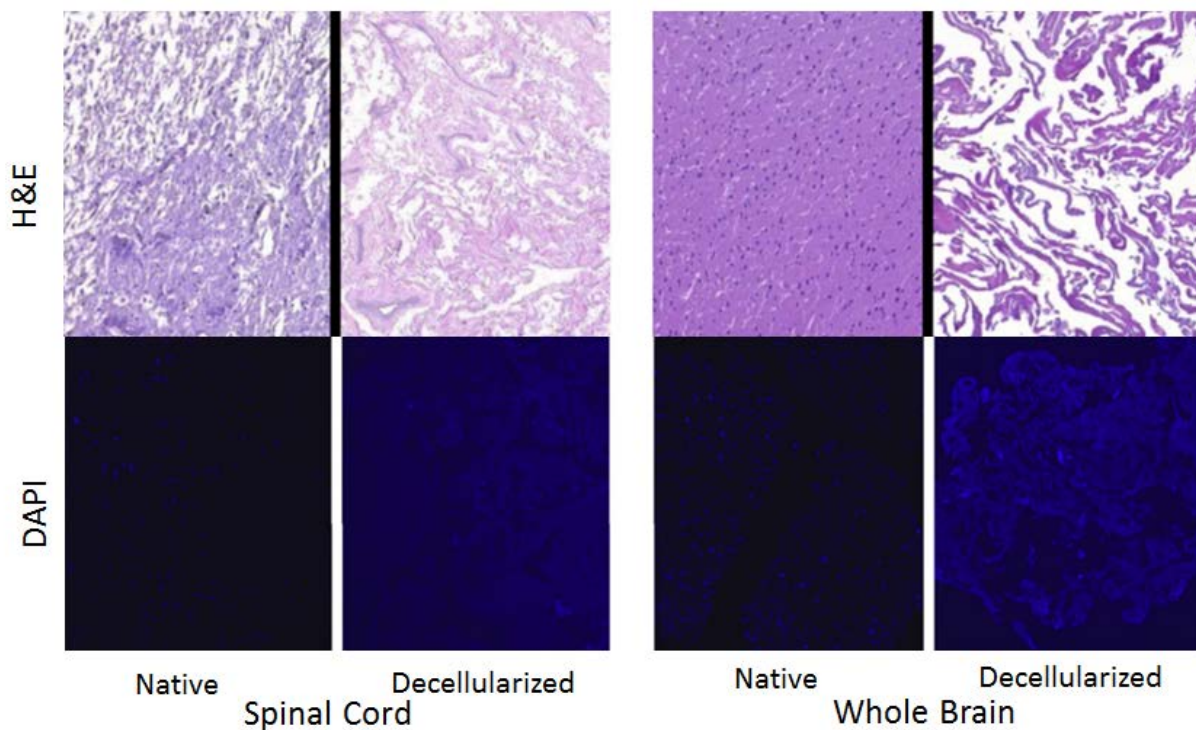


Figure 5. H&E and DAPI images of whole brain ECM and spinal cord ECM following decellularization. The decellularized scaffolds are compared to their native counterpart to demonstrate decellularization efficacy. All decellularized images have been over exposed to demonstrate the lack of nuclei found post decellularization.

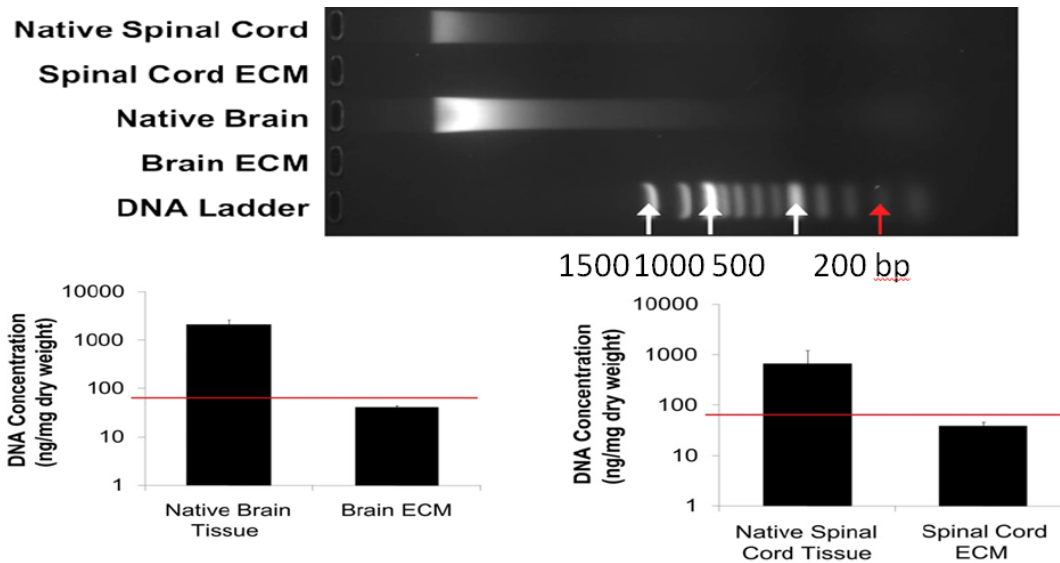


Figure 6. Spinal Cord ECM and Whole brain ECM contain less than 50ng DNA/ mg ECM as denoted by the red line. DNA remnants must less than 200bp to mitigate disease transmission

2.3.2 CNS-ECM Constituents

Histologic staining and immunohistochemistry showed that CNS-ECM scaffolds each retained laminin and myelin present in native tissues (Figure 7). Spinal cord ECM, and brain ECM also retained detectable concentrations of VEGF and bFGF, which were present in their tissues of origin (Figure 7). Concentrations of VEGF and bFGF in CNS-ECM scaffolds were comparable to concentrations in a non-CNS ECM scaffold derived from urinary bladder. In contrast, although all native CNS tissues contained NGF, spinal cord and brain ECM did not (Figure 8).

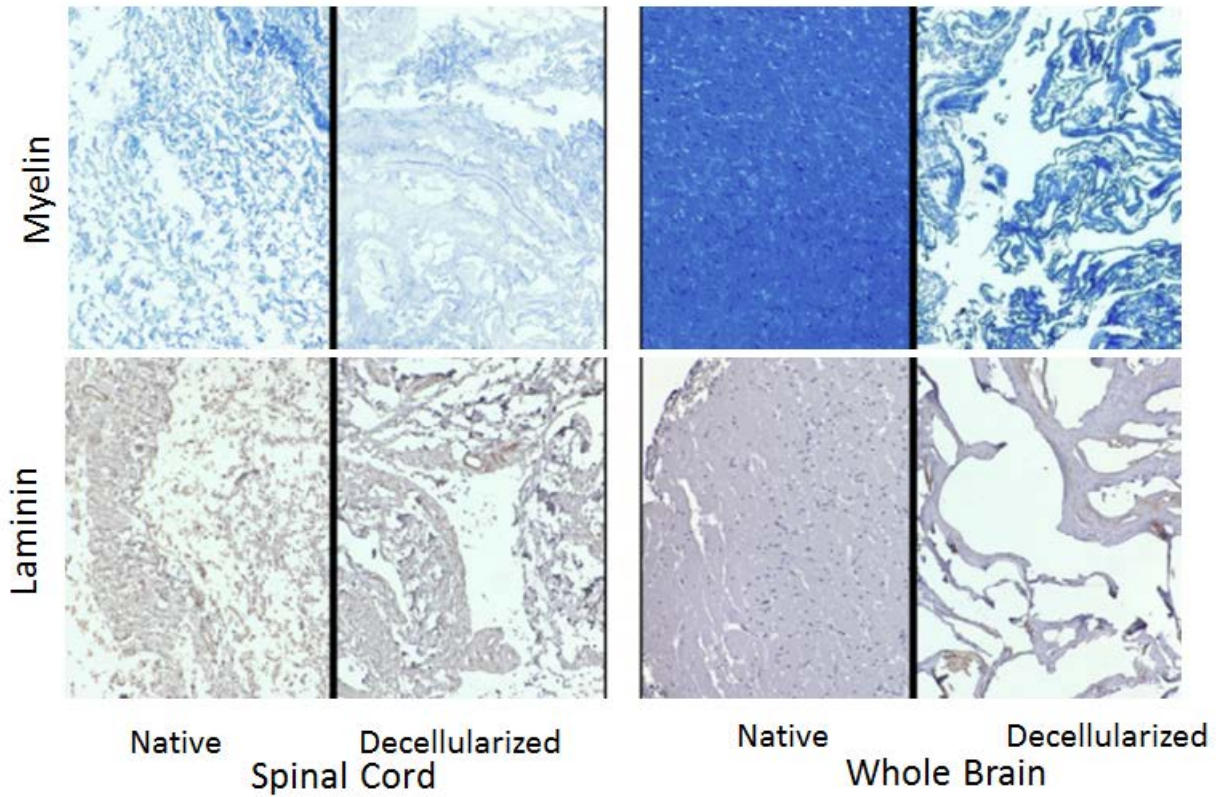


Figure 7. Myelin was present in the native brain, native spinal cord, decellularized brain, and decellularized spinal cord as shown by luxol fast blue staining. Laminin was also present in brain ECM, spinal cord ECM, and their native counterparts as shown by immunohistochemistry with hematoxylin counterstain. Magnification is 100x.

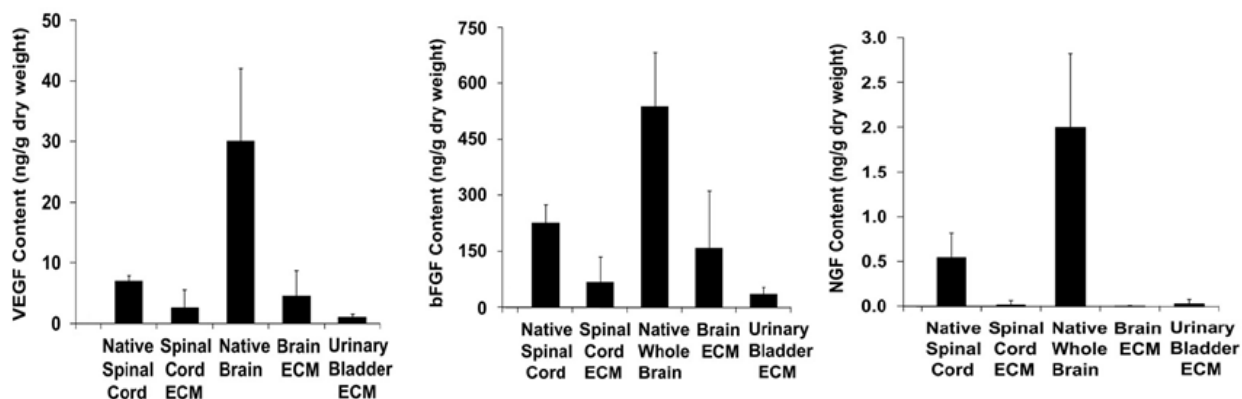


Figure 8. Growth factor content of CNS-ECM scaffolds. Spinal cord ECM, brain ECM, and urinary bladder ECM retained detectable concentrations of VEGF and bFGF, while only native tissues contain NGF.

2.3.3 In-vitro Characterization of CNS-ECM

Spinal cord ECM and brain ECM were cytocompatible in-vitro, as was a non-CNS ECM derived from urinary bladder (Figure 9). Both CNS and non-CNS ECM scaffolds increased undifferentiated PC12 cell mitogenesis up to 1.5-fold in vitro at the concentrations tested (Figure 10). CNS-ECM scaffolds induced PC12 chemotaxis in-vitro, resulting in up to 1.5-fold migration compared to unstimulated cells (Figure 11). In contrast, a non-CNS ECM scaffold attenuated migration to 0.5-fold control (Figure 11). Under the conditions assayed, CNS-ECM scaffolds induced PC12 differentiation at rates approaching 20% while a non-CNS-ECM scaffold induced differentiation at rates approaching 30% at an equivalent protein concentration (Figure 12). In summary, all PC12 cell functions except viability were modulated by CNS and non-CNS ECM scaffolds, including mitogenesis, chemotaxis, and differentiation.

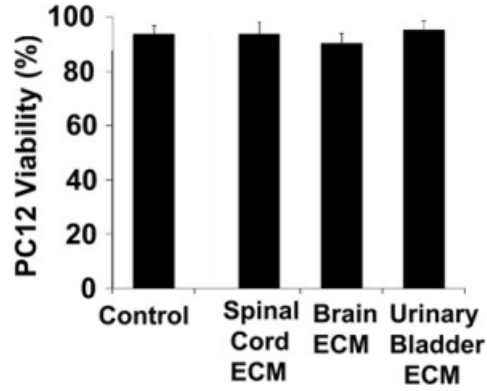


Figure 9. PC12 viability for CNS-ECMs and UBM-ECM is equivalent to the basal media control.

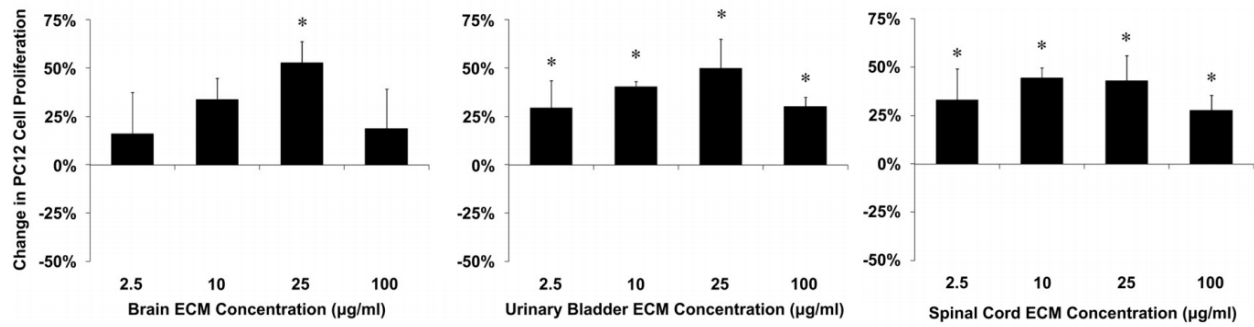


Figure 10. Mitogenic effects of CNS-ECM scaffolds. Undifferentiated PC12 cell proliferation was modulated by spinal cord ECM, brain ECM, and urinary bladder ECM as determined by BrdU incorporation during PC12 cell mitosis. Increases in mitogenesis peaked at 53% (brain ECM, 25 mg protein per ml). * Indicates $p < 0.05$ by one-way ANOVA.

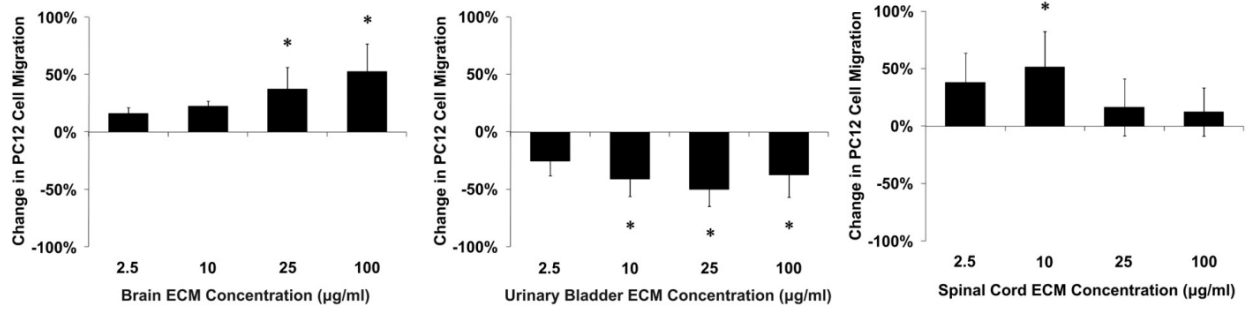


Figure 11. Chemotactic effects of CNS ECM scaffolds. Undifferentiated PC12 cell migration was modulated by spinal cord ECM, brain ECM, and urinary bladder ECM as determined by trans-membrane PC12 cell migration. Changes in chemotaxis ranged from increases of 53% (brain ECM, 100 µg protein per ml) to decreases of 50% (urinary bladder ECM, 25 µg protein per ml). * Indicates $p < 0.05$ by one-way ANOVA.

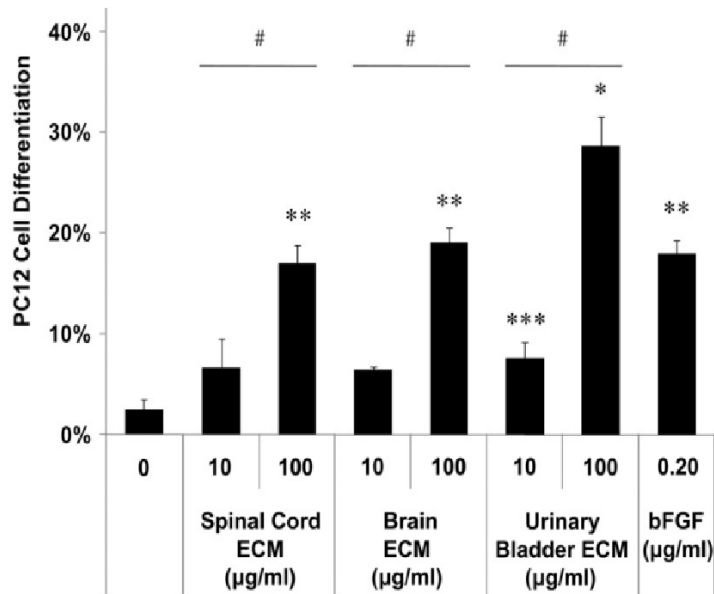


Figure 12. Differentiation effects of CNS-ECM scaffolds. PC12 neuronal differentiation induced by CNS and non-CNS ECM as indicated by neurite extension. Differentiation was compared using the following medium supplements: PBS as a negative control, spinal cord ECM at 100 µg/ml, brain ECM at 100 µg/ml, urinary bladder ECM at 100 µg/ml, or bFGF at 0.20 µg/ml as a positive control. *Urinary bladder ECM at 100 µg protein per ml induced greater differentiation than any other condition including the positive control (bFGF,

0.20 µg/ml). ** Spinal cord ECM or brain ECM at 100 µg/ml induced differentiation at rates comparable to the positive control which were greater than all other conditions except urinary bladder ECM at 100 µg protein per ml. ***Urinary bladder ECM at 10mg protein per ml induced differentiation at greater rates than the negative control (no ECM: 0mg/ml). # Differentiation rates increased with concentration for spinal cord ECM, brain ECM, and urinary bladder ECM (10 µg protein per ml vs. 100 µg protein per ml). Significant differences were determined between all groups shown by one-way ANOVA.

2.4 DISCUSSION

This study describes a versatile decellularization method that can be applied to two different CNS tissues: brain and spinal cord. The full protocol from tissue to ECM requires <24 h, a duration which compares favorably to previously reported CNS tissue decellularization methods (161-163). The resulting matrix is sufficiently acellular to obviate adverse host immune responses (73, 107, 125, 167) and contagion such as virus transmission (174-176) while retaining bioactive molecules, including myelin and laminin. In-vitro modulation of PC12 cell functions by CNS-ECM and the matrices' retention of neurosupportive proteins as well as growth factors, including neuroinductive bFGF and the neurotrophin NGF, suggest that the materials might influence behavior of other neural and neural-like cells in vitro and in-vivo.

Although the activity of growth factors, including neurotrophins, in CNS-ECM scaffolds is unknown, similar PC12 responses to CNS-ECM in-vitro suggests three nonexclusive possibilities: the amounts of NGF and other neurotrophins and growth factors (such as bFGF) with preserved bioactivity in each ECM are equivalent; spinal cord ECM and brain ECM contain

higher concentrations of neurotrophins other than NGF offset the lack of NGF; or, most likely, each CNS-ECM contains a unique profile of potent neurotrophins and growth factors which, in combination, yield similar effects.

Previous reports of ECM scaffolds derived from CNS tissues (161-163) have not explored tissue-specific functionality of these materials in contrast to non-CNS ECM. The present study clearly shows distinct cellular responses to CNS versus non-CNS ECM scaffolds, including divergent chemotactic and differentiation effects but similar mitogenic effects. These results mimic the ability of other non-CNS ECM scaffolds to support site-appropriate cell phenotype in several complex tissues (132, 134, 137-139) and suggest unique capabilities for CNS-ECM that may prove useful in regenerative medicine applications within the CNS.

Mitogenic and chemotactic effects of ECM scaffolds observed in this study were non-linear and generally conformed to an inverted-U curve commonly observed in neural cell responses to stimuli (177-179). Increasing differentiation rates correlated with moderating mitogenic and chemotactic effects at higher ECM concentrations, suggesting a dose dependent shift in cellular responses. The establishment of ECM cytocompatibilities at 100 $\mu\text{g/ml}$, the highest concentration used for in-vitro assays, further reinforced the concept that higher ECM concentrations caused alterations in cell behavior rather than apoptosis or functional impairment. Increased differentiation that coordinated with increased mitogenesis and chemotaxis at the same ECM concentration may indicate sub-populations of PC12 cells that respond differently to the ECM scaffolds or may reflect the complexity of each ECM composition as it influenced behavior of pluripotent cells (170). In considering this phenomenon, it is important to note that the differentiation assay used unique conditions, including starvation medium, greater duration, and lower cell density. Overall, responses of PC12 cells to ECM scaffolds in-vitro suggest that these

materials might be used in-vivo to control neural cell plasticity without adversely affecting viability.

Cell responses observed in this and other studies (110, 112, 136, 142, 144) suggest that ECM placed in-vivo has the potential (170) to attract endogenous progenitors such as neural stem cells to a site of CNS damage, induce proliferation, and cause differentiation into functional, site-appropriate cells to replace lost CNS tissue in cases of injury or neurodegenerative pathologies. If CNS-ECM proves to have advantages for in-vivo constructive remodeling of CNS tissues, then hydrogel forms of the scaffolds which crosslink in-situ would logically be desirable for minimally invasive application in the CNS. Ultimately and perhaps ideally, delivery of ECM (CNS or non-CNS) to a site of CNS injury in cases such as stroke or spinal cord injury might be achieved by localized injection of an ECM hydrogel (180) that would jointly fill the lesion, recruit endogenous stem cells, including neural stem cells, and enhance their regenerative responses (110). Hydrogel forms of ECM have been shown to induce rapid cell infiltration and site-appropriate constructive remodeling in vivo (152, 181). ECM bioscaffold remodeling in-vivo is likely to be further aided by the presence of VEGF and bFGF within the scaffolds, which suggests potential to promote neovascularization. Development of a microvascular network would not only support new tissue formation via transport, but could also deliver ECM degradation products as a signal to surrounding cells (110, 142), thereby inducing constructive remodeling and functional CNS recovery.

2.5 CONCLUSIONS

Acellular biologic scaffolds can be derived from CNS tissues such as spinal cord and brain by a combination of enzymatic and chemical processing. These CNS-ECM scaffolds meet or exceed established decellularization criteria (106), are cytocompatible, and retain neurosupportive proteins and growth factors present within the tissues of origin that are known to modify neural cell behaviors. The resultant acellular biologic scaffolds are able to modulate behaviors of model neural-like cell as demonstrated by increased proliferation, migration, and differentiation of the PC12 cell line in-vitro over a range of concentrations. Contrasting PC12 cell migration and differentiation responses to CNS versus non-CNS ECM suggest tissue-specific functionality for biologic scaffolds in neural applications. Overall, results of the study suggest that CNS and non-CNS ECM bioscaffolds may represent effective substrates for constructive neural tissue remodeling in-vivo and facilitate regenerative medicine approaches to CNS repair. Chapter 2 has been reprinted with permission from Elsevier (182).

2.6 FUTURE WORK

One metric not considered in this chapter was the age of the source tissue from which the ECM was harvested. The materials developed in this research were from market weight porcine. Previous studies have demonstrated that the age of the animal from which the material is derived is an important determinant of the success of the material. In-vitro analyses of bioscaffolds from different source ages of small intestinal submucosa showed distinct differences in terms of mitogenic, and chemotactic properties, two metrics of regenerative potential (110). Bioscaffolds

derived from the younger sources promoted increased chemotaxis, whereas those from the bioscaffolds derived from 26 and 52 week animals promoted increased mitogenesis (183). When the bioscaffolds were evaluated in an in-vivo model of biocompatibility, bioscaffolds from the youngest animals promoted increased alternative macrophage activation and increase skeletal muscle formation within the ECM bioscaffold (184). Bioscaffolds derived from the CNS, therefore, should be compared at different ages of development to enhance promotion of constructive remodeling.

3.0 HYDROGELS DERIVED FROM CENTRAL NERVOUS SYSTEM EXTRACELLULAR MATRIX

3.1 INTRODUCTION

Biologic scaffolds composed of extracellular matrix (ECM) can facilitate the constructive remodeling of numerous tissues including esophagus (95, 96), lower urinary tract (97, 98), muscle and tendon (99, 100), and myocardium (101, 102), among others. Although the mechanisms by which ECM scaffolds promote a constructive and functional remodeling response are only partially understood, recruitment of endogenous multipotent progenitor cells (141, 142), modulation of the innate immune response (73, 74), scaffold degradation with the generation of bioactive molecular cues (112, 185, 186), and innervation (122) have all been shown to be important events in this process. The contribution of the innate three-dimensional ultrastructure, unique surface ligand distribution, or molecular composition to constructive, functional remodeling is largely unknown. However, hydrogel formulations of matrix scaffolds lack the native three dimensional ultrastructure of the source tissue but still possess in vitro and in vivo biologic activity (180, 187-191), suggesting that the molecular composition of these materials is an active factor in remodeling events. There have also been reports that suggest tissue-specific biologic scaffold materials have properties that enhance greater site-appropriate

phenotypic cell differentiation compared to ECM scaffolds derived from non-homologous tissue sources (133, 134, 136, 182).

The use of biologic scaffold materials within either the central or peripheral nervous system has not been extensively investigated (192). However, it has been shown that innervation of remodeled scaffold materials is an early event when such materials are placed in several different anatomic locations and represents a predictor of constructive and functional outcomes (117, 122, 158). It has also been shown that innervation is a critical event in robust regenerative responses that occur in species such as the newt and axolotl (121, 193, 194). Methods for the isolation of central nervous system (CNS) ECM have recently been described. The objectives of the present study were to develop a method to create hydrogel forms of brain and spinal cord ECM, examine the biomolecular composition and mechanical properties of the resulting hydrogels, and evaluate the in-vitro neural cytocompatibility and neurotrophic potential of CNS-ECM hydrogels versus a hydrogel prepared from a non-CNS ECM; specifically, porcine urinary bladder matrix.

3.2 MATERIALS AND METHODS

3.2.1 Overview of Experimental Design

Following decellularization of porcine brain and spinal cord, the resulting brain and spinal cord ECM (B-ECM and SC-ECM, respectively) were solubilized. The ECM materials were analyzed for collagen and sulfated glycosaminoglycan content, ultrastructure, and hydrogel mechanical properties. A commonly used neural cell line for examining neurite extension, N1E-115 (195,

196), was used to identify the neurotrophic potential of ECM hydrogels in two- and three-dimensional culture. The results were compared to an ECM hydrogel manufactured from a non-CNS source, porcine urinary bladder matrix (UBM-ECM) (180).

3.2.2 ECM Biologic Scaffold Production

Porcine brain, spinal cord, and urinary bladder were obtained from market weight animals (Tissue Source, Lafayette, IN). Tissues were frozen immediately after harvesting at -80°C, thawed before use, and processed by tissue specific methods described previously (Table 1A) (182). In brief, CNS tissue was agitated (spinal cord tissue at 200 rpm; brain tissue at 120 rpm unless otherwise stated) in the following decellularization baths: deionized water (16 h at 4°C; 60 rpm), 0.02% trypsin / 0.05% EDTA (60 min at 37°C; 60RPM; Invitrogen Corp., Carlsbad, CA, USA), 3.0% Triton X-100 (60 min; Sigma-Aldrich Corp., St. Louis, MO, USA), 1.0 M sucrose (15 min; Fisher Scientific, Pittsburgh, PA, USA), water (15 min), 4.0% deoxycholic acid (60 min; Sigma), 0.1% peracetic acid (Rochester Midland Corp., Rochester, NY, USA) in 4.0% ethanol (v/v; 120 min), PBS (15 min; Fisher), deionized water (twice for 15 min each rinse), and PBS (15 min). Each bath was followed by rinsing the remaining tissue through a strainer with deionized water. Decellularized B-ECM and SC-ECM were lyophilized and stored dry until use.

Table 1. Methods for Decellularization and Solubilizing B-ECM, SC-ECM, and UBM-ECM.

Table 1			
A. Decellularization Methods			
<i>Step</i>	<i>B-ECM and SC-ECM (120 and 180 RPM respectively)</i>		<i>UBM-ECM (300 RPM)</i>
1.	Deionized Water Soak (18-24hours)		Mechanical Delamination
2.	0.025% Trypsin (1hour)		
3.	3% Triton X 100 (1hour)		
4.	1M Sucrose (30min.)		
5.	Deionized Water Soak (30min.)		
6.	4% Deoxycholic Acid (1hour)		
7.	0.01% Peracetic Acid		
B. Methods for Solubilizing and Digesting			
	<i>B-ECM</i>	<i>SC-ECM</i>	<i>UBM-ECM</i>
<i>Particle Size</i>	<400um	400-1000um	
<i>Solubilization</i>	0.01N HCl		
<i>Digestion</i>	1mg/mL Pepsin		

UBM-ECM was prepared as previously described (197). In brief, connective tissue was removed from the serosal surface of the bladder. The tunica serosa, tunica submucosa, and majority of the tunica muscularis mucosa were mechanically delaminated, which left the basement membrane and tunica propria intact. Luminal urothelial cells were dissociated from the basement membrane by soaking the UBM-ECM in deionized water. The UBM-ECM was then agitated in 0.1% peracetic acid in 4.0% ethanol (v/v; 120 min; 300 rpm) followed by a series of PBS and deionized water rinses and lyophilization.

3.2.3 ECM Digestion and Solubilization

Lyophilized and comminuted B-ECM (20 mesh), SC-ECM (20 mesh or hand cut), and UBM-ECM (20 mesh or hand cut; 400-1000µm largest particle dimension as measured by mesh diameter or ruler) were separately placed into a 0.01 N HCl solution containing 1mg/mL pepsin

(Sigma) at a concentration of 10 mg ECM/mL and stirred at room temperature for 48h as previously described (Table 1B) (180). After 48h, B-ECM, SC-ECM, and UBM-ECM were completely digested and formed a pre-gel solution (pH~2). The pre-gel ECM solution was brought to pH 7.4 using 0.01N NaOH and diluted to the desired volume/salt concentration using 10x and 1 x PBS. Pepsin is irreversibly inactivated at pH above 7.5 (198).

3.2.4 Collagen and sGAG Quantification

Collagen concentration of the pre-gel ECM solution was determined for samples from each production batch with the Sircol Assay Kit (Biocolor Ltd., UK) following the manufacturer's recommended protocol (n=4 in duplicate or triplicate). Sulfated glycosaminoglycan (sGAG) concentrations were determined using digested ECM at a concentration of 50 mg ECM/ml with 0.1 mg/ml proteinase K (Sigma) in buffer (10 mM Tris-HCl, pH 8.0, 100 mM NaCl, 25 mM EDTA for 48-72 hours at 50°C) using the Blyscan Sulfated Glycosaminoglycan Assay Kit (Biocolor Ltd., UK) and following the manufacturer's recommended protocol (n=3 in duplicate or triplicate).

3.2.5 Scanning Electron Microscopy

Scanning electron microscopy was used to examine the surface topography of brain, spinal cord, and UBM-ECM hydrogels. Five hundred micron thick hydrogels were prepared and then fixed in cold 2.5% glutaraldehyde (Electron Microscopy Sciences, Hatfield, PA) for 24 hours followed by three 30 minute washes in 1x PBS. Hydrogels were dehydrated in a graded series of alcohol (30, 50, 70, 90, 100% ethanol) for 30 minutes per wash, and then placed in 100% ethanol

overnight at 4°C. Hydrogels were washed 3 additional times in 100% ethanol for 30 minutes each and critical point dried using a Leica EM CPD030 Critical Point Dryer (Leica Microsystems, Buffalo Grove, IL, USA) with carbon dioxide as the transitional medium. Hydrogels were then sputter-coated with a 4.5 nm thick gold/palladium alloy coating using a Sputter Coater 108 Auto (Cressington Scientific Instruments, UK) and imaged with a JEOL JSM6330f scanning electron microscope (JEOL, Peabody, MA, USA)

3.2.6 Turbidity Gelation Kinetics

Turbidimetric gelation kinetics were determined as previously described (199). The pre-gel solution was diluted to 6mg/mL and maintained on ice at 4°C until placed into a 96 well plate (100µL/well). The plate was immediately transferred to a spectrophotometer (Molecular Devices) preheated to 37°C, and absorbance was measured at 405nm every 2 minutes for 50 minutes. Normalized absorbance was calculated using Equation 1 and then used to calculate the following parameters: time required to reach 50% and 95% maximum absorbance was denoted as $t_{1/2}$ and t_{95} , respectively, the lag phase, t_{lag} , calculated by extrapolating the linear portion of the curve, and the turbidimetric speed, S , of gelation was determined by calculating the growth portion slope of the curve normalized to absorbance (180). The assay was repeated three times with independent samples in triplicate.

$$\textit{Normalized Absorbance} = \frac{A - A_0}{A_{max} - A_0}$$

Equation 1. Normalized absorbance for turbidimetric analysis.

3.2.7 Rheological Measurements

The pH of the ECM digest was neutralized to 7.4 and diluted to 4, 6, or 8mg ECM/ml. The diluted pre-gel solution was then placed on a 40mm parallel plate rheometer (AR 2000, TA Instruments) at 1Pa stress and 10°C to ensure even distribution and the liquidity of the pre-gel solutions between the plates. A dynamic time sweep was run with the parameters of 5% strain (with the exception of spinal cord ECM gel at 8mg/mL, which was run with 0.5% strain), 1 rad/s (0.159 Hz) and rapidly increasing temperature from 10°C to 37°C to induce gelation as indicated by a sharp increase and plateauing of the storage modulus (G'), and the loss modulus (G'') (n=3 per gel per concentration).

3.2.8 N1E-115 ECM Cytocompatibility and Two Dimensional Neurite Extension

N1E-115 mouse neuroblastoma cells (ATCC No. CRL 2263), a commonly used experimental cell line to examine neurotrophic potential and differentiation (195, 196), were cultured in DMEM (Sigma) with 10% fetal bovine serum (FBS; Thermo Fisher Scientific, Waltham MA, USA) /1% pen/strep (Sigma) at a concentration of 100,000 cells per well in 12 well plate prior to the addition of ECM. B-ECM, SC-ECM, or UBM-ECM digest was added after cell attachment at a concentration of 100µg ECM/mL. Following 18-24hrs in culture with ECM, the medium was removed and 4µM calcein-AM and 4µM ethidium homodimer-1 was added to each well to evaluate cytotoxicity. Live cells that hydrolyze membrane-permeable calcein-AM, but not ethidium homodimer-1, fluoresce in green and dead cells that bind and activate ethidium homodimer-1, but not calcein-AM, fluoresce in red.

The effects of the B-ECM, SC-ECM, and UBM-ECM pre-gel digest upon N1E-115 neurite outgrowth were independently evaluated and used as an indicator of neurotrophic potential of the remaining bioactive molecules in ECM materials after enzymatic degradation. N1E-115 cells in DMEM with 10% FBS/1% pen strep were seeded at a density of 5,000 cells/well in a 24 well plate. After incubation for 24h, the media was removed and replaced with DMEM with 2.5% FBS, which promoted low levels of neurite extension and allowed changes in response to ECM to be quantified. Neutralized ECM pre-gel solutions at concentrations of 10 μ g/mL and 100 μ g/mL were added after cell attachment and cells were incubated for 48h. N1E-115 cells were fixed with 2% paraformaldehyde for 20 minutes at room temperature. Attached cells were stained with DAPI for nuclei and Alexa Fluor phalloidin 488 (Invitrogen) for F-actin filaments. Three images at 200x magnification were taken per well. The number of cells with neurite extensions were manually counted. The longest neurite of each cell was measured in pixels using ImageJ (NIH). The outgrowth assay was repeated six times per condition. Neurites were denoted as cell processes that extended a minimum length of twice the diameter of the cell body.

3.2.9 Neurite Extension in Three Dimensional Culture

N1E-115 cells were maintained in 10% FBS DMEM media at 37°C. B-ECM, SC-ECM, or UBM-ECM hydrogels (1ml) were cast with a cell density of 500,000 cells/hydrogel and a concentration of 6mg ECM/ml and after gelation for 1hr at 37°C in a non-humidified incubator. All hydrogels were then cultured for 24 hours in DMEM supplemented with 10% FBS/ 1% pen/strep. Serum concentration was reduced to 0% FBS and cells cultured for an additional 2 or 7 days. The hydrogels were then fixed with 4% paraformaldehyde (Fisher), stained for F-actin,

and imaged using multiphoton confocal microscopy to visualize three-dimensional cell morphology inside the hydrogel scaffolds.

Hydrogels cultured with N1E-115 cells were stained with 0.1% Alexa Fluor 488 Phalloidin (Invitrogen) for 2 hours and submerged in PBS solution in a hanging drop slide and coverslipped. To visualize neurite outgrowth in three dimensions, the slide was mounted beneath an Olympus FV1000 multiphoton system. The system was equipped with a Chameleon ultra-diode-pumped laser, and a 25x XL Plan N objective with a N.A. of 1.05 and a field of view of 500 μ m. The excitation wavelength was chosen at 830 nm at a 6% laser transmissivity. The sampling speed was set to 2 μ s/pixel with a 2 line kalman filter, and the scanning had an incremental z-step of 1 μ m. Image stacks were then compiled into a maximum intensity z-projection in ImageJ. Image stacks were imported into Imaris software (Bitplane, South Windsor CN, USA) for 3-D visualization.

3.2.10 Statistical Analysis

An independent Student's t-test was used to compare the effect of ECM pre-gel digests on N1E-115 cell differentiation to the effect of the no ECM control ($p < 0.05$). A one-way ANOVA was used for all other comparisons ($p < 0.05$). All statistical analysis methods used SPSS Statistical Analysis Software (SPSS, IBM, Chicago, IL, USA).

3.3 RESULTS

3.3.1 Collagen and sGAG Quantification

Collagen concentration of B-ECM was 537.5 ± 26.9 μg collagen/mg dry weight, which was less than SC-ECM and UBM-ECM at 703.2 ± 47.3 and 702.5 ± 113.5 μg collagen/mg dry weight, respectively ($p < 0.01$) (Figure 13A). B-ECM and UBM-ECM had a higher sGAG concentration, 5.1 ± 1.4 ($p < 0.009$) and 4.4 ± 0.4 ($p < 0.02$) μg sGAG/mg dry weight, respectively, compared to SC-ECM, which was 1.3 ± 0.9 μg sGAG/mg dry weight (Figure 13B).

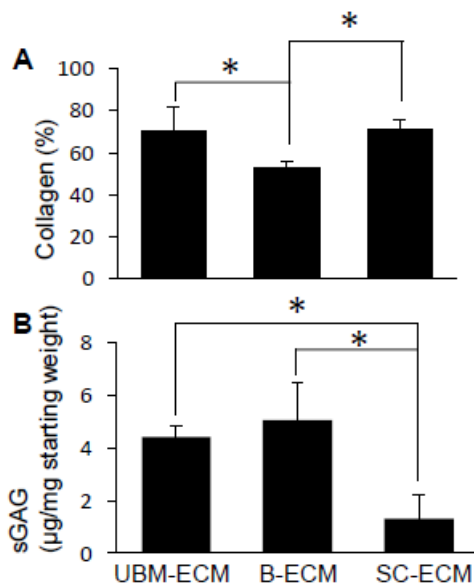


Figure 13. Collagen and sGAG composition in B-ECM and SC-ECM scaffolds. (A) SC-ECM contains a significantly higher percentage of collagen than B-ECM. (B) B-ECM contains a significantly higher concentration of sGAGs than SC-ECM.

3.3.2 Qualitative Assessment

B-ECM, SC-ECM, and UBM-ECM pre-gel solutions polymerized to form a hydrogel at physiologic pH (7.4) and temperature (37°C). Qualitatively, SC-ECM hydrogels were more rigid than B-ECM and UBM-ECM hydrogels (Figure 14A-C). SEM micrographs showed dense, moderately organized collagen fibrils in B-ECM, SC-ECM, and UBM-ECM hydrogels (Fig. 14D-I). B-ECM contained the thickest fibrils (Figure 14G), while SC-ECM hydrogels contained the most dense arrangement of fibrils (Figure 14H). SC-ECM and UBM-ECM hydrogels contained moderately organized collagen fibers, while B-ECM contained dense clusters of randomly distributed collagen fibers.

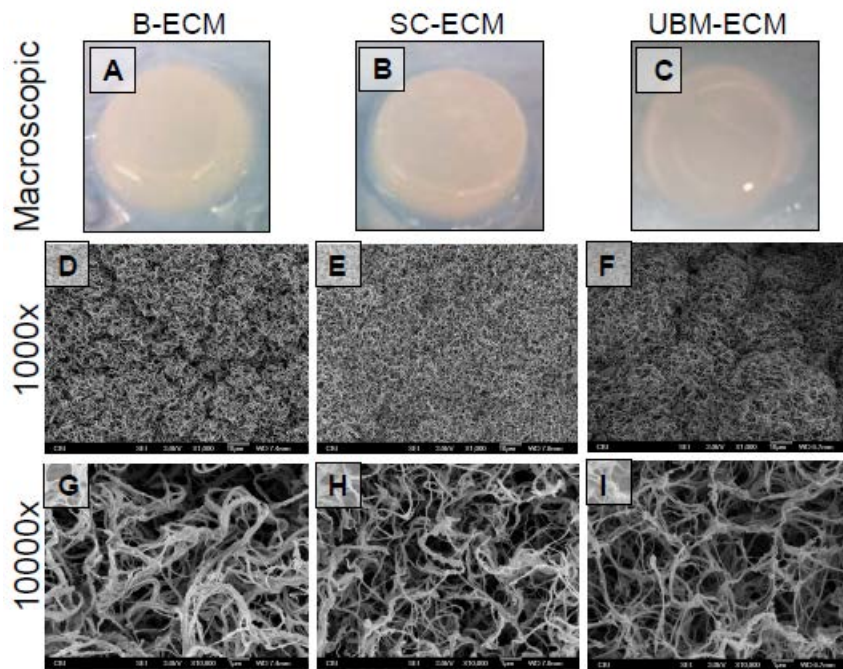


Figure 14. B-ECM, SC-ECM, and UBM-ECM hydrogels and their respective Scanning Electron Micrographs (6mg/mL). (A) B-ECM hydrogel; (B) SC-ECM hydrogel; (C) UBM-ECM hydrogel; (D) B-ECM 1000x; (E) SC-ECM 1000x; (F) UBM-ECM 1000x; (G) B-ECM 10000x; (H) SC-ECM 10000x; (I) UBM-ECM 10000x.

3.3.3 Turbidimetric Gelation Kinetics

The gelation kinetics between hydrogel forms of B-ECM, SC-ECM, and UBM-ECM were evaluated using a normalized absorbance (Figure 15A) to define the lag phase, times to reach half and 95% of the final turbidity, and speed to reach complete gelation using turbidimetric gelation kinetics as previously described (Table 2) (180, 199). Turbidimetric gelation kinetics showed a sigmoidal shape for SC-ECM and UBM-ECM hydrogels, whereas B-ECM showed an exponential shape (Figure 15B). Differences observed in kinetic curve shapes translated to a longer lag phase (t_{lag} ; Figure 15C) for UBM-ECM hydrogels (7.2 ± 1.4 min) than B-ECM (28 ± 4.2 min) or SC-ECM hydrogels (3.6 ± 5.6 min). The time required to reach half of the final turbidity ($t_{1/2}$; Figure 15D) was also longer for UBM-ECM (11.0 ± 5.8 min.) than B-ECM (8.9 ± 5.4 min) or SC-ECM hydrogels (8.2 ± 5.1 min.). The time required to reach 95% of the final turbidity (t_{95} ; Figure 15E) was also longer for UBM-ECM hydrogels (21.6 ± 2.9 min) compared to B-ECM (15.1 ± 5.5 min) and SC-ECM hydrogels (12.2 ± 4.6 min). The velocity to complete gelation (S ; Figure 15F) was faster for SC-ECM hydrogels (0.11 ± 0.02 min⁻¹) compared to B-ECM (0.08 ± 0.01 min⁻¹) and UBM-ECM (0.07 ± 0.02 min⁻¹) ($p < 0.05$). These results suggest that during hydrogel assembly, SC-ECM hydrogels reach the steady state plateau faster than B-ECM or UBM-ECM hydrogels.

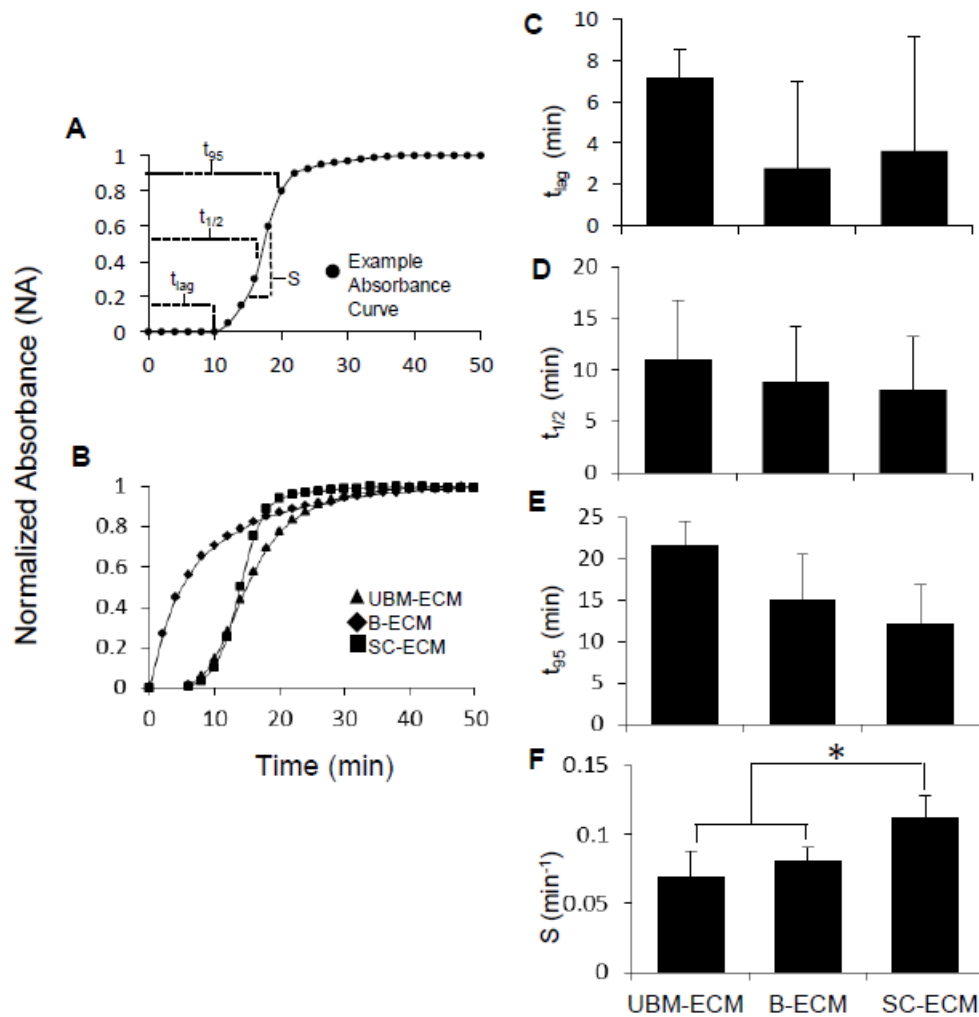


Figure 15. B-ECM and SC-ECM representative turbidimetric and normalized turbidimetric curves. (A) Example absorbance curve and the metrics analyzed. (B) Normalized absorbance for B-ECM (diamonds), SC-ECM (squares), and UBM-ECM (triangles). (C) Lag time comparison for B-ECM, SC-ECM, and UBM-ECM. (D) Time to 50% complete gelation for B-ECM, SC-ECM, and UBM-ECM. (E) Time to 95% complete gelation for B-ECM, SC-ECM, and UBM-ECM. (F) Velocity to complete gelation for B-ECM, SC-ECM, and UBM-ECM following the lag time.

Table 2. Summary of Rheologic and Turbidity Values for B-ECM, SC-ECM, and UBM-ECM. * Indicates statistical significance at $p < 0.05$ when one group is statistically different from the other two.

Rheology	B-ECM (Average (STDEV))			SC-ECM (Average (STDEV))			UBM-ECM (Average (STDEV))		
	4mg	6mg	8mg	4mg	6mg	8mg	4mg	6mg	8mg
Storage Modulus (G' ; Pa)	20.31 (15.96)	49.9 (16.81)	61.75 (10.97)	138.5* (33.81)	235.5 (63.11)	757* (74.87)	11.43 (4.9)	72.78 (2.17)	143.8 (84.1)
Loss Modulus (G'' ; Pa)	2.6 (1.94)	9.44 (4.64)	10.15 (1.8)	16.31* (4.93)	37.51* (11.39)	93.61* (10.9)	1.4 (0.59)	10.14 (0.48)	19.31 (12.27)
Complete gelation (Time; min)	34.8 (28.87)	2.4 (1.25)	8.33 (2.76)	11.7 (5.63)	7.0 (3.56)	28.97 (4.68)	52.53 (2.15)	8.47 (1.71)	19.8 (19.1)
Turbidity	B-ECM (Average (STDEV))			SC-ECM (Average (STDEV))			UBM-ECM (Average (STDEV))		
	6mg			6mg			6mg		
Speed (S ; min^{-1})	0.8 (0.1)			0.11 (0.02)			0.07 (0.02)		
50% gelation ($t_{1/2}$; min)	8.87 (5.40)			8.15 (5.06)			11.00 (5.75)		
95% gelation (t_{95} ; min)	15.08 (5.48)			12.23 (4.63)			21.57 (2.93)		
Lag Phase (t_{lag} ; min)	2.79 (4.22)			3.62 (5.57)			7.16 (1.35)		

3.3.4 Rheologic Measurements

The storage modulus (G') and the loss modulus (G'') for B-ECM, SC-ECM, and UBM-ECM hydrogels changed over time as the sample temperature increased rapidly from 10°C to 37°C. Sigmoidal storage and loss moduli curves showed increased maximum storage modulus, maximum loss modulus, and time to complete gelation as concentration increased (Figure 16A-C). SC-ECM hydrogels had the largest storage modulus at all hydrogel concentrations (Figure 16D). At 8mg/mL, the storage modulus for SC-ECM, 757.0 ± 74.8 Pa, was greater than both UBM-ECM and B-ECM ($p < 0.05$), which showed storage moduli of 143.8 ± 84.1 Pa and 61.8 ± 11.0 Pa, respectively. While B-ECM hydrogels have lower storage moduli than SC-ECM and UBM-ECM hydrogels, B-ECM hydrogels at a concentration of 6mg/mL reached the steady state plateau in 2.4 ± 1.3 min.; a time that was faster than UBM-ECM and SC-ECM, which had times of 8.5 ± 1.7 min. and 7.0 ± 3.6 min., respectively. Table 2 summarizes the storage modulus, loss

modulus, and time to complete gelation for each ECM hydrogel at concentrations of 4, 6, and 8mg/mL.

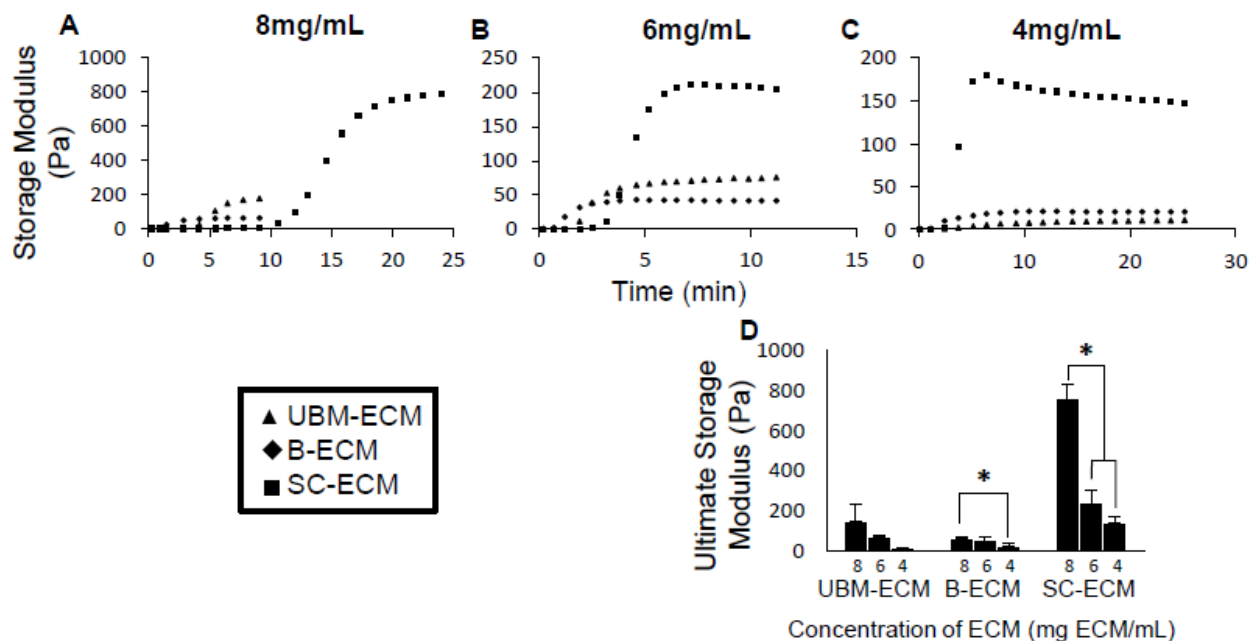


Figure 16. Representative rheologic gelation kinetics for B-ECM and SC-ECM hydrogels (4, 6, and 8 mg/mL). G' represents the storage modulus and G'' represents the loss modulus. SC-ECM is significantly stiffer than B-ECM at each hydrogel concentration. (A) Storage modulus time sweep for B-ECM, SC-ECM, and UBM-ECM at 8mg/mL. (B) Storage modulus time sweep for B-ECM, SC-ECM, and UBM-ECM at 6mg/mL. (C) Storage modulus time sweep for B-ECM, SC-ECM, and UBM-ECM at 4mg/mL. (D) Final storage modulus for B-ECM, SC-ECM, and UBM-ECM at each concentration. * Indicates statistical significance of $p < 0.05$.

3.3.5 N1E-115 ECM Cytocompatibility and Two Dimensional Neurite Extension

The live/dead assay showed all ECMs to be non-cytotoxic for N1E-115 cells (Figure 17). B-ECM, SC-ECM, and UBM-ECM pre-gel solutions at concentrations of 10 and 100 μ g ECM/mL increased the number of cells extending neurites (differentiated cells) compared to cells cultured

without ECM digest. At 100 μ g ECM/mL, SC-ECM digest promoted the highest percentage of differentiation, with $69.7 \pm 14.0\%$ of the cells extending neurites, whereas UBM-ECM and B-ECM promoted, $57.4 \pm 12.1\%$ and $54.3 \pm 11.7\%$ respectively. At 10 μ g and 100 μ g ECM/mL, B-ECM, SC-ECM, and UBM-ECM increased the percentage of cells with neurite extensions compared to the buffered control; however B-ECM was the only scaffold that showed an increase in neurite extension length for both 10 and 100 μ g ECM/ml compared to cells cultured without ECM (Figure 18).

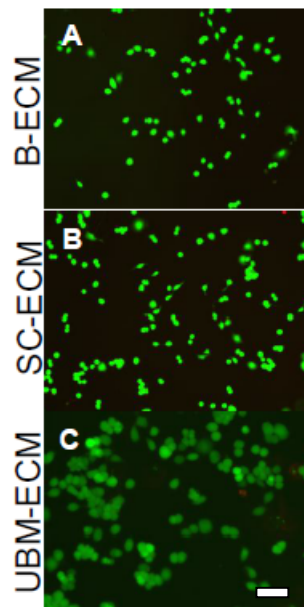


Figure 17. Live/dead cytotoxicity analysis for B-ECM, SC-ECM, and UBM-ECM. (A) B-ECM, (B) SC-ECM, and (C) UBM-ECM pre-gel solutions are non-cytotoxic when added to culture medium of N1E-115 cells (10x; scale bar is approximately 200 μ m).

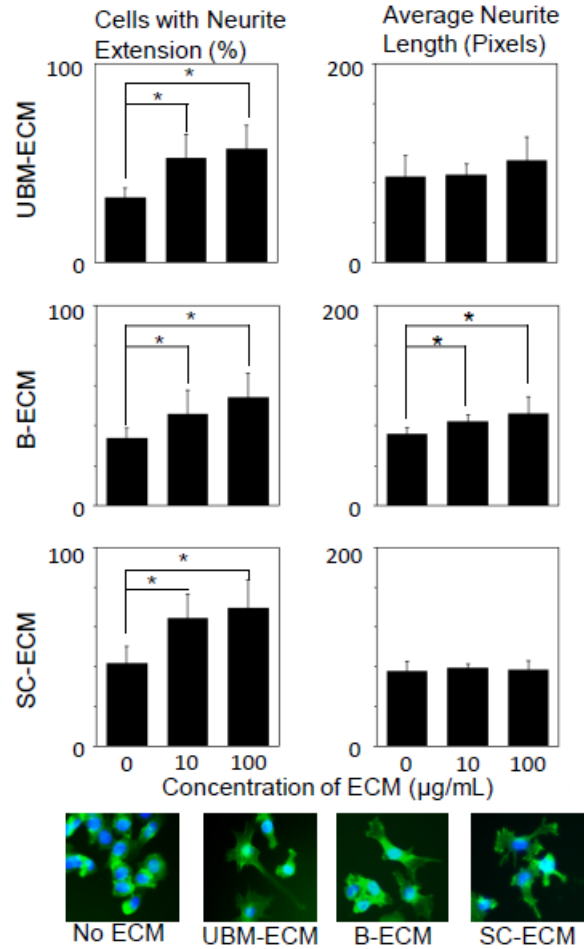


Figure 18. B-ECM and SC-ECM pre-gel solutions increase the number of cells with neurite extensions. All Scaffolds show a dose dependent increase for the number of cells with neurite extension, while only B-ECM shows a dose dependent increase in neurite length with increasing concentrations of ECM. * Indicates statistical significance of $p < 0.05$.

3.3.6 Neurite Extension in Three Dimensional Culture

B-ECM, SC-ECM, and UBM-ECM supported the formation of three-dimensional neurite extensions at 2 and 7 days following removal of serum (Figure 19). N1E-115 cells seeded in B-ECM hydrogels promoted a short arborizing growth pattern at two days, while SC-ECM and

UBM-ECM hydrogels induce unipolar extensions. By 7-days, all ECM hydrogels promoted unipolar or bipolar extensions (Figure 19).

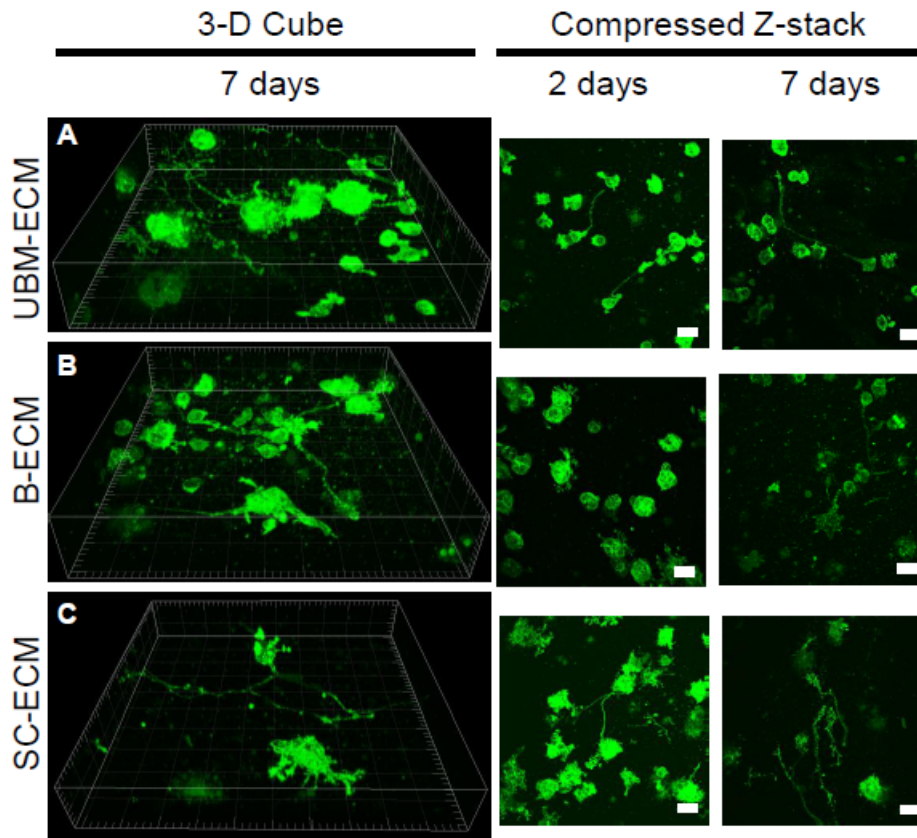


Figure 19. Neurite Extension in B-ECM, SC-ECM, and UBM-ECM in 6mg/mL hydrogels in a 3-D cube or compressed Z-stack. (A) N1E-115 cell extension following 7 days culture in B-ECM in 3-D cube. (B) N1E-115 cell extension following 7 days culture in SC-ECM in 3-D cube. (C) N1E-115 cell extension following 7 days culture in UBM-ECM in 3-D cube. The compressed Z-stack shows B-ECM has short arborizing extensions at two days, while SC-ECM and UBM-ECM have uni- or bi-polar extensions. At 7 days all ECM hydrogels support uni- or bi-polar N1E-115 cell extensions. For 3-D cubes the major tick mark represents 50 μ m and the minor tick mark represents 10 μ m. For the Z-stacks the scale bar represents 50 μ m.

3.4 DISCUSSION

The present study shows that biologic scaffolds derived from porcine brain and spinal cord can be processed to form hydrogels that retain selected ECM-specific constituents. At comparable ECM concentrations, these hydrogel forms of CNS-ECM have distinctive composition and biomechanical properties. Furthermore, CNS-ECM hydrogels are cytocompatible, promote N1E-115 cell differentiation, and support three-dimensional neurite extension.

The mechanical properties of SC-ECM hydrogels are similar to those previously shown to support neuronal differentiation of stem cells (0.1-1kPa) (200). It is therefore plausible that the rheologic and turbidimetric properties of CNS-ECM hydrogels could be used to influence the differentiation of endogenous or therapeutically administered stem cells following CNS injury (200). The gelation kinetics and storage moduli of CNS-ECM hydrogels can be manipulated to a certain extent by varying ECM concentrations, such that following polymerization a hydrogel could be made with tailored in-vivo pre-polymerization lag time, final storage modulus, and rate of polymerization (201). Altering these parameters may enhance not only the ability of the gels to modulate stem cell behaviors, but also the cell and drug delivery properties of CNS-ECM hydrogels (202, 203).

It is logical that the distinctive collagen and sGAG concentrations play a role in ECM hydrogel gelation and rheologic properties; therefore, quantification of the collagen and sGAG concentrations provides valuable insight. Furthermore, the collagen monomers aggregate and self-assemble into thin filaments that can then crosslink into collagen fibers that interweave with themselves and other ECM components to contribute to hydrogel formation (204). The shorter polymerization time and smaller storage modulus of B-ECM hydrogel compared to SC-ECM hydrogel may result from the higher sGAG concentration found in B-ECM hydrogels.

Concentration of sGAGs has been shown to alter gelation kinetics and mechanical properties of hydrogels (205, 206). While UBM-ECM hydrogel has a similar concentration of sGAGs compared to B-ECM hydrogel, the increased storage modulus could be due to a possible increased ratio of collagen I to collagen III in UBM-ECM hydrogel (207, 208). The increased storage modulus of SC-ECM hydrogel compared to UBM-ECM hydrogel may result from relatively low sGAG concentration found in SC-ECM. Although collagen composition of B-ECM contains approximately 50% collagen, native brain contains very limited amounts of ECM components including collagen (209). It should be noted that the percent collagen described herein represents a percentage of the isolated ECM, rather than a percentage of the mass of the intact brain prior to decellularization. While collagen and sGAGs affect hydrogel mechanical properties, further studies are needed to determine those additional molecules present in the ECM hydrogels that may contribute to polymerization.

Both composition and material properties of the CNS derived hydrogels are distinct from a hydrogel derived from a non-CNS tissue source (UBM-ECM) (180). The unique ECM composition of different organs (210, 211), suggests that ECM scaffolds derived from the same tissue type as that of the injury site may contain bioactive components uniquely able to induce constructive remodeling of that tissue type. An array of proteins and peptides will be generated during ECM solubilization (142, 180) that is reflective of the molecular profile of the organ from which the ECM is derived. Thus, a hydrogel derived from solubilized and digested CNS-ECM will contain a unique composition of molecular constituents resembling those found within the ECM of healthy CNS tissue. The bioactive factors retained in the ECM hydrogels in the present study are neurotrophic as evident by the formation of N1E-115 cell neurite extensions when cultured in the presence of ECM digests. In addition, the present study shows that B-ECM

hydrogels increase the length of N1E-115 neurite extensions in two-dimensional culture. This effect is not seen in UBM-ECM or SC-ECM digest, a possible indication of a tissue-specific effect of B-ECM upon these brain derived cells (195, 212).

3.5 CONCLUSIONS

B-ECM and SC-ECM hydrogels, while derived by similar decellularization methods from their source tissue, each have a unique biochemical composition, mechanical properties, and neurotrophic potential. The increase in neurite length for N1E-115 cells in response to B-ECM suggests a tissue specific effect of B-ECM hydrogels on a brain derived cell line. Each ECM elicited unique cell responses as demonstrated by neurotrophic potential in their solubilized form and support of considerable three-dimensional neurite growth and extension in their re-polymerized hydrogel forms; this finding suggests that the molecular constituents of the source ECM play an important role in the bioactivity of these scaffolds. Support of three-dimensional neurite extension by CNS-ECM hydrogels also suggests the possibility that these hydrogels provide the scaffolding necessary to promote in-vivo axonal repair and warrants further study.

3.6 FUTURE WORK

Future research into hydrogels derived from the CNS for CNS repair should focus on evaluating functional neuronal networks within the hydrogel. While this research evaluated hydrogel's ability to support neurite extension in three-dimensions, there was no evaluation of the functional

connections and functional networks that may have formed within the hydrogel. To accomplish this, primary neurons should be isolated and cultured within the hydrogels. Following 2-3 weeks in culture cells can be evaluated for expression of markers such synaptophysin (213) and evaluate GABA activation triggers (214). Further, using three-dimensional multi-electrode arrays, it is possible to evaluate the ability of these isolated cells to excite spontaneously. By evaluating these metrics, further insight into the ability of the CNS-ECM hydrogel materials to impact neural repair will be developed.

4.0 ALTERNATIVE MACROPHAGE POLARIZATION AND ENHANCED NEURAL STEM CELL REGENERATIVE POTENTIAL WITH BIOSCAFFOLDS DERIVED FROM CENTRAL NERVOUS SYSTEM EXTRACELLULAR MATRIX

4.1 INTRODUCTION

The human central nervous system (CNS) has a limited capacity for repair (215), and the majority of severe traumatic CNS injuries yield neurologic deficits that lead to irrecoverable impairments. While researchers have increased their understanding of the mechanisms behind CNS injury, clinical therapeutics that significantly improve neurologic impairments have not been developed (216). Recent efforts have focused on the neural stem cell (NSC) and macrophage response as possible therapeutics capable of shifting the natural healing response towards one associated with tissue reconstruction.

Following injury neural stem cells (NSCs) are pathotrophic (217) and migrate to the site of CNS trauma. NSCs can secrete neurotrophic factors that include nerve growth factor, brain-derived neurotrophic factor, NT-3, and glial-derived neurotrophic factor, which may play important roles in wound resolution and mediating repair following injury (218). NSCs also have been shown to play roles in remyelination (219) and may undergo neuro- and oligogenesis (220) under appropriate microenvironmental conditions. Macrophage response following

traumatic CNS injuries can also mediate neural reconstruction and as such should be considered when developing neural reconstructive therapeutics.

Macrophage response to traumatic CNS injury has recently been highlighted as a dichotomy of behaviors that can contribute to wound resolution and tissue repair (78) or contribute to a pro-inflammatory environment (221). Macrophages are highly plastic cells that respond to their microenvironmental signals along a response spectrum that ranges from the classic, M1 response, to the alternatively activated, M2 response (62, 63). M1 macrophages are polarized via LPS/IFN γ and initiate pro-inflammatory (67-69) responses and are responsible for pathogen resistance (70, 71). M2 macrophages, polarized via IL-4, IL-10, IL-13 or IL-1R signals, promote Th2 responses, provide parasite resistance, mediate immunoregulation, participate in IL-10 secretion, and deposit new ECM for functional tissue remodeling (20, 72). Following spinal cord injury (SCI) macrophages and microglia polarize towards the M1 phenotype and greatly contribute to secondary injury. Recently, it has been demonstrated that their contributions can shift towards the M2 phenotype and contribute to tissue repair and wound resolution if provided with a permissive microenvironment (60). A regenerative medicine therapeutic that can enhance the reconstructive potential of stem cells, as well as create a permissive environment for alternate activation of macrophages would be a significant advancement in therapies for traumatic CNS injuries.

Bioscaffolds derived from the ECM of tissues and organs through decellularization have promoted site specific constructive tissue remodeling in several preclinical studies and clinical applications, including those of the peripheral nerve (159), dura matter (127), esophagus (95, 96), lower urinary tract (97, 98), muscle and tendon (99, 100), and myocardium (101, 102), among others. The success of these scaffolds is due, in part, to the ability to increase

regenerative potential and recruitment of stem cells (99, 110-112) and the modulation of the innate immune response towards an alternatively activated, pro-regenerative phenotype (73, 74, 125, 222). Furthermore, bioscaffolds derived from homeostatic tissue homologous to the wound site enhance maintenance of site appropriate cellular phenotypes (131, 134, 136, 186). Recently ECM bioscaffolds have been derived from the CNS (161-163, 182). A bioscaffold derived from homeostatic CNS tissue may contain site-appropriate molecular signals necessary for tissue reconstruction. Currently, these scaffolds have not been evaluated for their ability to enhance the reconstructive potential of clinically relevant human cell types. The objectives of this work were to evaluate the ability of CNS-ECM scaffolds to (1) enhance human spinal cord stem cell's (SPC) regenerative potential and (2) create a permissive microenvironment that promotes alternative, pro-regenerative, macrophage polarization. The present study is focused on the mitogenic, chemotactic, and differentiation properties of CNS-ECM bioscaffolds in comparison to a non-CNS-ECM scaffold, urinary bladder matrix (UBM).

4.2 MATERIALS AND METHODS

4.2.1 UBM-ECM and CNS-ECM Scaffold Preparation

4.2.1.1 UBM-ECM

UBM-ECM was prepared as previously described. In brief, porcine urinary bladders were harvested from market weight (240–260 lbs) pigs immediately following euthanasia. UBM-ECM was prepared from the bladders using previously described methods (166, 223, 224). The connective and adipose tissue were trimmed and the tunica serosa, tunica submucosa, and

majority of the tunica muscularis mucosa were mechanically delaminated, leaving the basement membrane and tunica propria intact. Luminal urothelial cells were dissociated from the basement membrane by soaking the UBM-ECM in deionized water. The UBM-ECM was decellularized using a 0.1% peracetic acid/4% ethanol treatment with mechanical shaking at 300RPM. The UBM-ECM was then subjected to a series of phosphate buffered saline and deionized water rinses to ensure complete peracetic acid removal.

4.2.1.2 CNS-ECM

Immediately following euthanasia, whole brain and spinal cords were frozen at -80°C until use. Whole brains with dura matter removed were sliced into 1cm³ cubes before placement in decellularization agents. Whole spinal cords with dura removed were longitudinally quartered and cut into less than 3cm long segments. CNS tissue was mechanically shaken (spinal cord tissue at 200 rpm; brain tissue at 120 rpm unless otherwise stated) in the following decellularization agents: deionized water (16 h at 4°C; 60 rpm), 0.02% trypsin / 0.05% EDTA (60 min at 37°C; 60RPM; Invitrogen Corp., Carlsbad, CA, USA), 3.0% Triton X-100 (60 min; Sigma-Aldrich Corp., St. Louis, MO, USA), 1.0 M sucrose (15 min; Fisher Scientific, Pittsburgh, PA, USA), water (15 min), 4.0% deoxycholate (60 min; Sigma), 0.1% peracetic acid (Rochester Midland Corp., Rochester, NY, USA) in 4.0% ethanol (v/v; 120 min), PBS (15 min; Fisher), deionized water (twice for 15 min each rinse), and PBS (15 min). Each bath was followed by rinsing the remaining tissue through a strainer with deionized water. Decellularized B-ECM and SC-ECM were lyophilized and stored dry until use.

4.2.2 ECM Digestion and Solubilization

Lyophilized and mechanically powdered B-ECM (20 mesh), SC-ECM (20 mesh or hand cut), and UBM-ECM (20 mesh or hand cut; 400-1000 μ m largest particle dimension as measured by mesh diameter or ruler) were separately placed into a 0.01 N HCl solution containing 1mg/mL pepsin (Sigma) at a concentration of 10 mg ECM/mL and stirred at room temperature for 48h as previously described (180). After 48h, B-ECM, SC-ECM, and UBM-ECM were completely digested and formed a viscous pre-gel solution (pH~2). The pre-gel ECM solution was brought to pH 7.4 using 0.01N NaOH and diluted to the desired volume/salt concentration using 10x and 1 x PBS. Pepsin is irreversibly inactivated at pH above 7.5 (198).

4.2.3 Human Macrophage Description

Human peripheral blood monocytes were isolated by negative selection (CD3, CD7, CD16, CD19, CD56, CD123 and Glycophorin A, Monocyte Isolation Kit II (Macs, Miltenyi Biotec)) from human blood obtained at a local blood bank. Freshly isolated monocytes matured into macrophages (M Φ) over 7 days in RPMI media supplemented with 20% fetal calf serum and 100ng/mL macrophage colony stimulating factor (M-CSF). To drive macrophages to the M1 phenotype, macrophages were placed in RPMI media supplemented with 5% fetal calf serum and 100ng/mL LPS (Sigma I3650) and 20ng/ml IFN γ (Sigma, I3275) for 24 hours. To drive to an M2 phenotype macrophages were placed in RPMI media supplemented with 5% fetal calf serum and 20ng/mL IL-4 (PeproTech, 200-04) for 24 hours.

4.2.3.1 Human Macrophage Polarization with ECM Bioscaffolds

Following monocyte maturation in MCSF, 250,000 naïve (MΦ) macrophages per well (24 well plate) were cultured in media supplemented with CNS-ECM pre-gel digests at concentrations ranging from 50µg/mL to 1mg/mL for 48 hours. Cells were fixed with 2% paraformaldehyde and stained for M1 marker CCR7 staining and M2 marker CD206 to determine the polarization state induced by ECM scaffolds.

4.2.3.2 Human Macrophage Chemotaxis

Chemotactic effects of CNS-ECM bioscaffolds were determined by transmembrane migration using blind-well chambers and polycarbonate filters with 8.0 µm pore size (AP48; Neuro Probe Inc., Gaithersburg, MD, USA). Filters were coated in 5 µg/cm² laminin (Sigma) for 30 min and allowed to dry completely. Wells were loaded with 50,000 cells per well. After 4hours in RPMI the filter was removed, the upper (non-migratory) surface scraped, and the lower (migratory) surface fixed with methanol, stained with DAPI, imaged, and quantified.

4.2.4 Mouse Macrophage Description

Mouse macrophages were isolated through the following established protocol as it has been used as a reliable and reproducible model for macrophage isolation. In brief, mouse bone marrow was isolated and cultured with L929 fibroblast enriched MCSF media to mature myeloid precursor cells to mouse macrophages (225-227). Before use, macrophage phenotype was confirmed with F4/80 (90% F4/80 positive), a standard mouse pan macrophage marker.

4.2.4.1 Mouse Bone Isolation

Mice were euthanized with rapid cervical dislocation and sprayed with 70% ethanol. A shallow incision was made on the leg severing the skin and exposing musculoskeletal tissue. Quadriceps were clamped for hip dislocation and distal femur was exposed. Mouse foot was then articulated to expose the tibia, excess tissue removed from the bone, and was placed on ice before bone marrow removal.

4.2.4.2 Mouse Macrophage Culture

Mouse macrophage complete media was added to a sterile petri dish and using 30 gauge needles the bone marrow rinsed out into sterile media until bone appears white. Bone marrow aspirates were then centrifuged for 5 minutes at 1500 RPM and resuspended in 10mL of fresh mouse macrophage complete media. Bone marrow aspirates were triturated to mix the pellet and strained through a 100 μ m cell strainer and counted using a hemacytometer. Cells were then placed in a 12 or 6 well plate, with 1 or 2 mL of cells per well, respectively, and incubated for 18 hours at 37°C. After 18 hours, an additional 1mL of macrophage complete media was added, and changed every 48 hours thereafter.

4.2.4.3 Mouse Macrophage Polarization and Treatment with ECM Conditioned Media

Seven days following bone marrow harvest and cell isolation, cells were treated with polarizing cytokines or media conditioned with UBM-ECM or CNS-ECMs (200 μ g/mL). M1 macrophages were polarized with 20ng/mL IFN γ and 100ng/mL LPS (Miltenyi Biotec). M2 macrophages were polarized with 20ng/mL IL-4 (Miltenyi Biotec).

4.2.4.4 Mouse Macrophage Immunolabeling

Following 18 hours in cytokine polarization or ECM conditioned media, media was aspirated and replaced with 2% paraformaldehyde for 20 minutes and rinsed thoroughly with 1xPBS. Cells were then blocked in 0.01% Tween-20, 0.01% Triton X-100, 2% Bovine Serum Albumin, and 2% Horse serum for 1 hour at room temperature. Primary antibody incubation overnight at 4°C included, F4/80 (Abcam, AB6640) (rat anti-mouse; 1:200), iNOS (Abcam #ab3523) (rabbit anti-mouse; 1:100), Fizz1 (Peprotech, #500-P214) (rabbit anti-mouse; 1:200). Antibodies were chosen based on a literature search to determine markers that denote an M1 or M2 macrophage phenotype. Secondary antibody incubation for 45 minutes at room temperature included Alexa Fluor 488 (donkey anti- rat or rabbit; 1:200). Nuclei were counterstained with 500mM DAPI. All wells were rinsed thoroughly with 1xPBS between staining solutions.

4.2.5 Spinal Cord Stem Cell (SPC) Description

Spinal cord stem cells were a kind gift from Dr. Jack Price at King's College London and isolated with the following protocol (228). In brief 10 week old human spinal cord from the cervical region was finely chopped with a scalpel in 0.25% trypsin in DMEM:F12 at 37°C followed by 0.25mg/mL trypsin soybean inhibitor (Sigma). Cells were conditionally immortalized using a retroviral system with the cMYC-ER^{TAM} gene (229). Individual colonies were passaged using glass cloning cylinders (Sigma) and SPC-01 cell population was selected following over 20 uniform doublings. Continuous cell culture was completed as previously described (228). In brief, cells were grown on laminin-coated (Sigma-Aldrich), NUNC treated, tissue-culture flasks in DMEM/F12 supplemented with bFGF (10 ng/ml; PeproTech), EGF (20 ng/ml; PeproTech), human serum albumin (0.03%; Baxter Healthcare), L-glutamine (2 mM;

Gibco); human transferrin (100 µg/ml; Sigma), putrescine dihydrochloride (16.2 µg/ml; Sigma) , human insulin (5 µg/ml; Fisher Scientific), progesterone (60 ng/ml; Sigma), sodium selenite (40 ng/ml; Sigma), 4-OHT (100 nM; Sigma), and Pen/Strep (1%; Fisher Scientific) . Cell differentiation was triggered by the removal of growth factors and 4-OHT from the media.

4.2.5.1 Spinal Cord Stem Cell Chemotaxis

The migration response of SPCs to CNS-ECM degradation products was quantitatively evaluated with the Neuroprobe 48-well micro-chemotaxis chamber (Neuro Probe Inc. Gaithersburg, MD). An 8 µm pore polycarbonate filter was coated with 20 µg/mL laminin for 1 hour and dried completely. B-ECM, SC-ECM, or UBM-ECM conditioned media was evaluated at concentrations of 50, 100, 250, 500 and 1000 µg/ml. SPCs were added to the chamber at concentrations of 50,000 cells per well and incubated for 4 hours at 37°C. After 4 hours filters were fixed with methanol and stained with DAPI. Experimental conditions were evaluated in triplicate three times.

4.2.5.2 Spinal Cord Stem Cell Proliferation.

SPC proliferation was determined through methods previously used to evaluate ECM products on perivascular stem cells (110). The well-established 5-bromo-2'-deoxyuridine (BrdU) colorimetric assay (Roche, Nutley, NJ) was used. Cells were plated at 5,000 cells/well in a 96 well plate with CNS-ECM pre-gel digest for 48hr. Following this 48hr period, BrdU (10mM) was placed into the media to label proliferating cells. Plates were then fixed and manufacturer's instructions followed. Relative proliferation was quantified at 370nm and 492nm in a molecular spectrophotometer. The assay was performed in triplicate for a total of three times.

4.2.5.3 Spinal Cord Stem Cell Differentiation

Undifferentiated SPCs were plated in laminin coated wells at the following concentration at 25,000 cells per well in a 48 well plate (230). Verification of stemness was completed before differentiation assays using Nestin and Sox2 (Figure 20). The cells were allowed to attach to the wells for 24 hours. Media supplemented with CNS-ECM or UBM-ECM digestion products was then replaced every two days and the cells fixed in 2% paraformaldehyde (230). Cells were immunolabeled for β 3-tubulin (1:200; Thermo-Scientific; MA1-19187) and GFAP (1:500; Abcam; 53554) to quantify neuronal and astrocyte differentiation.

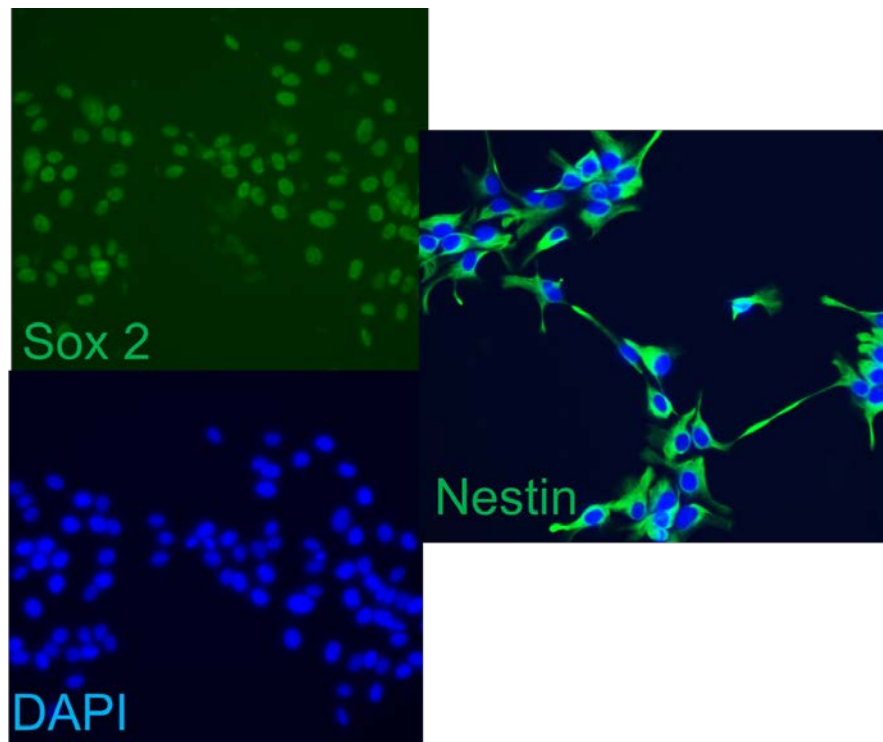


Figure 20. Prior to differentiation assays, SPCs were examined for their expression of neural stem cell markers Sox 2 and Nestin. Transcription factor Sox 2 colocalizes with the nuclei of the SPC cells, while Nestin can be seen as an intermediate filament.

4.2.6 Cytocompatibility Analysis

ECM cytocompatibility was evaluated using isolated human macrophages using an established live/dead assay. In brief, 100,000 cells per well in a 48 well plate were cultured for 24 hours, at which time the media was replaced with ECM supplemented media at a concentration of 500 μg ECM/mL. Cytotoxicity was evaluated for macrophages cultured with and without cytokines, and with ECM supplemented media. Following 24 hours in culture with ECM, the medium was removed and 4 μM calcein-AM and 4 μM ethidium homodimer-1 was added to each well to evaluate cytotoxicity. Live cells that hydrolyze membrane-permeable calcein-AM, but not ethidium homodimer-1, fluoresce in green and dead cells that bind and activate ethidium homodimer-1, but not calcein-AM, fluoresce in red.

4.2.7 Statistical Analysis

A one-way ANOVA was used for all comparisons ($p < 0.05$) with a Tukey post-hoc for group comparisons. All statistical analysis methods used SPSS Statistical Analysis Software (SPSS, IBM, Chicago, IL, USA).

4.3 RESULTS

4.3.1 Cellular Cytocompatibility

Live/dead assay assessed B-ECM, SC-ECM, UBM-ECM, and pepsin with M0, M1, or M2 macrophages. No scaffold exhibited a cytotoxic effect towards human macrophages, and there was an approximately 98% or greater viability for human macrophages in the presence of ECM bioscaffolds (Figure 21).

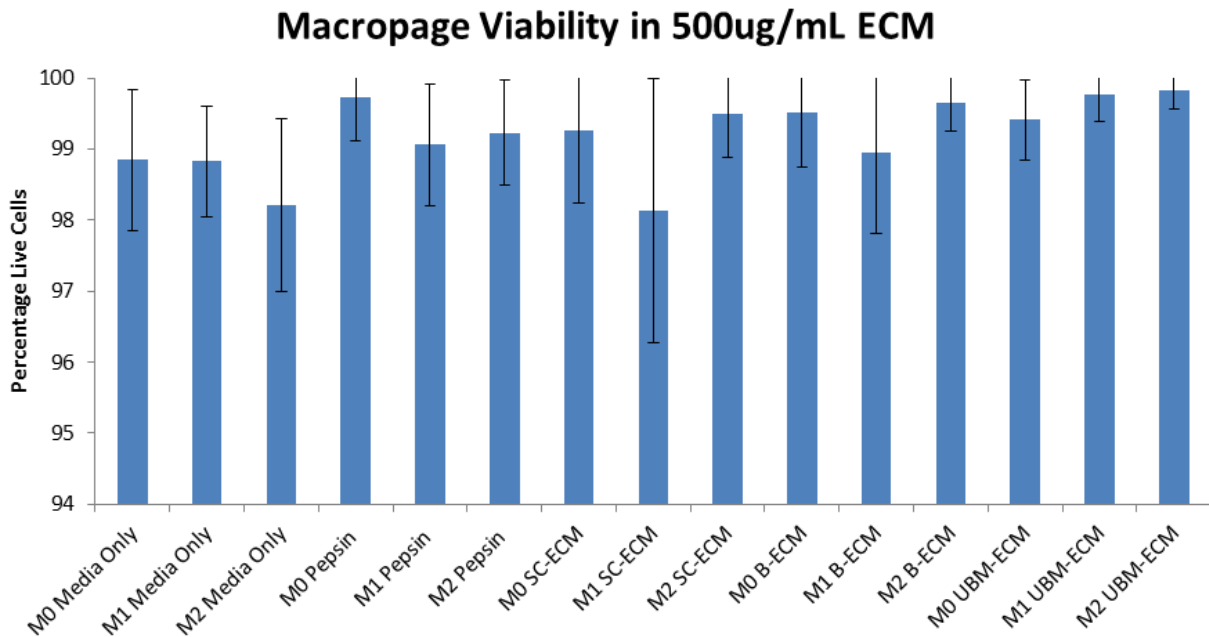


Figure 21. ECM bioscaffolds are not cytotoxic to human monocyte derived macrophages.

4.3.2 Macrophage Chemotaxis

Table 3 summarizes the macrophage chemotaxis data towards each of the ECM scaffolds. Only UBM-ECM was the only ECM scaffold to contain degradation products capable of promoting

macrophage migration. Naïve macrophages do not show significantly increased migration as compared to the pepsin digestion control (1.19 ± 0.14 and 1.24 ± 0.13 fold increase for 50 and 500 μg , respectively). M1 macrophages do not show significantly increased migration as compared to the pepsin digestion control (1.26 ± 0.28 and 1.14 ± 0.17 fold increase for 50 and 500 μg , respectively). M2 macrophages promoted a significant increase in migration ($p < 0.05$) as compared to the pepsin digestion control (2.91 ± 0.52 and 2.56 ± 0.40 fold increase for 50 and 500 μg , respectively) (Figure 22).

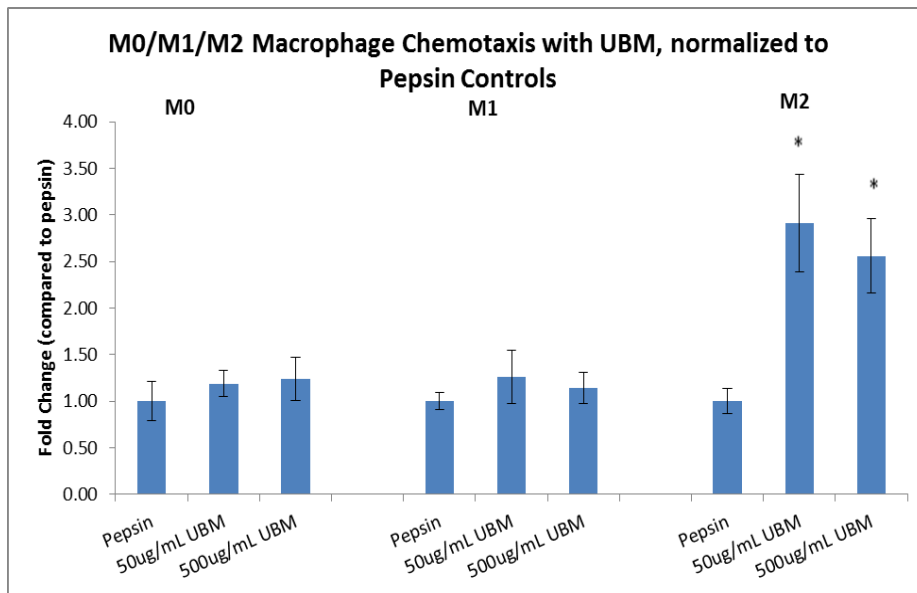


Figure 22. Only M2 macrophages increase their chemotactic ability in response to UBM-ECM digestion products, suggesting an additional mechanism for how ECM scaffolds polarize macrophages at an injury site.

*** indicates a significant difference ($p < 0.05$) compared to pepsin digestion buffer control.**

Table 3. Summary of data for macrophage chemotaxis in response to SC-ECM, B-ECM, and UBM-ECM. Only UBM-ECM significantly increase migration. Data expressed as fold change of cells migrated normalized to the pepsin digestion buffer.

Mac. Polarization	ECM Conc.	Avg SC-ECM	St Dev SC-ECM	Avg B-ECM	St Dev B-ECM	Avg UBM-ECM	St Dev UBM-ECM
M0	50µg/mL	1.07	0.54	2.10	1.36	1.19	0.14
M0	500µg/mL	1.40	0.68	1.40	0.98	1.24	0.23
M1	50µg/mL	0.80	0.11	1.47	0.65	1.26	0.28
M1	500µg/mL	1.03	0.31	3.30	2.27	1.14	0.17
M2	50µg/mL	1.04	0.59	1.47	0.48	2.91	0.52
M2	500µg/mL	1.34	1.03	1.72	0.75	2.56	0.40

4.3.3 Macrophage Polarization

Human monocyte derived macrophages were first evaluated for their ability to be polarized with CNS and UBM-ECMs. These preliminary studies showed high variability and monocytes were subsequently used. The monocytes were manipulated less prior to use, and this was hypothesized to decrease variability in cell surface marker expression (231). The polarization effect found with human monocytes showed similar trends to that shown in-vivo with UBM-ECM, however with CNS-ECMs the variability was still increased, and a non-variable mouse model was then evaluated.

4.3.3.1 Human Macrophage Polarization

Moderate M1 polarization in response to CNS-ECM scaffolds with human monocyte derived macrophages, however this response was not significantly greater than the pepsin digestion control. Both B-ECM and SC-ECM showed two to three-fold increase in M1 macrophage marker CCR7 expression, however the variability was too high in these cells to

draw significant conclusions. UBM-ECM did not show significantly increased M1 expression at any concentration (Figure 23).

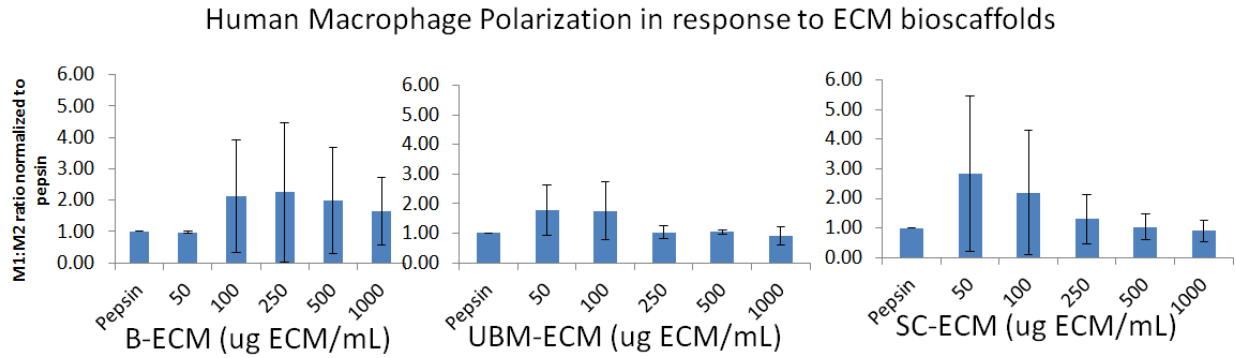


Figure 23. Moderate M1 responses to B-ECM and SC-ECM after 48 hours in polarization.

4.3.3.2 Human Monocyte Polarization

The variability in polarization in response to all ECM conditioned medias was again increased (Figure 24). Macrophages treated with UBM-ECM, however, showed the lowest variability among the ECM treated cells. Further, the trend for these cells in response to UBM-ECM treatment was towards an M2 phenotype as indicated by all UBM-ECM treated groups having averages below the pepsin digestion buffer control. In response to the CNS-ECMs, there was a trend towards an M1 phenotype, however the cell surface marker expression was highly variable within each treatment group.

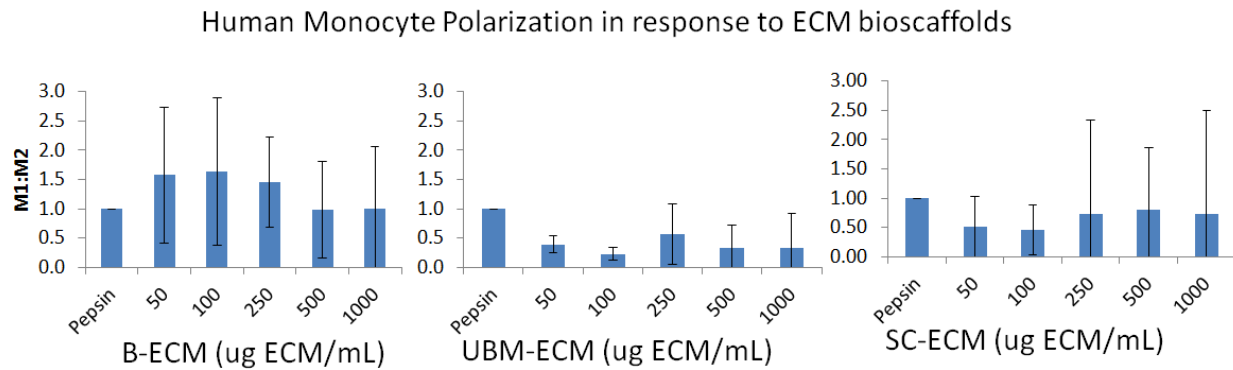


Figure 24. Human Monocytes show a decreased M1 response as anticipated with UBM-ECM, however high variability makes interpretation difficult.

4.3.3.3 Mouse Macrophage Polarization

Mouse macrophage polarization was assessed using immunofluorescence. Fizz1 is an M2 marker and iNOS is an M1 marker. In this assay, a control polarization plate (Figure 25) was used to verify proper staining. Once verified, the ECM test treatments were assessed. In this assay, we saw consistent positive upregulation of Fizz1 expression for all ECM scaffolds, but not for pepsin (Figure 26). B-ECM has the lowest percentage of Fizz1 positive macrophages, with only 36.70 ± 1.08 percent of the cells expressing Fizz 1 (Figure 27). SC-ECM, while containing the highest percentage of Fizz 1 expressing cells (59.89 ± 19.9 percent), is the most variable among the ECM treated groups. UBM-ECM, in comparison, polarizes almost 50% of the cells (44.88 ± 2.10 percent) and maintains low variability. This data suggests that there may be some mechanism conserved between the ECM of different tissues and organs capable of modulating macrophage behavior.

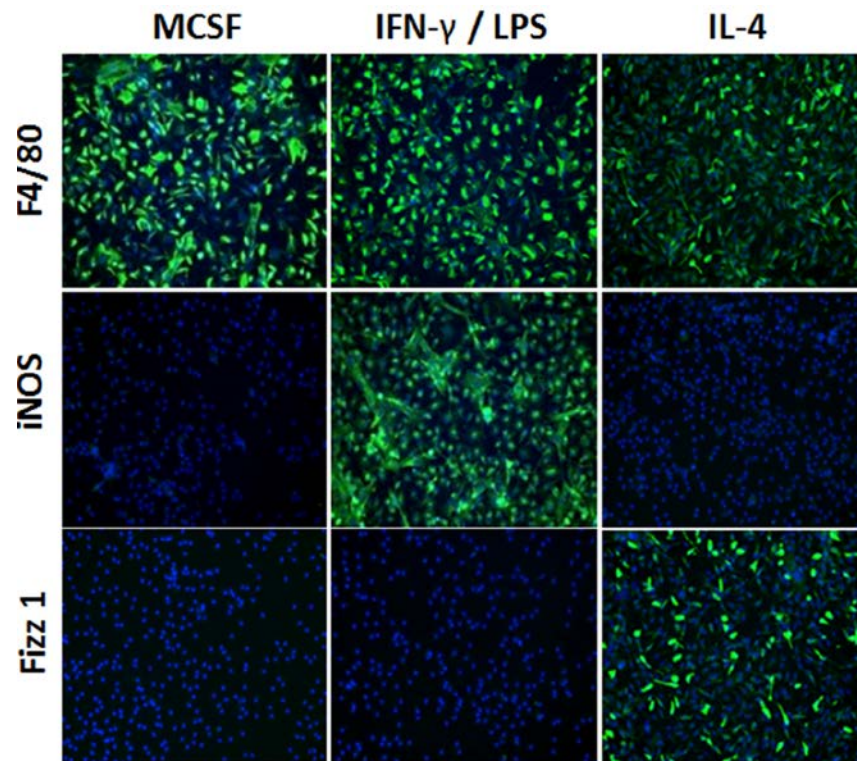


Figure 25. Control plate for mouse macrophage staining shows positive M1 iNOS marker when macrophages are polarized with IFN γ /LPS and Fizz1 when polarized with IL-4.

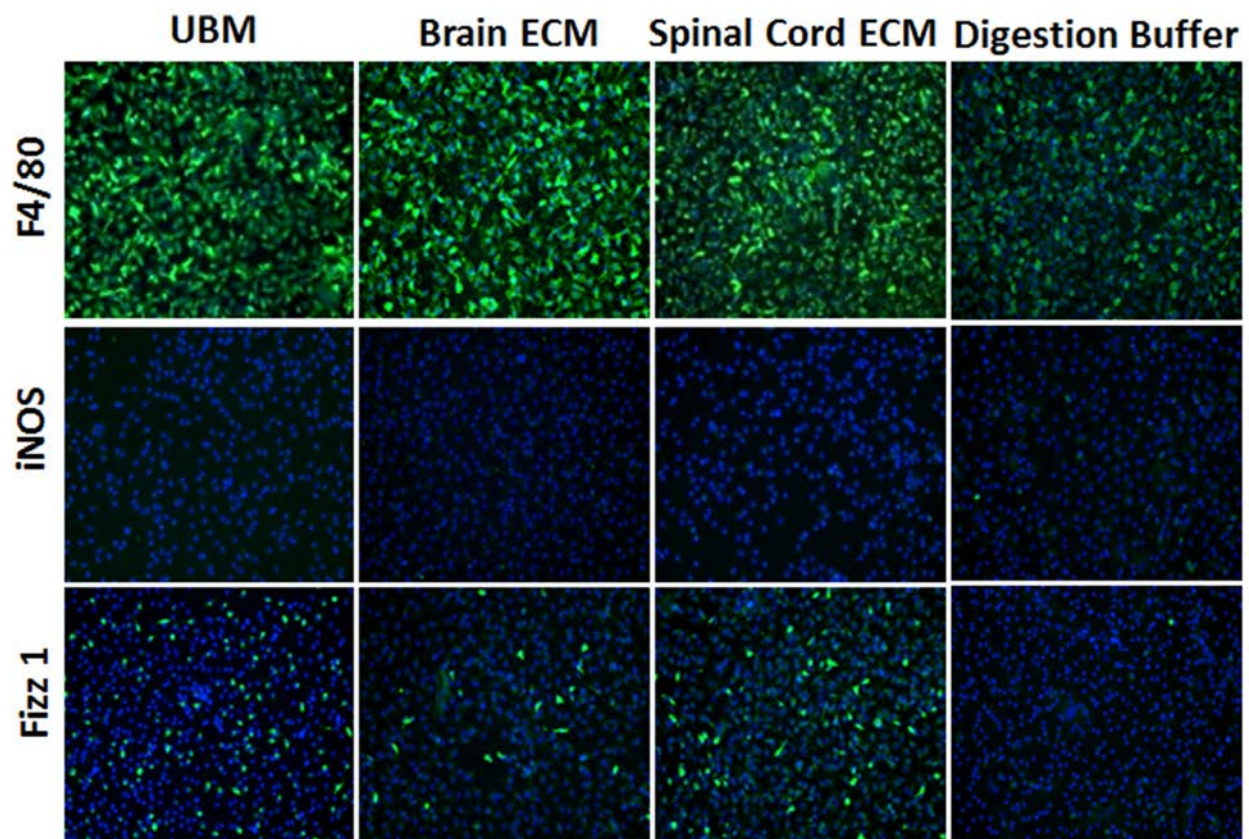


Figure 26. All ECM scaffolds exhibit M2 macrophage activation (via Fizz1 expression), however expression appears to be higher in UBM-ECM and SC-ECM as compared to B-ECM. The digestion buffer does not show iNOS or Fizz1 expression.

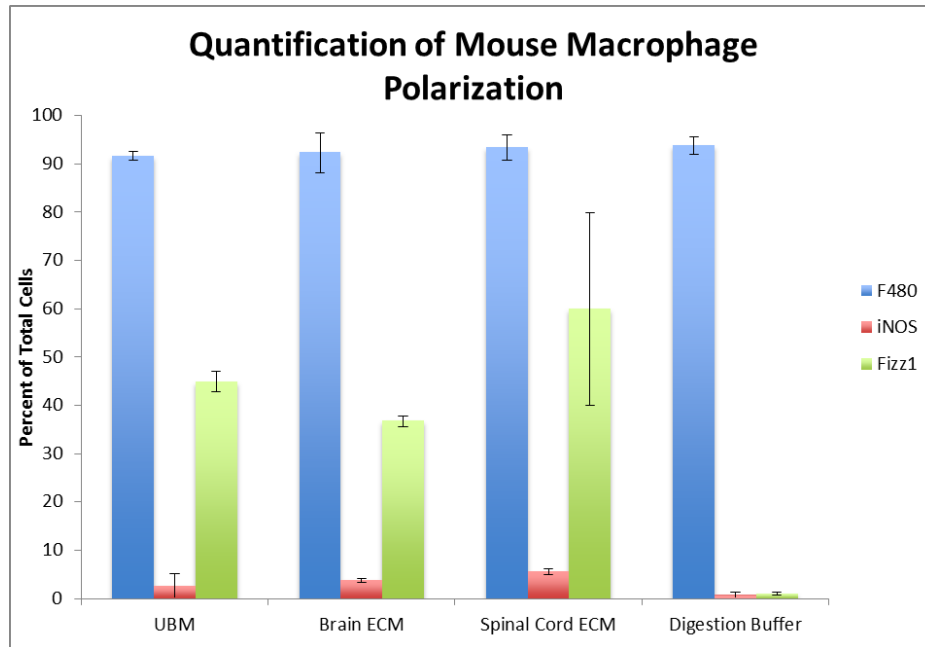


Figure 27. Quantification of mouse macrophage polarization shows that all ECM bioscaffolds promote an M2 polarization through an increase in Fizz1 expression with minimal M1 (iNOS) activation. The digestion buffer control does not show an increase in either iNOS or Fizz 1.

4.3.4 SPC Behavioral Response to ECM Bioscaffolds

4.3.4.1 Chemotaxis

SPCs increase chemotactic behavior by two-fold in response to 100 and 250 μ g/mL SC-ECM (Figure 28). This is markedly different from both B-ECM and UBM-ECM where chemotaxis is inhibited with increasing concentration reaching approximately a two-fold decrease in chemotaxis. It is possible that this is a site specific response of these spinal cord stem cells towards SC-ECM (Figure 28).

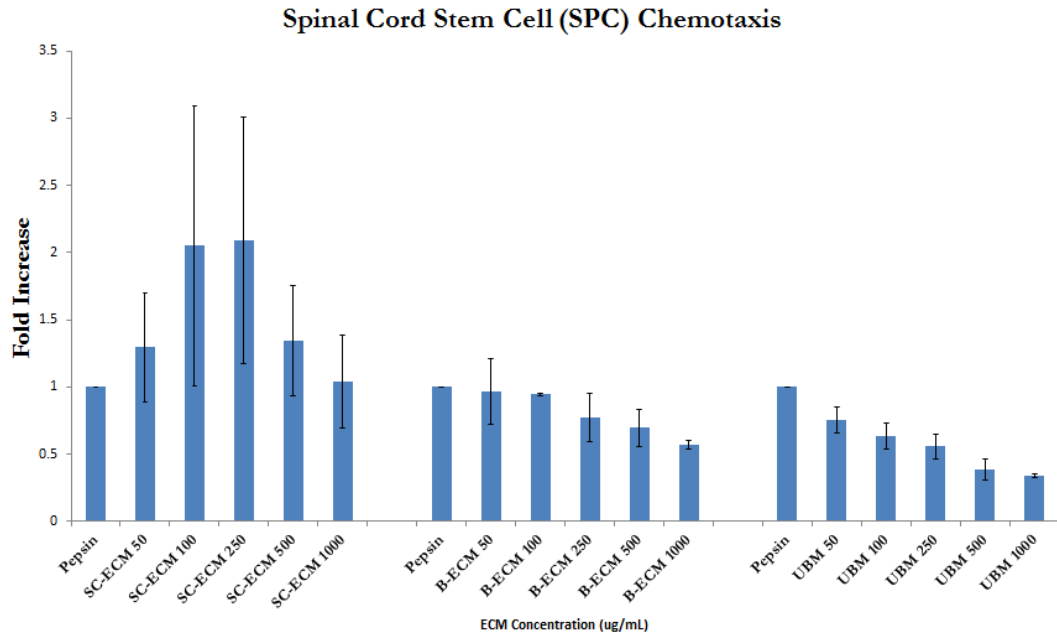


Figure 28. SPCs respond to SC-ECM with an increase in migration, whereas to B-ECM and UBM-ECM, the SPCs exhibit a dose dependent decrease in migration.

4.3.4.2 Proliferation

SPCs exhibit differential mitogenic potential in response to CNS-ECMs and UBM-ECM as shown through the BrdU proliferation assay (Figure 29). In response to UBM-ECM, mitogenesis not differ in comparison to the pepsin buffer. However, there was a unique response to the CNS-ECM scaffolds. In response to high concentrations of SC-ECM SPC mitogenesis decreases back to basal media levels and is significantly less than the pepsin digestion buffer control ($p < 0.05$). In response to low concentrations of B-ECM mitogenesis has a significant 1.3 fold increase ($p < 0.05$) in comparison to the basal media and pepsin controls. These results speak to the compositional and bioactive differences within the unique CNS-ECM scaffolds.

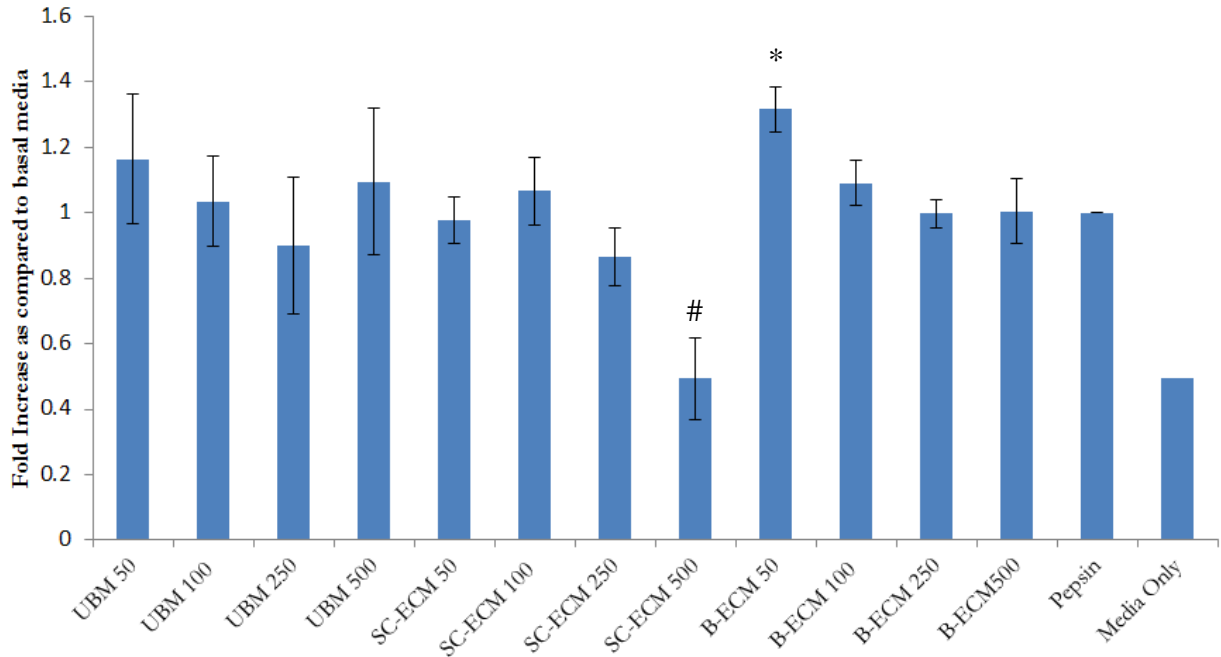


Figure 29. SPCs exhibit differential effects in mitogenesis following exposure to ECM scaffolds. In response to high levels of SC-ECM, mitogenesis is maintained at basal levels, whereas in response to high levels of B-ECM, mitogenesis is increased. * indicates a significant increase in comparison to the pepsin and basal media controls. # indicates a significant decrease in comparison to the pepsin digestion buffer control.

4.3.4.3 Differentiation

Following 21 days in culture with media conditioned with 250 μ g ECM/mL SPCs were stained for β 3-tubulin denoting neuronal differentiation or GFAP denoting astrocyte differentiation. While astrocyte differentiation remains constant between the CNS-ECM scaffolds, pepsin buffer, and the basal differentiation media (growth media with growth factors and 4-OHT removed), it was significantly decreased in the UBM-ECM group. Also, UBM-ECM promoted significantly increased neural differentiation, where the CNS-ECM scaffolds did not (Figure 30).

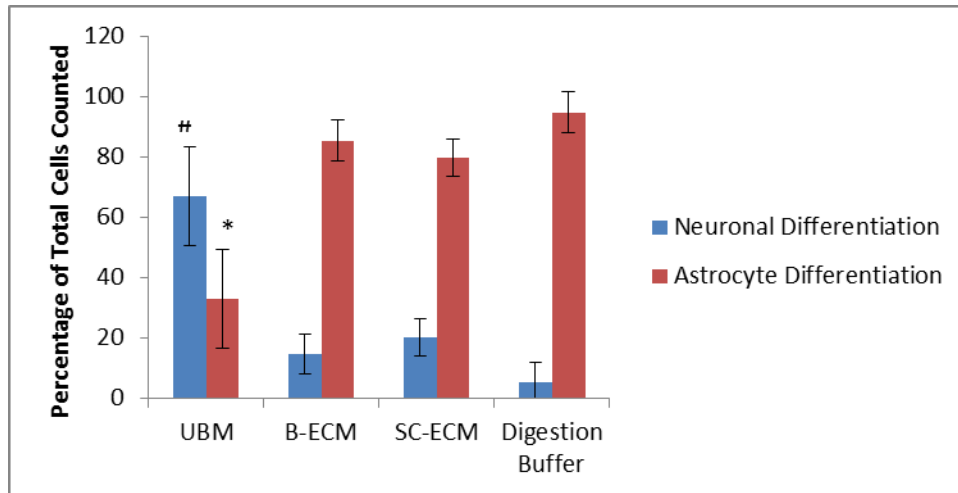


Figure 30. Following 21 days in culture with media conditioned with 250ug ECM/mL SPCs were stained for B3-tubulin denoting neuronal differentiation or GFAP denoting astroglial differentiation. UBM-ECM had significantly increased neuronal differentiation (# = p <0.05) and significantly decreased astrocyte differentiation (* = p<0.05) when compared to all other groups. ECM conditioned media was at a concentration of 250 g ECM/mg.

Spinal Cord ECM and pepsin, in rare occasions, produced GFAP+ cell populations with morphologies similar to reactive astrocytes (Figure 31) (232). The hypertrophy was also similar to astrocytes commonly found after SCI (16).

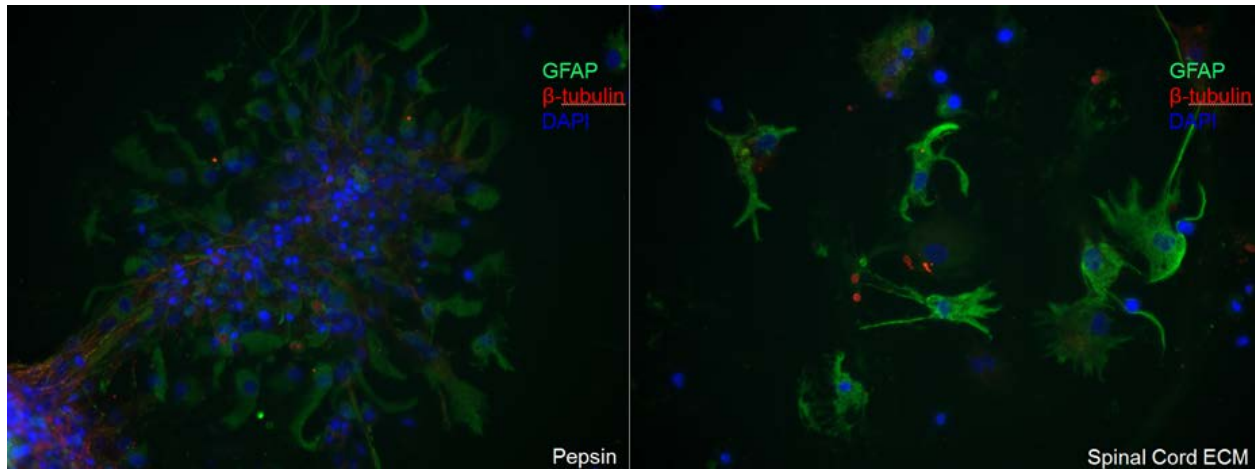


Figure 31. Pepsin and SC-ECM occasionally produced GFAP differentiated cells with morphology commonly expressed by reactive astrocytes.

4.4 DISCUSSION

ECM bioscaffolds have been shown to promote functional constructive remodeling in numerous preclinical and clinical applications. While several mechanisms mediate ECM bioscaffold tissue reconstruction, modulation of the endogenous stem cell response and polarizing the innate immune system towards a pro-reconstructive phenotype are paramount. These mechanisms, among others, will be crucial for ECM bioscaffolds to mediate repair following traumatic CNS injury.

Endogenous neural stem cell populations have been demonstrated in both the brain (233) and the spinal cord (234) and are known to contribute to population maintenance for both neural and glial cells (234). The regenerative potential of such cells is not currently harnessed to produce significant behavioral and cognitive recovery following injury. Regenerative

therapeutics, such as ECM bioscaffolds, may harness the regenerative potential of such neural stem cells to promote neural recovery. In this work, a spinal cord derived neural stem cell was evaluated in terms of mitogenesis, chemotaxis, and differentiation for CNS-ECMs and compared with properties of a non-CNS ECM, UBM-ECM. Previous research demonstrated increased mitogenesis and chemotaxis of stem cells in response to ECMs (110), as well as recruitment and ultimately differentiation of multiple stem cell populations (99, 111, 112). These results of this study confirm that ECM bioscaffolds may be able to not only recruit stem cells, but also to have mitogenic and differentiation capacities that can contribute to constructive remodeling following CNS injury. The SPCs in this study, demonstrated an increased chemotaxis towards an ECM derived from the spinal cord. This may suggest that SC-ECM retains specific neurotrophic factors following decellularization that these cells recognize as behavior altering molecules. The decrease in mitogenesis with increasing concentration suggests that the cells may be undergoing a change in their molecular machinery towards differentiation.

As stem cells begin differentiation, their rate of proliferation can decrease significantly (228). The differentiation studies conducted in this work may add to the understanding of bioscaffold induced innervation. CNS-ECM scaffolds promote an astroglial differentiation as demonstrated through GFAP staining, while UBM-ECM promoted neuronal differentiation. UBM-ECM and other bioscaffolds have induced innervation into newly reconstructed tissues, which may suggest that the highly innervated ECM of the bladder retains some component of the peripheral neural microenvironmental niche following decellularization. The work completed in this study suggests that ECM bioscaffolds may have the capacity to enhance the minimal regeneration found following CNS injury and promote tissue reconstruction. Alternatively activated macrophages also have been shown to increase the regenerative potential of neural

stem cells in addition to providing the necessary immunomodulatory milieu for wound resolution and tissue repair.

This work evaluated the ability of CNS-ECM bioscaffolds to polarize human macrophages towards an alternatively activated state. In-vitro studies of primary human macrophages can be highly variable, in part, due to high donor variation. Variance may be increased as the monocytes are responding to both the tissue culture plastic (235) and the maturation cytokines that are known to alter macrophages from their M0 state (236). The present study, then, evaluated human monocytes. The decrease in cell culture manipulation by using monocytes immediately after harvest can significantly reduce variation. The polarization studies demonstrated effects of UBM-ECM scaffolds similar to the ratios seen in-vivo that are known to be a determinant for ECM mediated constructive remodeling. However, for CNS-ECM scaffolds the variance remained. To further understand the ability of CNS-ECM scaffolds to modulate macrophage phenotype in-vitro, we then used a non-variable mouse macrophage model. This model demonstrated that, like UBM-ECM, the CNS-ECM scaffolds retain factors that can contribute to alternative macrophage activation and may possibly aid in CNS tissue reconstruction. This study also furthered the understanding of macrophage response to ECM scaffolds through looking at their chemotactic effect.

There is debate in the literature as to whether monocyte derived macrophages arrive to the site of injury in a pre-polarized state, or polarize upon interacting with the local microenvironment of a wound site. While in reality it is likely a combination of the two theories. Following SCI, a subset of the monocyte population was shown to take a unique migratory route to the site of injury and subsequently was alternatively activated (237). In the work of this manuscript, only M2 macrophages were shown to migrate towards UBM-ECM bioscaffolds.

This is an interesting concept as in-vivo, using an elegant radioactive tracking method for ECM degradation, ECM bioscaffolds were shown to begin degradation within the first 60 minutes and degradation products were found in the blood stream. This study may have demonstrated a unique method for an ECM mediated alternative macrophage response through recruitment of pre-polarized M2 cells from distal locations to the injury site. Further research should evaluate peripheral blood macrophages and monocytes following ECM implantation a for M1 and M2 polarization markers that could shed light onto this mechanisms of innate immune system modulation.

4.5 CONCLUSION

CNS-ECM bioscaffolds retain a unique molecular composition that alters the spinal cord stem cell differentiation, mitogenic, and chemotactic responses. The neuronal differentiation potential of UBM-ECM may demonstrate a mechanism for innervation found following bioscaffold remodeling. In addition, this work demonstrated an in-vitro model of human macrophage and monocyte polarization that matches in-vivo descriptions of the innate immune response towards ECM bioscaffolds. The research here also demonstrated novel chemotactic responses of M2 macrophages towards UBM-ECM, which may aid in the understanding of ECM bioscaffold induced mediation of the innate immune response. In conclusion, this study furthers the understanding of ECM induced constructive remodeling and sets the foundation for future studies evaluating combinatory therapies that involve ECM scaffolds as cell or pharmaceutical delivery vehicles.

4.6 LIMITATIONS AND FUTURE WORK

A significant limitation to this study was the limited markers to denote differentiation. SPC differentiation only evaluated neuronal and astrocyte differentiation, and was only confirmed with 1 marker each. The next steps in the differentiation of these cells should be to evaluate maintenance of stem cell stemness or oligodendrocyte differentiation. Further, the neuronal differentiation did not validate which type of neuron that the cells may have differentiated into, nor did the differentiation mark the cells as mature neuronal cells. Thus future work should be done to discern a more complete differentiation profile of these spinal cord stem cells.

In regards to the macrophage polarization, while it was limited to only 1 marker was used per M1 or M2 polarization, this was accounted for through evaluating several cell types in terms of macrophage polarization. For future work in discerning macrophage polarization, a more functional descriptor should be used. By evaluating in-vitro macrophage secretions in response to the ECM bioscaffolds (83), it would add insight into the mechanisms behind ECM mediated alternative macrophage polarization. Furthermore, future work should evaluate the paracrine effects and cross talk between these two essential cell types. This would set the foundation for research into macrophage, neural stem cell, and ECM combinatory therapeutics.

5.0 CONTUSION SPINAL CORD INJURY TREATMENT WITH INJECTABLE EXTRACELLULAR MATRIX BIOSCAFFOLDS

5.1 INTRODUCTION

Approximately 200,000 people live with spinal cord injury in the United States alone (238). Of the estimated 20,000 new cases occurring each year, less than 1% of patients experience complete neurologic recovery by hospital discharge (2). Accompanying chronic paralysis are long term physiologic conditions that include chronic pain (239), depression (240), reduced bladder and bowel control (241, 242), and sexual dysfunction (243), among others. SCI also leads to significant economic burdens on the patient and the healthcare system, with the estimated lifetime cost of care are between 2 and 4.6 million dollars for quadriplegics and 1.4 and 2.2 million dollars (3) for paraplegics. While much of the paralysis is due to the primary insult, secondary injury also contributes to tissue disruption.

There are two mechanisms to spinal cord damage following severe SCI (244). The primary injury consists of acute trauma to the spinal cord resulting in cellular necrosis (245) and vascular hemorrhaging (246), and secondary injury, which is composed of the sub-acute and chronic pro-inflammatory microenvironment that can lead to Wallerian degeneration. Wallerian degeneration can include oligodendrocyte apoptosis (247), further axonal demyelination, and development of post traumatic syringomyelia (248). The continued pro-inflammatory

microenvironment is partially controlled by the macrophage and microglial response. While macrophages and microglia can secrete molecules associated with tissue repair including TGF-beta and arginase-1, following SCI the cells contribute to the secretion of TNF- α , IL-1 β , NO, Superoxide, and hydrogen peroxide (51). A regenerative medicine therapeutic that can alter the normal macrophage and microglia response could be beneficial following SCI.

Regenerative medicine bioscaffolds composed of decellularized extracellular matrix (ECM) retain much of their native composition following removal of cellular and antigen components. ECM bioscaffolds alter the innate response to injury towards and have promoted constructive tissue remodeling in several preclinical studies and clinical applications (95-102, 127), in part, by modulation of peripheral macrophage response towards one correlated with tissue repair (73, 74, 125, 222). Bioscaffold efficacy can be further enhanced when derived from homeostatic tissue homologous to the wound site (131, 134, 136, 186). Recently, bioscaffolds have been isolated from CNS-ECM for use in CNS reconstruction applications (161-163, 182), however their application in preclinical models has been limited (130, 192). This study aimed to evaluate the histologic response towards implanted bioscaffolds derived from the brain and spinal cord as site specific materials in comparison to a well-established non-CNS ECM, urinary bladder matrix (UBM-ECM). A secondary objective of this study was to evaluate animal behavior over 28 days.

5.2 MATERIALS AND METHODS

5.2.1 Overview and Experimental Design

Sprague-Dawley rats underwent laminectomy and contusion injury. Immediately following injury (less than 5 minutes), ECM bioscaffolds were injected into the center of the lesion site. Animals were then placed in behavior or histologic evaluation groups. Histologic animals were sacrificed at days 7, 14, and 28 post injury for lesion site and macrophage analyses. Behavioral animals were preconditioned and evaluated for locomotor and sensorimotor recovery over 4 weeks. Results compared ECM bioscaffolds derived from the CNS, brain (B-ECM) and spinal cord (SC-ECM), to those derived from a non-CNS source, porcine urinary bladder (UBM-ECM).

5.2.2 UBM-ECM and CNS-ECM Scaffold Preparation

UBM-ECM, was prepared as previously described. In brief, porcine urinary bladders were harvested from market weight (240–260 lbs) pigs immediately following euthanasia. UBM-ECM was prepared from the bladders using previously described methods (166, 223, 224). The connective and adipose tissue were removed and the tunica serosa, tunica submucosa, and majority of the tunica muscularis mucosa were mechanically delaminated, leaving the basement membrane and tunica propria intact. Luminal urothelial cells were dissociated from the basement membrane by soaking the UBM-ECM in deionized water. The UBM-ECM was decellularized using a 0.1% peracetic acid/4% ethanol treatment with mechanical shaking at 300RPM. The UBM-ECM was then subjected to a series of phosphate buffered saline and deionized water rinses to ensure all peracetic acid was removed from the tissue.

5.2.2.1 CNS-ECM

Immediately following euthanasia, whole brain and spinal cords were frozen at -80°C until use. Whole brains with dura matter removed were sliced into 1cm^3 cubes before placement in decellularization agents. Whole spinal cords with dura removed were longitudinally quartered and cut into less than 3cm long segments. CNS tissue was mechanically shaken (spinal cord tissue at 200 rpm; brain tissue at 120 rpm unless otherwise stated) in the following decellularization agents: deionized water (16 h at 4°C ; 60 rpm), 0.02% trypsin / 0.05% EDTA (60 min at 37°C ; 60RPM; Invitrogen Corp., Carlsbad, CA, USA), 3.0% Triton X-100 (60 min; Sigma-Aldrich Corp., St. Louis, MO, USA), 1.0 M sucrose (15 min; Fisher Scientific, Pittsburgh, PA, USA), water (15 min), 4.0% deoxycholic acid (60 min; Sigma), 0.1% peracetic acid (Rochester Midland Corp., Rochester, NY, USA) in 4.0% ethanol (v/v; 120 min), PBS (15 min; Fisher), deionized water (twice for 15 min each rinse), and PBS (15 min). Each bath was followed by rinsing the remaining tissue through a strainer with deionized water. Decellularized B-ECM and SC-ECM were lyophilized and stored dry until use.

5.2.3 ECM Digestion and Solubilization

Lyophilized and mechanically powdered B-ECM (20 mesh), SC-ECM (20 mesh or hand cut), and UBM-ECM (20 mesh or hand cut; 400-1000 μm largest particle dimension as measured by mesh diameter or ruler) were separately placed into 0.01 N HCl solutions containing 1mg/mL pepsin (Sigma) at a concentration of 10 mg ECM/mL and stirred at room temperature for 48h as previously described (180). After 48h, B-ECM, SC-ECM, and UBM-ECM were completely digested and formed a viscous pre-gel solution (pH \sim 2). The pre-gel ECM solution was brought

to pH 7.4 using 0.01N NaOH and diluted to the desired volume/salt concentration using 10x and 1 x PBS. Pepsin is irreversibly inactivated at pH above 7.5 (198).

5.2.4 Spinal Cord Injury

All animal surgical research was approved by the Institution of Animal Care Committee at the University of Pittsburgh. Animals were placed under deep anesthesia with 60mg/kg ketamine HCl and 0.4mg/kg medetomidine throughout all surgical procedures. Animals received a laminectomy at the T7-T10 vertebrae to expose the spinal cord. Following cord exposure the animals were attached to the infinite horizon impactor (Precision Systems, IL) for piston contusion injury. Contusion injuries within +/-5% of the 175kDyne injury were placed into one of 4 groups, B-ECM, SC-ECM, UBM-ECM, or pepsin control buffer. Following contusion the animals were injected immediately with 5 μ L of the 8mg ECM/mL material or equivalent buffer from their respective group into the center of the spinal cord lesion. Muscle overlaying the spine was sutured together and the skin closed with Michel wound clips. A total of 8 animals per group were underwent surgical procedures for functional recovery and an additional 8 animals per group (4 for 1 week time point and 4 for 2 week time point) were contused and injected with bioscaffolds for histologic analysis.

5.2.4.1 Post-surgical Animal Care and Euthanasia

Following surgery animals were immediately given 1.5mg/kg atipamezole HCl to reverse the sedative effects, 10mL of Ringer's solution, and 6mg/kg gentamicin intramuscularly. Animal bladders were expressed twice daily for 14 days and received 5mL Ringer's solution (subcutaneously), 6mg/kg gentamicin (intramuscularly), and 0.03 mg/kg buprenorphine

(subcutaneously) daily 7-10 days post operation. Animals were deeply sedated using 60mg/kg ketamine HCl and 0.4 mg/kg medetomidine, and 500IU of heparin was injected into the left heart ventricle prior to euthanization. This was followed by 300mL 1xPBS and 500mL of 4% paraformaldehyde. Spinal cord was exposed via tissue removal and laminectomy along the cord. Brain and spinal cords were placed in 4% PFA for 24 hours followed by 30% sucrose for an additional 24 hours and embedded in OCT.

5.2.5 Immunofluorescence and Histochemistry

Injured spinal cords were embedded in OCT leaving approximately 1cm proximal and distal to the lesion site. Cords were cut into 12 series of 10 μ m thick horizontal sections and stored at -20°C until histochemical or immunofluorescence processing. Sections were stained with Masson's trichrome or processed through a triple immunolabeling procedure to perform a temporospatial macrophage phenotype analysis.

5.2.5.1 Macrophage Triple Immunolabeling

Macrophages/microglia were immunolabeled for classically or alternatively using modified previously established methods (73). In brief, the OCT embedded sections were rinse thrice in 1xPBS for 10 minutes per wash. Following this, slides were incubated in blocking solution (0.01% Triton X-100, 0.01% Tween-20, 5% Horse Serum, and 2% Bovine Serum Albumin) for 45 minutes. Primary and secondary antibody incubations were done using the blocking solution as the antibody diluent. Primary antibody incubation included CD11b (mouse anti-rat; 1:250), pan macrophage/microglia, CD86 (rabbit anti-rat; 1:300), M1 marker, and CD206 (goat anti-rat; 1:250), M2 marker overnight at 4°C. Secondary antibodies incubated (all

dilutions were 1:300) for 45 minutes at room temperature and included Alexa Fluor 488 donkey anti-goat, Alexa Fluor 594 donkey anti-mouse, and Percp Cy5.5 donkey anti-rabbit. All slides were counterstained with DAPI and imaged using Nuance multispectral software (PerkinElmer). Between primary incubation, secondary incubation, and the DAPI counterstain the slides were rinsed thrice in 1xPBS for 10-15 minutes per wash.

5.2.6 Behavioral Testing

Prior to behavioral testing, all animals were given 3-5 habituation treatments that allowed them to equilibrate and become comfortable with their environment before evaluation. Throughout the behavioral testing, researchers directly performing the evaluation were blinded to the animal's treatment group. Blinding was accomplished using a double labeling system such that during surgery the animal was assigned an identifier that was then hidden during the injection. The animal was then assigned a second identifier that related to the treatment group. The second identifier was then removed and the animal returned to the appropriate housing location. Only the study coordinator had access to the key matching final identifiers to the treatment group. The key was then released following completion of the behavioral testing and analysis.

5.2.6.1 BBB

Basso, Beattie, and Brennhahan open field locomotor (249) examination evaluates complex kinematic movements of animals following SCI as they move around an open field. Animals were observed for 4 minutes at days 1, 3, 7, 14, 21, and 28 post injury. The movements were evaluated according to the BBB examination criteria. A healthy animal scores 21 points,

while a completely paralyzed animal scores a 0. The scoring progresses as the animal regains limb control and function.

5.2.6.2 Gridwalk

Sensorimotor testing was evaluated using a horizontal ladder walk (250) that scores the animal based on the number of slip as the animal moves across the ladder. Small (paw), medium (foot to the part of the lower leg), and large (whole leg) slips were counted during the 60 cm length at the middle of the ladder. Results displayed as a percentage of steps to normalize between the number of steps varying by animal.

5.2.6.3 Digigait

While classic locomotion pattern is evaluated using an ink footpad (251), this experiment used a motorized treadmill and camera to track the motion of the footprints. Through the Digigait analysis four metrics were assessed: individual paw stride length, paw angle of rotation, limb stance width, and step angle.

5.2.7 Statistical Analysis

A repeated-measures one-way ANOVA was used for statistical comparison for the BBB and gridwalk analyses. All statistical analysis methods used SPSS Statistical Analysis Software (SPSS, IBM, Chicago, IL, USA).

5.3 RESULTS

5.3.1 Masson's Trichrome Lesion Assessment

Masson's trichrome was used as an evaluative histologic stain as it can detect collagen present in the ECM bioscaffolds as well as some levels of glial scar components. The lesions for all SCIs appear smaller at the dorsal edge of the spinal cord and grow in size towards the ventral region. Dorsal images were taken from 0 - 400 μ m, central from 500-700 μ m, and ventral beyond the 700 μ m marker. All ECM scaffolds maintain a fibrous structure throughout the volume of the lesion as compared to the pepsin control. UBM-ECM maintains a consistent fibrous architecture within the lesion volume across all time points. Samples injected with the pepsin digestion buffer contain less fibrous structure at the lesion site. A dense mononuclear cell accumulation can be seen in all accounts, with the ECM bioscaffolds supporting this cell infiltration throughout the wound lesion up to 28 days post injury (Figure 32).

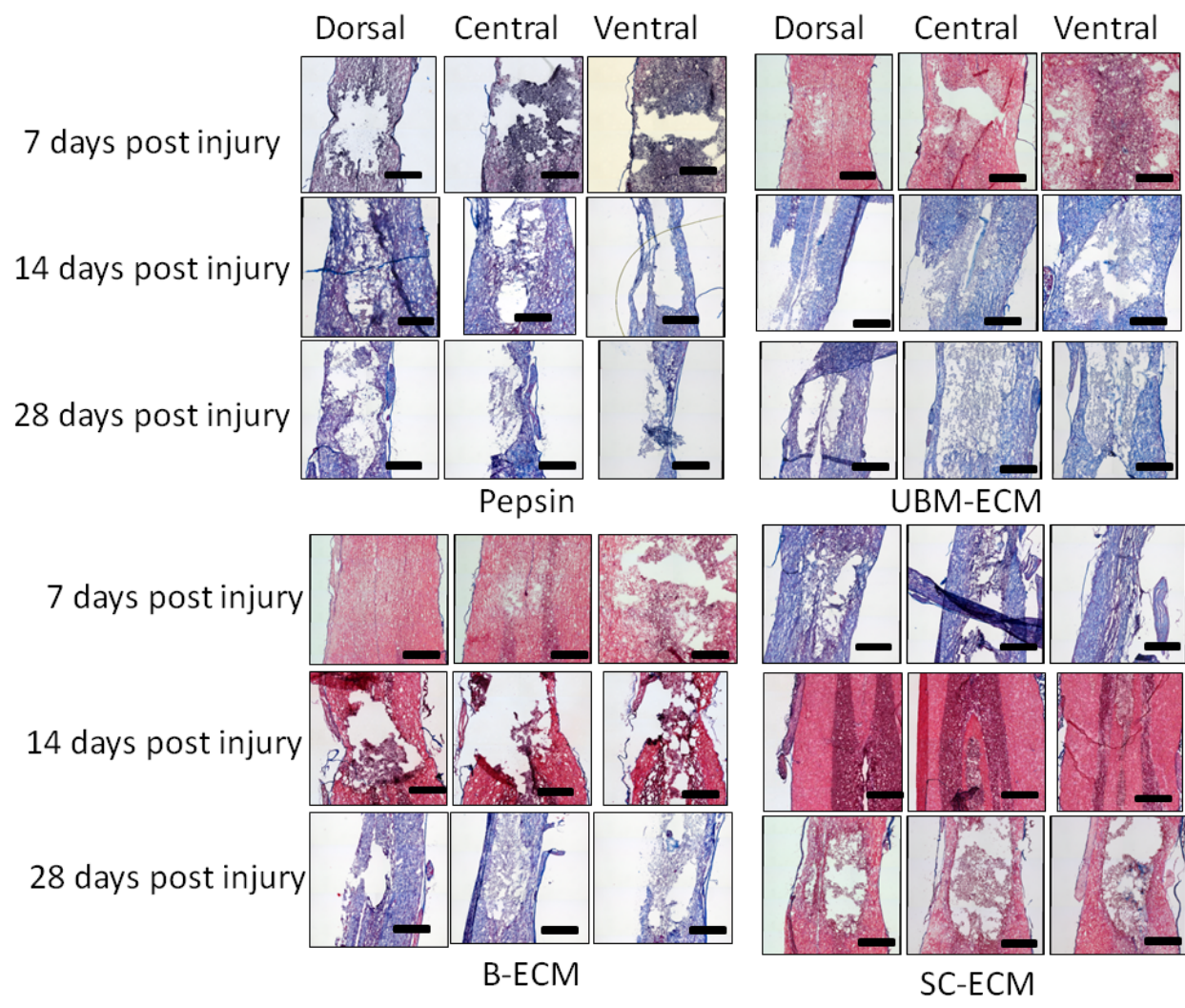


Figure 32. Trichrome staining of UBM, B-ECM, SC-ECM treated spinal cords as compared to a pepsin buffer control. All ECM scaffolds maintain a fibrous structure throughout the volume of the lesion as compared to the pepsin control.

5.3.2 Temporospatial Macrophage Evaluation

A macrophage temporospatial analysis was completed using M1 marker CD86 and M2 marker CD206 with CD11b as a pan macrophage marker. Representative images shown in Figures 33-36, were taken from the central region of the spinal cord to demonstrate the macrophage spatial locations over the 7, 14, and 28 day time points. All spinal cords contained a dense population of CD11b positive cells throughout the lesion area. All treatments show cells expressing CD206 and CD86. Pepsin buffer controls exhibit low levels of CD206 that maintain constant over 28 days. By 28 days, the CD86 positive cells are diffuse throughout the lesion site (Figure 33). Spinal cords treated with UBM-ECM shows a dense accumulation of CD206 positive cells over 28 days. CD86 positive cells are maintained throughout the 28 days (Figure 34). B-ECM treatment animals displayed a moderate CD206 expression at 7 and 14 days post injury, however the CD206 expression becomes more diffuse by day 28. CD86 cell population was present throughout the spinal cords at all time points (Figure 35). SC-ECM shows a dense expression of CD206 and CD86 positive cells throughout the lesion site, however by day 28 the expression localized to the edge of the lesion (Figure 36).

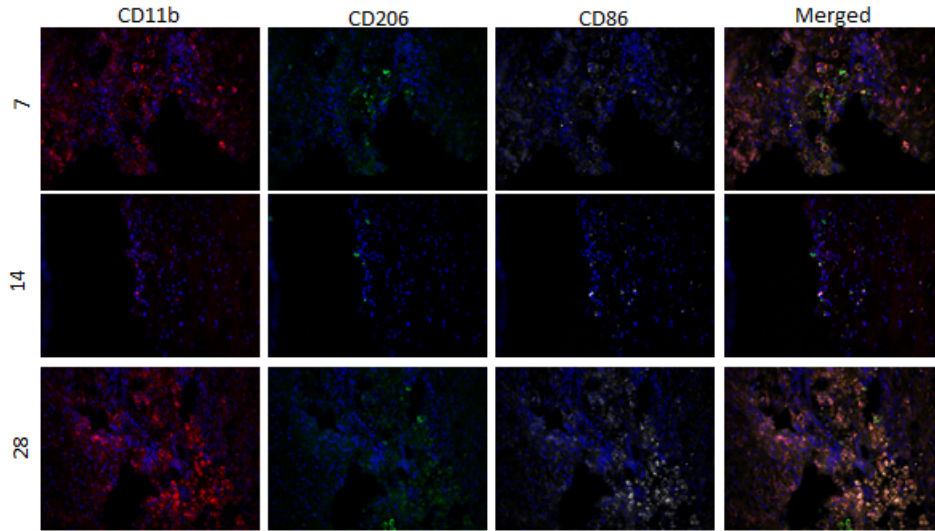


Figure 33. Pepsin buffer control macrophage response over 28 days following injury. The pepsin treated animals show CD206 expression, and a dense accumulation of CD86 positive cells at day 28.

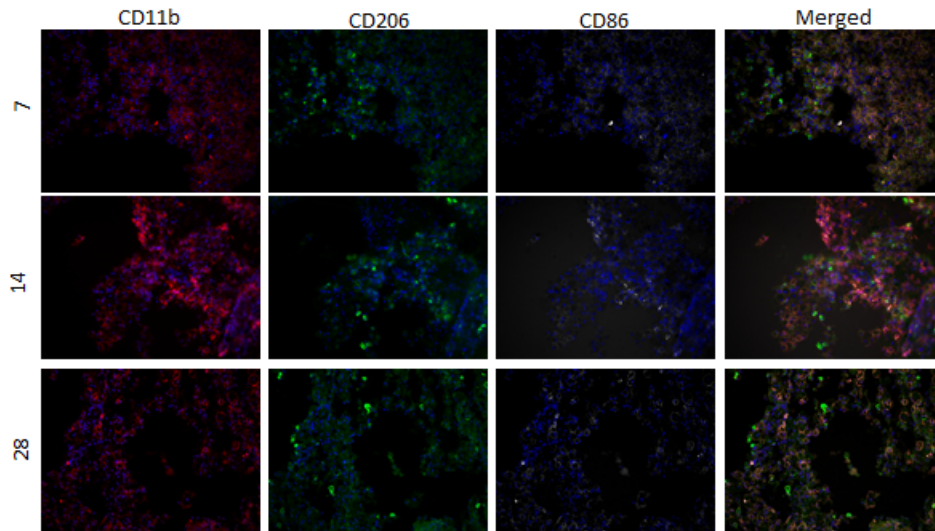


Figure 34. SCI repair with UBM-ECM over 28 days showed a dense accumulation of CD206 positive cells that maintained over 28 days. The CD86 positive cells were diffuse through the lesion area throughout the time points examined.

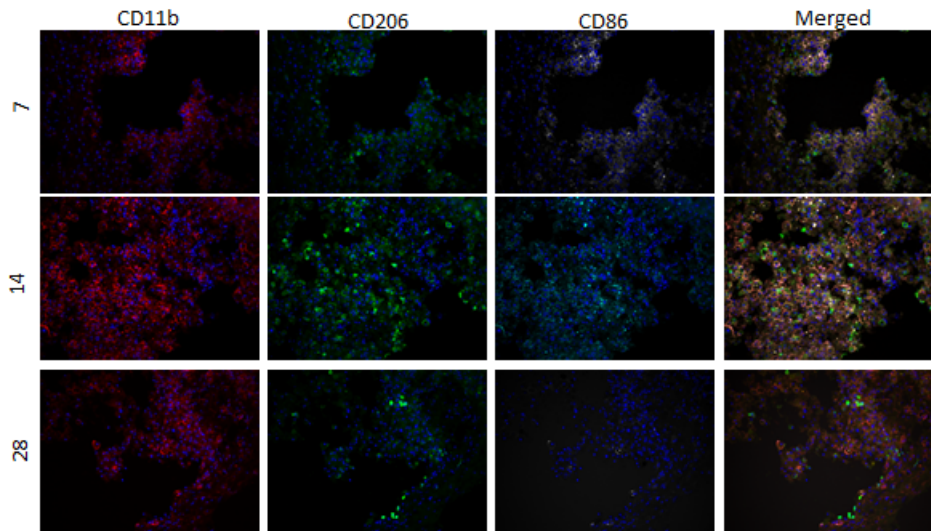


Figure 35. SCI repaired with B-ECM showed a moderate CD206 population that became more diffuse by 28 days. The CD86 cell population is present throughout the lesion site.

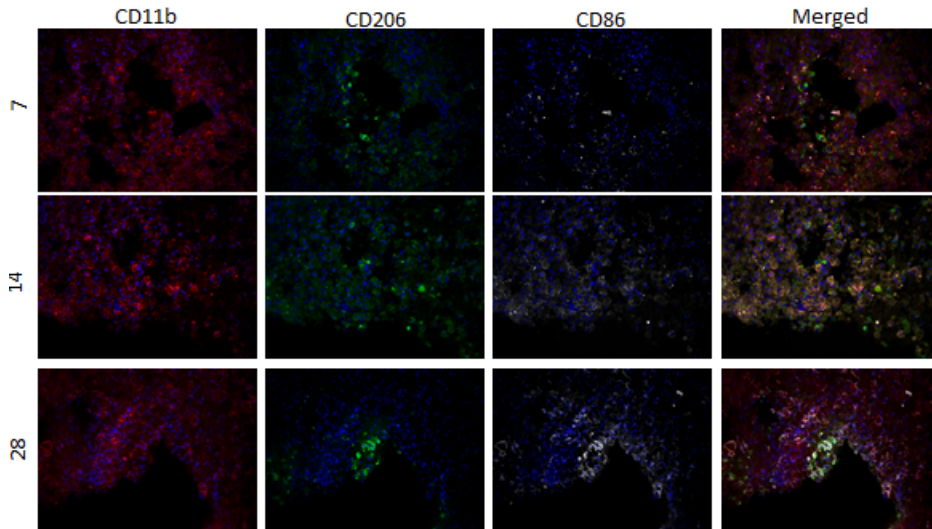


Figure 36. SCI repaired with SC-ECM shows dense CD206 and CD86 cell populations throughout the lesion at days 7 and 14. By day 28, CD206 positive cells were found closer to cavity edges, whereas CD86 remained diffuse.

5.3.3 Locomotor and Sensorimotor Recovery

Assessment of locomotor and sensorimotor recovery was evaluated through 3 comprehensive behavioral recovery metrics. The first, BBB scoring (Figure 37), showed no differences through 28 days of evaluation. The second, gridwalk horizontal ladder assessment showed large variance in groups and no differences between treatments at 14 (Figure 38) and 28 (Figure 39) days post injury. The third metric was the Digigait paw analysis that evaluated stride length (Figure 40), paw angle (Figure 41), step angle (Figure 42), and limb stance width (Figure 43). While there were no behavioral differences between treated and untreated control in this metrics, there was a trend to increase the limb stance width for animals that underwent injury (Figure 43).

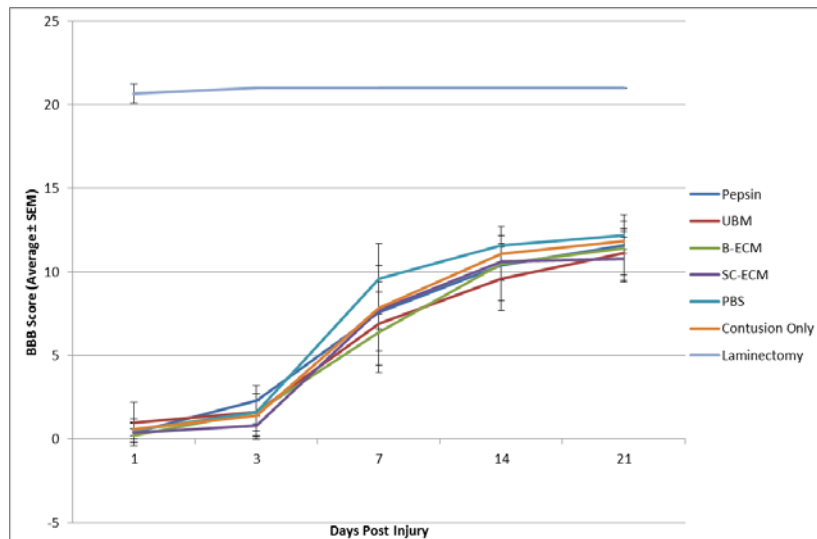


Figure 37. BBB open field locomotor assessment shows all animals recovering to approximately a 12 on the BBB scale. There are no differences between injury controls and treatment groups. Additional controls were added to the graph that include laminectomy only, PBS injection, and contusion with no injection.

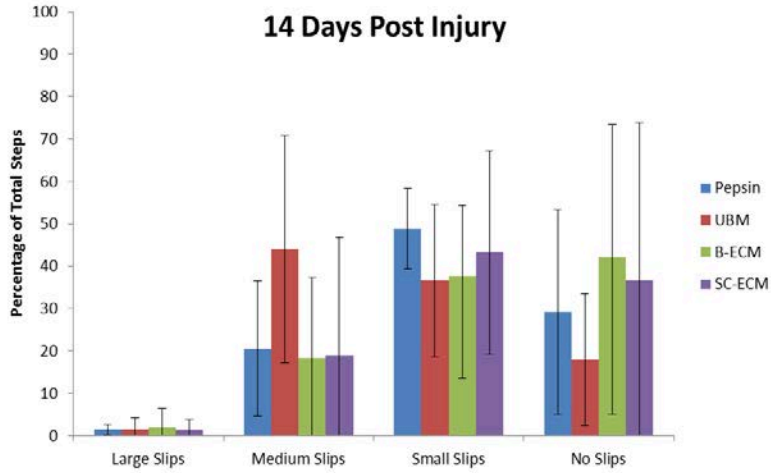


Figure 38. At 14 days post injury, there are no sensorimotor differences between treatment groups as shown through the gridwalk analysis.

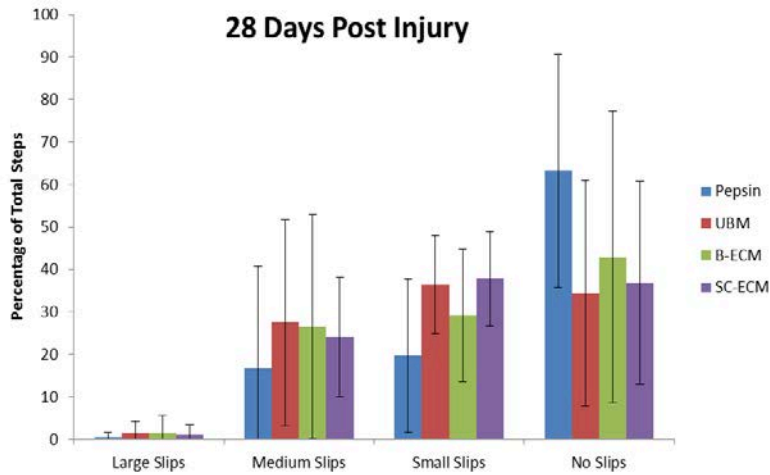


Figure 39. At 28 days post injury, gridwalk slip analysis shows no differences between treatment groups and injection buffer control.

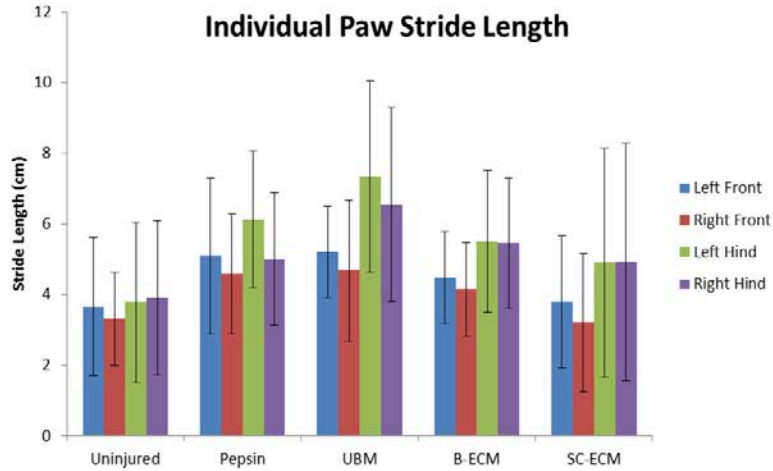


Figure 40. Digigait stride length assessment between CNS-ECM and a non-CNS ECM scaffold show no differences between treatment groups and controls.

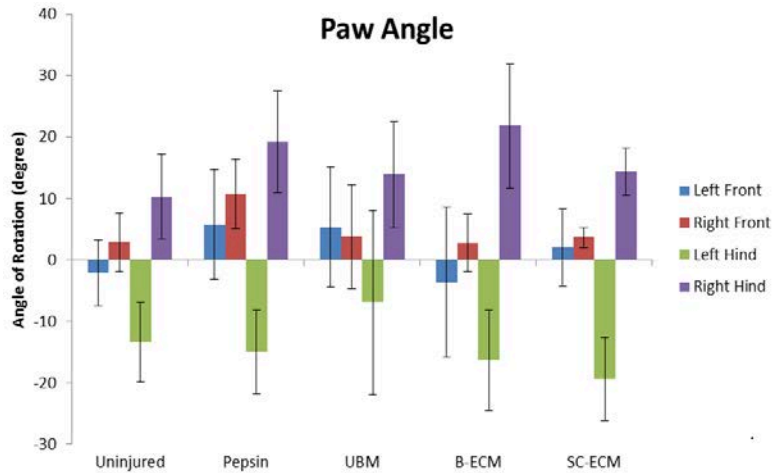


Figure 41. Digigait paw angle assessment shows no difference between the uninjured control, pepsin, UBM-ECM, B-ECM, and SC-ECM.

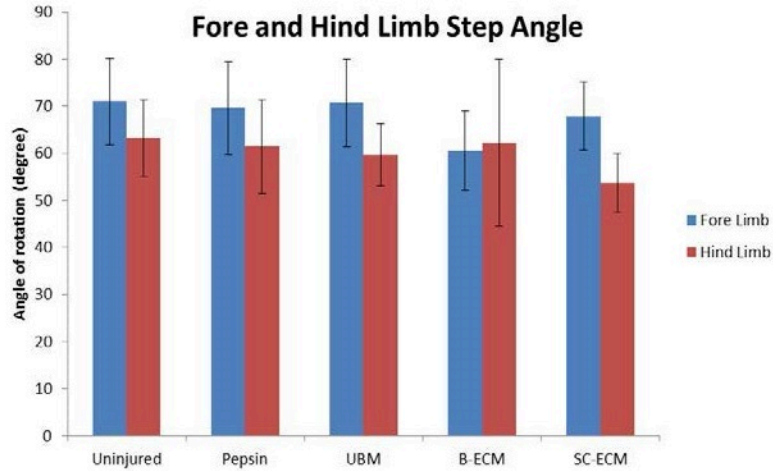


Figure 42. Digigait fore and hind limb step angle assessment shows no difference between uninjured animals, pepsin control, or ECM treatment groups.

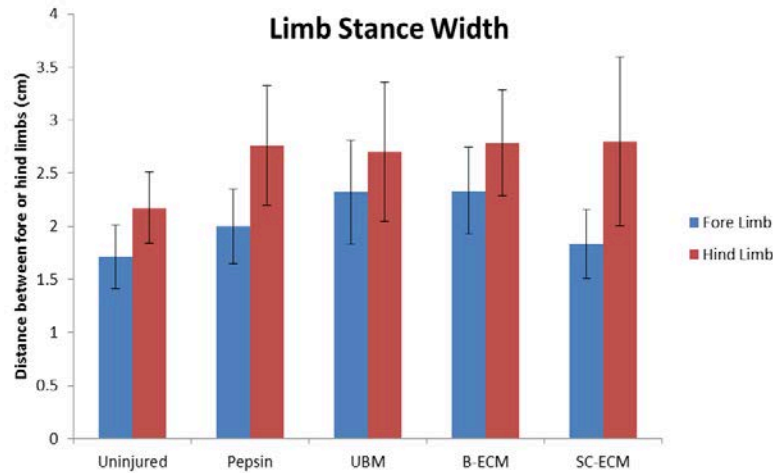


Figure 43. Digigait assessment of limb stance width shows a moderate increase in the hind limb stance width between uninjured and injured animals. There are no differences between injury controls and treatment groups.

5.4 DISCUSSION

In this study, injectable bioscaffolds derived from decellularized whole tissue and organ ECM were successfully delivered to the spinal cord following traumatic injury via syringe injection. Implantation of acellular ECM scaffolds has shown promise for treatment of traumatic neural injuries by promoting locomotor recovery, remyelination, and stimulated regenerative neural fibers (128, 129, 192, 252, 253). These promising benefits of ECM bioscaffolds for CNS applications may be due, in part, to the ability of the ECM scaffold to promote innervation following tissue reconstruction and recruit cells that play a role in neural repair (122). The SCI models previously evaluated with ECM bioscaffolds were either hemi- or transection. In models such as these, the wound area is debrided before the implantation of acellular constructs that replace whole segments of the cord. While this previous research demonstrated functional improvements, the removal of a segment of the spinal cord may not be as clinically relevant as a contusion injury model. Further, the studies did not evaluate the role of the immune response to aid in tissue reconstruction.

In this study, following a severe contusion injury, the lesion area of the spinal cords were first evaluated through a histologic examination of the lesion site using Masson's trichrome staining. The staining revealed a dense fibrous architecture found at the center of the lesion volume for all ECM scaffolds, while this structure was not present or reduced for the pepsin digestion control samples. Further, a dense mononuclear cell population was associated with the lesion site throughout 28 days for all treatment groups. While this dense mononuclear cell population is classically associated with inflammation, it has recently been seen as a step in ECM mediated tissue remodeling (222). To further examine this mononuclear cell population, an evaluation of the macrophage/microglia phenotype was completed.

The present study evaluated the temporospatial macrophage/microglia response to SCI repair to injectable ECM scaffolds. M2 polarized macrophages were present most commonly at the edge of, and often, in the center of the lesion over 28 days. M1 macrophages, on the other hand, were evenly distributed surrounding and within the lesion. Center of the lesion was found using brightfield imaging and macrophage/microglia phenotyping was completed at this location. ECM bioscaffolds all maintained a CD206 cell population at the lesion site, however only UBM-ECM maintained a dense accumulation over 28 days. Previous research demonstrated that macrophages can be polarized towards an M2 phenotype at the edge of a lesion by the proteoglycan glial scar (254-256). This phenomenon may explain the high levels of CD206 positive cells at the cavity boundary. ECM bioscaffold composition has also been shown to contain proteoglycans and future research should evaluate the role that the glycosaminoglycans and their degradation products play in creating a permissive environment for alternative macrophage activation. The macrophages polarized towards an M2 phenotype in models of SCI have been shown to decrease secondary injury and size of lesion cavity (257). Although the microenvironment was permissive for M2 macrophages, no ECM scaffold mediated behavioral recovery was found 28 days post injury. Further, there did not appear to be a benefit for the use of site specific CNS-ECMs in this model.

5.5 CONCLUSIONS

ECM bioscaffolds can be syringe injected into the center of a SCI lesion and maintain a fibrous architecture within the lesion site. The fibrous structure within the lesion supported cellular in-growth and a dense mononuclear cell accumulation. No significant benefit was found for the use

of CNS-ECM scaffolds in either maintaining structure at the lesion site or with the dense mononuclear cell accumulation. While many of the mononuclear cells present at the lesion were M1 macrophages, M2 positive cells were also associated with the lesion site. In combination with other therapeutics, the ability to maintain a fibrous structure and promote cellular in-growth within the lesion site could be harnessed for spinal cord tissue reconstruction efforts.

5.6 LIMITATIONS AND FUTURE WORK

A major limitation of this work was the singular markers for the M1 and M2 evaluation. The markers CD86 and CD206, while commonly used for M1 and M2 macrophage profiling, respectively, do not provide a complete profile of the current activation state. Future work should evaluate a gene expression profile, such as the one completed by Kigerl et. al. in 2009. In this experiment, a set of markers including CD206, CD163, and arginase 1 could be used to evaluate M2 polarization and iNOS, CD16, CD86 could be examined to determine M1 functional upregulation (60). A second limitation when evaluating the innate immune response was the lack of understanding how macrophages versus microglia played a role following ECM implantation. As research continues to shed light upon the differential behaviors of macrophages and microglia, understanding the role that each plays in promotion of constructive CNS remodeling following ECM implantation is crucial (61). Future studies should be conducted with transgenic animals in models of SCI that can interrogate this crucial information. While these limitations did not allow for a complete profile of the activation state for macrophage polarization, the results showed a comprehensive temporospatial analysis of the macrophage/microglia polarization and showed M2 macrophages can be found at the lesion site

28 days post injury. This suggests that future work should include the evaluation of ECM bioscaffolds in other models of traumatic injury including stroke and TBI.

The final limitation in this study was the hyper acute injection of the ECM bioscaffolds, which is not as realistic as waiting a short period or evaluating the materials in a chronic lesion. Future work should evaluate ECM bioscaffolds in a chronic model where the lesion has been allowed to form. This would allow for the ECM bioscaffolds to be injected as a liquid and fill an irregularly shaped three-dimensional lesion commonly found in CNS pathology. The hydrogels would then provide a form filling scaffold for the infiltration of neural and immune cells.

6.0 DISSERTATION SYNOPSIS

6.1 MAJOR FINDINGS

The present work described the development, production, and use of CNS-ECM bioscaffolds as CNS therapeutics. When the development of these scaffolds began there was only study on the isolation of brain derived extracellular matrix for angiogenic applications. The formulation of CNS-ECM bioscaffolds into hydrogel materials made them appropriate for clinical application as minimally invasive surgical procedures could be used. Compositional analyses demonstrated differences between ECMs isolated from different parts of the CNS, and mechanical evaluations of both brain and spinal cord ECM bioscaffolds demonstrated properties similar to the native CNS. Brain, spinal cord, and UBM-ECM hydrogels supported extensive in-vitro three-dimensional neurite extension as well as promoted differential differentiation, mitogenic, and chemotactic effects as demonstrated through stringent assays completed with human macrophages and spinal cord stem cells. Finally, the scaffolds were evaluated in a rat model of contusion spinal cord injury. While no functional recovery was shown in this model of contusion SCI and hyper-acute repair with ECM bioscaffolds, a fibrous tissue structure that supported cellular in-growth was found at the center of the lesion that could be harnessed in combinatorial therapies for neural tissue reconstruction applications.

The following are major findings of the present work:

Specific Aim 1

- Brain and spinal cord ECM can be harvested from whole porcine tissue sources through decellularization that removes residual cells and DNA
- Presence of extracellular matrix molecules including: laminin, soluble collagens I-IV, growth factors VEGF and bFGF, sGAGs, and myelin
- Neurotrophic potential within CNS-ECMs increases model neural cell differentiation responses
- Formulation into injectable hydrogel materials with tunable mechanical properties that supports three-dimensional neurite extension

Specific Aim 2

- SPC response to CNS-ECMs and UBM-ECM shows unique properties of each ECM to influence mitogenesis, chemotaxis, and neuronal and astrocyte differentiation, with UBM promoting the most neuronal differentiation as denoted by β 3-tubulin staining
- Only M2 macrophages are chemotactic towards UBM-ECM
- Increases in Fizz1 expression in an in-vitro mouse model of macrophage polarization in response to UBM-ECM and CNS-ECM degradation products suggest a component of the ECM that is conserved between tissue types can modulate macrophage phenotype

Specific Aim 3

- CNS-ECM hydrogel scaffolds can be successfully delivered to the site of SCI using syringe injection techniques

- A fibrous tissue structure was maintained within the lesion for ECM bioscaffolds
- The fibrous tissue structure supports cellular in-growth into the lesion site

6.2 OVERALL CONCLUSIONS

The work contained in this dissertation describes the isolation and characterization of ECM derived from whole brain or spinal cord tissue. The novel decellularization process described herein maintained ECM structural and bioactive molecules known to be neurotrophic and capable of supporting in-vitro three-dimensional neural growth. Hydrogels developed in this dissertation can be applied as neural therapeutics using minimally invasive surgical techniques and could be used in the future for combinatorial therapies that deliver pharmaceutical agents and or cells for cellular therapy. While ECM bioscaffolds did not improve behavioral outcomes following hyperacute injection, a permissive microenvironment was created for cellular in-growth into the lesion site. This research sets the foundation for future evaluation of bioscaffolds in traumatic neural injuries including stroke and traumatic brain injury.

APPENDIX

PRESENTATION AND PUBLICATION LIST

Published Manuscripts:

1. T.J. Keane, R. Londono, R.M. Carey, C.A. Carruthers, J.E. Reing, C.L. Dearth, A. D'Amore, **C.J. Medberry**, S.F. Badylak. Preparation and Characterization of a Biologic Scaffold from Esophageal Mucosa. *Biomaterials*, 2013.
2. M.T. Wolf, C.A. Carruthers, C.L. Dearth, P.M. Crapo, A. Huber, O.A. Burns, R. Londono, S.A. Johnson, K.A. Daly, E.C. Stahl, J.M. Freund, **C.J. Medberry**, L.E. Carey, A. Nieponice, N.J. Amoroso, S.F. Badylak. Polypropylene surgical mesh coated with extracellular matrix mitigates the host foreign body response. *Journal of Biomedical Materials Research Part A*, 2013.
3. W.S. Turner, X. Wang, S.A. Johnson, **C.J. Medberry**, J. Mendez, S.F. Badylak, M.G. McCord, K.E. McClosky. Cardiac tissue development

for delivery of embryonic stem cell-derived endothelial and cardiac cells in natural matrices. *Journal of Biomedical Materials Research Part B: Applied Biomaterials*, 2012.

4. **C.J. Medberry***, P.M Crapo*, B.F. Sui, C.A. Carruthers, M.T. Wolf, S. Nagarkar, V. Agrawal, K.E. Jones, J. Kelly, S. Velankar, S.C. Watkins, M. Modo, S.F. Badylak. Hydrogels derived from central nervous system extracellular matrix. *Biomaterials*, 2012.
5. B.M. Sicari, V. Agrawal, B.F. Sui, **C.J. Medberry**, C.L. Dearth, N.J. Turner, S.F. Badylak. A Murine Model of Volumetric Muscle Loss and a Regenerative Medicine Approach for Tissue Replacement. *Tissue Engineering*, 2012.
6. P.M. Crapo*, **C.J. Medberry***, J.E. Reing, S. Tottey, Y. van der Merwe, K.E. Jones, S.F. Badylak. Biologic Scaffolds composed of central nervous system extracellular matrix. *Biomaterials*, 2012.
7. V. Agrawal, B.F. Sui, H. Chao, K.K. Hirschi, E. Raborn, S.A. Johnson, S. Tottey, K.B. Hurley, **C.J. Medberry**, S.F. Badylak. Partial Characterization of a Sox2+ Cell Population in an Adult Murine Model of Digit Amputation. *Tissue Engineering*, 2012.

8. B.M. Sicari, S.A. Johnson, B.F. Sui, P.M. Crapo, K.A. Daly, H. Jiang, **C.J. Medberry**, S. Tottey, N.J. Turner, S.F. Badylak. The effect of source animal age upon the in vivo remodeling characteristics of an extracellular matrix scaffold. *Biomaterials*, 2012.
9. A. Huber, A.V. Boruch, A. Nieponice, H. Jiang, **C.J. Medberry**, S.F. Badylak. Histopathologic host response to polypropylene-based surgical mesh materials in a rat abdominal wall defect model. *Journal of Biomedical Materials Research Part B: Applied Biomaterials*, 2012.
10. **C.J. Medberry**, S. Tottey, H. Jiang, S. Johnson, and S.F. Badylak. Resistance to infection of five different materials in a rat body wall model. *J Surg Res*, 2012.
11. K.A. Daly, S. Liu, V. Agrawal, B.N. Brown, S.A. Johnson, **C.J. Medberry**, S.F. Badylak. Damage associated molecular patterns within xenogeneic biologic scaffolds and their effects on host remodeling. *Biomaterials*, 2012.
12. A. Huber, G.P. McCabe, A.V. Boruch, **C.J. Medberry**, M. Honerlaw, S.F. Badylak. Polypropylene-containing synthetic mesh devices in soft tissue repair: A meta-analysis. *Journal of Biomedical Materials Research Part B: Applied Biomaterials*, 2012.

13. A. Soto-Gutierrez, L. Zhang, **C.J. Medberry**, K. Fukumitsu, D. Faulk, H. Jiang, J. Reing, R. Gramignoli, J. Komori, M. Ross, M. Nagaya, E. Lagasse, D. Stolz, S.C. Strom, I.J. Fox, S.F. Badylak. A Whole-Organ Regenerative Medicine Approach for Liver Replacement. *Tissue Eng Part C Methods*, 2011.

14. S. Tottey, S. Johnson, B. Reines, H. Jiang, J. Reing, P. Crapo, **C.J. Medberry**, and S.F. Badylak. Effect of Source Animal Age Upon ECM Scaffold Properties. *Biomaterials*, 2011.

**= Authors contributed equally to this work.*

Filed Patents:

1. S.F. Badylak, B. Brown, P.M. Crapo, S.A. Johnson, C.J. Medberry. Injectable CNS-Derived ECM for Tissue Reconstruction. W.O. Patent 2,013,009,595. Filing date 7/12/12.

Presentations and Published Abstracts:

1. **C.J. Medberry**, P.M. Crapo, B.F. Sui, C.A. Carruthers, M.T. Wolf, S. Nagarkar, V. Agrawal, K.E. Jones, J. Kelly, S. Velankar, M. Modo, S.F. Badylak. Hydrogels derived from Central Nervous System Extracellular Matrix as Therapeutic Scaffolds for Neural Repair (Poster). Hilton Head Regenerative Medicine Workshop. March 2013.

2. D. M. Faulk, A. Soto-Gutiérrez, L. Zhang, **C.J. Medberry**, S.F. Badylak. Whole Organ Liver Engineering With Three Dimensional ECM Biologic Scaffolds (Oral Presentation). TERMIS-NA 2011 Annual Conference, Houston, TX. December, 2011.

3. P.M. Crapo, E. Bible, **C.J. Medberry**, S. Tottey, K.E. Jones, M.M. Modo, S.F. Badylak. CNS-ECM biologic scaffold for the treatment of cortical defects secondary to middle cerebral artery occlusion (Oral Presentation). TERMIS-NA 2011 Annual Conference, Houston, TX. December, 2011.

4. P.M. Crapo, S. Tottey, **C.J. Medberry**, S.F. Badylak. A regenerative medicine approach for optic nerve reconstruction using biologic scaffold materials (Poster). Vision Restoration: Regenerative Medicine in Ophthalmology, Pittsburgh, PA. May, 2011.

5. P.M. Crapo, S. Tottey, **C.J. Medberry**, S.F. Badylak. Biologic scaffolds derived from mammalian CNS for regenerative medicine (Oral Presentation). Society for Biomaterials 2011 Annual Conference, Orlando, FL. April, 2011.

6. **C.J. Medberry**, L. Zhang, J. Komori, E. Lagasse, and S.F. Badylak. Liver Regeneration Using a Three Dimensional Hepatic Extracellular Matrix (Poster). 2nd TERMIS World Congress and Seoul Stem Cell Symposium, Seoul, South Korea. August 31-September 3, 2009.

7. L. Zhang, **C.J. Medberry**, N. Marasco, D. Faulk, T. Hoppo, E. Lagasse, S.F. Badylak. Organ Engineering With Hepatic ECM (Poster). Tissue Engineering and Regenerative Medicine International Society, North American Chapter Meeting. 2008, San Diego, United States. December 7-10, 2008.

8. **C.J. Medberry**, L. Zhang, J. Komori, E. Lagasse, and S.F. Badylak. Maintenance of Functional Hepatocytes with a Three-Dimensional Liver Extracellular Matrix (Invited Speaker). Cellular Approaches to Tissue Engineering and Regenerative Medicine Seminar. November 6, 2008.

BIBLIOGRAPHY

1. Foundation R. Paralysis Facts and Figures 2013 [cited 2013 September 17]. Available from: http://www.christopherreeve.org/site/c.mtKZKGMWKwG/b.5184189/k.5587/Paralysis_Facts_Figures.htm.
2. Bernhard M, Gries A, Kremer P, Bottiger BW. Spinal cord injury (SCI)--prehospital management. Resuscitation. 2005 Aug;66(2):127-39. PubMed PMID: 15950358. Epub 2005/06/14. eng.
3. DeVivo MJ, Chen Y, Mennemeyer ST, Deutsch A. Cost of Care Following Spinal Cord Injury. Topics in spinal cord injury rehabilitation. 2011;16(4):8.
4. Beattie MS, Farooqui AA, Bresnahan JC. Review of current evidence for apoptosis after spinal cord injury. Journal of neurotrauma. 2000 Oct;17(10):915-25. PubMed PMID: 11063057.
5. Springer JE, Azbill RD, Knapp PE. Activation of the caspase-3 apoptotic cascade in traumatic spinal cord injury. Nature medicine. 1999 Aug;5(8):943-6. PubMed PMID: 10426320.
6. Lou J, Lenke LG, Ludwig FJ, O'Brien MF. Apoptosis as a mechanism of neuronal cell death following acute experimental spinal cord injury. Spinal cord. 1998 Oct;36(10):683-90. PubMed PMID: 9800272.
7. Lu J, Ashwell KW, Waite P. Advances in secondary spinal cord injury: role of apoptosis. Spine. 2000 Jul 15;25(14):1859-66. PubMed PMID: 10888960.
8. Sekhon LH, Fehlings MG. Epidemiology, demographics, and pathophysiology of acute spinal cord injury. Spine. 2001 Dec 15;26(24 Suppl):S2-12. PubMed PMID: 11805601.

9. Salgado-Ceballos H, Guizar-Sahagun G, Feria-Velasco A, Grijalva I, Espitia L, Ibarra A, et al. Spontaneous long-term remyelination after traumatic spinal cord injury in rats. *Brain research*. 1998 Jan 26;782(1-2):126-35. PubMed PMID: 9519256.
10. Waxman SG. Demyelination in spinal cord injury. *Journal of the neurological sciences*. 1989 Jun;91(1-2):1-14. PubMed PMID: 2664092.
11. Guest JD, Hiester ED, Bunge RP. Demyelination and Schwann cell responses adjacent to injury epicenter cavities following chronic human spinal cord injury. *Experimental neurology*. 2005 Apr;192(2):384-93. PubMed PMID: 15755556.
12. Fleming JC, Norenberg MD, Ramsay DA, Dekaban GA, Marcillo AE, Saenz AD, et al. The cellular inflammatory response in human spinal cords after injury. *Brain : a journal of neurology*. 2006 Dec;129(Pt 12):3249-69. PubMed PMID: 17071951.
13. Happel RD, Smith KP, Banik NL, Powers JM, Hogan EL, Balentine JD. Ca²⁺-accumulation in experimental spinal cord trauma. *Brain research*. 1981 May 4;211(2):476-9. PubMed PMID: 7237138.
14. Liu D, Xu GY, Pan E, McAdoo DJ. Neurotoxicity of glutamate at the concentration released upon spinal cord injury. *Neuroscience*. 1999;93(4):1383-9. PubMed PMID: 10501463.
15. Tator CH, Koyanagi I. Vascular mechanisms in the pathophysiology of human spinal cord injury. *Journal of neurosurgery*. 1997 Mar;86(3):483-92. PubMed PMID: 9046306.
16. Norenberg MD, Smith J, Marcillo A. The pathology of human spinal cord injury: defining the problems. *Journal of neurotrauma*. 2004 Apr;21(4):429-40. PubMed PMID: 15115592.
17. Berry M, Maxwell WL, Logan A, Mathewson A, McConnell P, Ashhurst DE, et al. Deposition of scar tissue in the central nervous system. *Acta neurochirurgica Supplementum*. 1983;32:31-53. PubMed PMID: 6581703.
18. Sadowsky C, Volshteyn O, Schultz L, McDonald JW. Spinal cord injury. *Disability and rehabilitation*. 2002 Sep 10;24(13):680-7. PubMed PMID: 12296983.

19. Ball MJ, Dayan AD. Pathogenesis of syringomyelia. *Lancet*. 1972 Oct 14;2(7781):799-801. PubMed PMID: 4116236.
20. Gordon S, Taylor PR. Monocyte and macrophage heterogeneity. *Nature reviews Immunology*. 2005 Dec;5(12):953-64. PubMed PMID: 16322748.
21. van Furth R, Cohn ZA, Hirsch JG, Humphrey JH, Spector WG, Langevoort HL. The mononuclear phagocyte system: a new classification of macrophages, monocytes, and their precursor cells. *Bulletin of the World Health Organization*. 1972;46(6):845-52. PubMed PMID: 4538544. Pubmed Central PMCID: 2480884.
22. Van Furth R, Diesselhoff-den Dulk MC, Mattie H. Quantitative study on the production and kinetics of mononuclear phagocytes during an acute inflammatory reaction. *The Journal of experimental medicine*. 1973 Dec 1;138(6):1314-30. PubMed PMID: 4762549. Pubmed Central PMCID: 2139470.
23. van oud Alblas AB, van Furth R. Origin, Kinetics, and characteristics of pulmonary macrophages in the normal steady state. *The Journal of experimental medicine*. 1979 Jun 1;149(6):1504-18. PubMed PMID: 448291. Pubmed Central PMCID: 2184895.
24. Qu C, Edwards EW, Tacke F, Angeli V, Llodra J, Sanchez-Schmitz G, et al. Role of CCR8 and other chemokine pathways in the migration of monocyte-derived dendritic cells to lymph nodes. *The Journal of experimental medicine*. 2004 Nov 15;200(10):1231-41. PubMed PMID: 15534368. Pubmed Central PMCID: 2211916.
25. Hickey WF. Leukocyte traffic in the central nervous system: the participants and their roles. *Seminars in immunology*. 1999 Apr;11(2):125-37. PubMed PMID: 10329499.
26. Kierdorf K, Erny D, Goldmann T, Sander V, Schulz C, Perdiguero EG, et al. Microglia emerge from erythromyeloid precursors via Pu.1- and Irf8-dependent pathways. *Nature neuroscience*. 2013 Mar;16(3):273-80. PubMed PMID: 23334579.
27. Bertrand JY, Jalil A, Klaine M, Jung S, Cumano A, Godin I. Three pathways to mature macrophages in the early mouse yolk sac. *Blood*. 2005 Nov 1;106(9):3004-11. PubMed PMID: 16020514.

28. Geissmann F, Manz MG, Jung S, Sieweke MH, Merad M, Ley K. Development of monocytes, macrophages, and dendritic cells. *Science*. 2010 Feb 5;327(5966):656-61. PubMed PMID: 20133564. Pubmed Central PMCID: 2887389.
29. Lawson LJ, Perry VH, Gordon S. Turnover of resident microglia in the normal adult mouse brain. *Neuroscience*. 1992;48(2):405-15. PubMed PMID: 1603325.
30. de Groot CJ, Huppes W, Sminia T, Kraal G, Dijkstra CD. Determination of the origin and nature of brain macrophages and microglial cells in mouse central nervous system, using non-radioactive in situ hybridization and immunoperoxidase techniques. *Glia*. 1992;6(4):301-9. PubMed PMID: 1281462.
31. Massberg S, Schaerli P, Knezevic-Maramica I, Kollnberger M, Tubo N, Moseman EA, et al. Immunosurveillance by hematopoietic progenitor cells trafficking through blood, lymph, and peripheral tissues. *Cell*. 2007 Nov 30;131(5):994-1008. PubMed PMID: 18045540. Pubmed Central PMCID: 2330270.
32. Yona S, Kim KW, Wolf Y, Mildner A, Varol D, Breker M, et al. Fate mapping reveals origins and dynamics of monocytes and tissue macrophages under homeostasis. *Immunity*. 2013 Jan 24;38(1):79-91. PubMed PMID: 23273845.
33. Varvel NH, Grathwohl SA, Baumann F, Liebig C, Bosch A, Brawek B, et al. Microglial repopulation model reveals a robust homeostatic process for replacing CNS myeloid cells. *Proceedings of the National Academy of Sciences of the United States of America*. 2012 Oct 30;109(44):18150-5. PubMed PMID: 23071306. Pubmed Central PMCID: 3497743.
34. Kettenmann H, Kirchhoff F, Verkhratsky A. Microglia: new roles for the synaptic stripper. *Neuron*. 2013 Jan 9;77(1):10-8. PubMed PMID: 23312512.
35. Neumann H, Wekerle H. Brain microglia: watchdogs with pedigree. *Nature neuroscience*. 2013 Mar;16(3):253-5. PubMed PMID: 23434975.
36. Blinzinger K, Kreutzberg G. Displacement of synaptic terminals from regenerating motoneurons by microglial cells. *Zeitschrift für Zellforschung und mikroskopische Anatomie*. 1968;85(2):145-57. PubMed PMID: 5706753.

37. Schafer DP, Lehrman EK, Kautzman AG, Koyama R, Mardinly AR, Yamasaki R, et al. Microglia sculpt postnatal neural circuits in an activity and complement-dependent manner. *Neuron*. 2012 May 24;74(4):691-705. PubMed PMID: 22632727. Pubmed Central PMCID: 3528177.
38. Cardona AE, Piroo EP, Sasse ME, Kostenko V, Cardona SM, Dijkstra IM, et al. Control of microglial neurotoxicity by the fractalkine receptor. *Nature neuroscience*. 2006 Jul;9(7):917-24. PubMed PMID: 16732273.
39. Ransohoff RM, Perry VH. Microglial physiology: unique stimuli, specialized responses. *Annual review of immunology*. 2009;27:119-45. PubMed PMID: 19302036.
40. Ohsawa K, Imai Y, Nakajima K, Kohsaka S. Generation and characterization of a microglial cell line, MG5, derived from a p53-deficient mouse. *Glia*. 1997 Nov;21(3):285-98. PubMed PMID: 9383038.
41. Giulian D, Baker TJ. Characterization of ameboid microglia isolated from developing mammalian brain. *The Journal of neuroscience : the official journal of the Society for Neuroscience*. 1986 Aug;6(8):2163-78. PubMed PMID: 3018187.
42. Shechter R, London A, Varol C, Raposo C, Cusimano M, Yovel G, et al. Infiltrating blood-derived macrophages are vital cells playing an anti-inflammatory role in recovery from spinal cord injury in mice. *PLoS medicine*. 2009 Jul;6(7):e1000113. PubMed PMID: 19636355. Pubmed Central PMCID: 2707628.
43. Saederup N, Cardona AE, Croft K, Mizutani M, Cotleur AC, Tsou CL, et al. Selective chemokine receptor usage by central nervous system myeloid cells in CCR2-red fluorescent protein knock-in mice. *PloS one*. 2010;5(10):e13693. PubMed PMID: 21060874. Pubmed Central PMCID: 2965160.
44. Hefendehl JK, Neher JJ, Suhs RB, Kohsaka S, Skodras A, Jucker M. Homeostatic and injury-induced microglia behavior in the aging brain. *Aging cell*. 2013 Aug 16. PubMed PMID: 23953759.
45. Kreutzberg GW. Microglia: a sensor for pathological events in the CNS. *Trends in neurosciences*. 1996 Aug;19(8):312-8. PubMed PMID: 8843599.

46. Nimmerjahn A, Kirchhoff F, Helmchen F. Resting microglial cells are highly dynamic surveillants of brain parenchyma in vivo. *Science*. 2005 May 27;308(5726):1314-8. PubMed PMID: 15831717.
47. Rice T, Larsen J, Rivest S, Yong VW. Characterization of the early neuroinflammation after spinal cord injury in mice. *Journal of neuropathology and experimental neurology*. 2007 Mar;66(3):184-95. PubMed PMID: 17356380.
48. Perry VH, Andersson PB, Gordon S. Macrophages and inflammation in the central nervous system. *Trends in neurosciences*. 1993 Jul;16(7):268-73. PubMed PMID: 7689770.
49. Popovich PG, Wei P, Stokes BT. Cellular inflammatory response after spinal cord injury in Sprague-Dawley and Lewis rats. *The Journal of comparative neurology*. 1997 Jan 20;377(3):443-64. PubMed PMID: 8989657.
50. Donnelly DJ, Popovich PG. Inflammation and its role in neuroprotection, axonal regeneration and functional recovery after spinal cord injury. *Experimental neurology*. 2008 Feb;209(2):378-88. PubMed PMID: 17662717. Pubmed Central PMCID: 2692462.
51. Bethea JR, Dietrich WD. Targeting the host inflammatory response in traumatic spinal cord injury. *Current opinion in neurology*. 2002 Jun;15(3):355-60. PubMed PMID: 12045737.
52. Schwartz M, Kipnis J, Rivest S, Prat A. How do immune cells support and shape the brain in health, disease, and aging? *The Journal of neuroscience : the official journal of the Society for Neuroscience*. 2009 Jun 24;29(25):7897-902. PubMed PMID: 19478237.
53. Sicard RE. Differential inflammatory and immunological responses in tissue regeneration and repair. *Annals of the New York Academy of Sciences*. 2002 Jun;961:368-71. PubMed PMID: 12081942.
54. Wilson K. Wound healing: the role of macrophages. *Nursing in critical care*. 1997 Nov-Dec;2(6):291-6. PubMed PMID: 9887766.
55. Ydens E, Cauwels A, Asselbergh B, Goethals S, Peeraer L, Lornet G, et al. Acute injury in the peripheral nervous system triggers an alternative macrophage response. *Journal of neuroinflammation*. 2012;9:176. PubMed PMID: 22818207. Pubmed Central PMCID: 3419084.

56. Yin Y, Henzl MT, Lorber B, Nakazawa T, Thomas TT, Jiang F, et al. Oncomodulin is a macrophage-derived signal for axon regeneration in retinal ganglion cells. *Nature neuroscience*. 2006 Jun;9(6):843-52. PubMed PMID: 16699509.
57. Cox G. IL-10 enhances resolution of pulmonary inflammation in vivo by promoting apoptosis of neutrophils. *The American journal of physiology*. 1996 Oct;271(4 Pt 1):L566-71. PubMed PMID: 8897903.
58. London A, Cohen M, Schwartz M. Microglia and monocyte-derived macrophages: functionally distinct populations that act in concert in CNS plasticity and repair. *Frontiers in cellular neuroscience*. 2013;7:34. PubMed PMID: 23596391. Pubmed Central PMCID: 3625831.
59. Bogdan C, Vodovotz Y, Nathan C. Macrophage deactivation by interleukin 10. *The Journal of experimental medicine*. 1991 Dec 1;174(6):1549-55. PubMed PMID: 1744584. Pubmed Central PMCID: 2119047.
60. Kigerl KA, Gensel JC, Ankeny DP, Alexander JK, Donnelly DJ, Popovich PG. Identification of two distinct macrophage subsets with divergent effects causing either neurotoxicity or regeneration in the injured mouse spinal cord. *The Journal of neuroscience : the official journal of the Society for Neuroscience*. 2009 Oct 28;29(43):13435-44. PubMed PMID: 19864556. Pubmed Central PMCID: 2788152.
61. David S, Kroner A. Repertoire of microglial and macrophage responses after spinal cord injury. *Nature reviews Neuroscience*. 2011 Jul;12(7):388-99. PubMed PMID: 21673720.
62. Tidball JG, Villalta SA. Regulatory interactions between muscle and the immune system during muscle regeneration. *American journal of physiology Regulatory, integrative and comparative physiology*. 2010 May;298(5):R1173-87. PubMed PMID: 20219869. Pubmed Central PMCID: 2867520.
63. Mantovani A, Sica A, Sozzani S, Allavena P, Vecchi A, Locati M. The chemokine system in diverse forms of macrophage activation and polarization. *Trends in immunology*. 2004 Dec;25(12):677-86. PubMed PMID: 15530839.
64. Lucas T, Waisman A, Ranjan R, Roes J, Krieg T, Muller W, et al. Differential roles of macrophages in diverse phases of skin repair. *Journal of immunology*. 2010 Apr 1;184(7):3964-77. PubMed PMID: 20176743.

65. Wan J, Benkdane M, Teixeira-Clerc F, Bonnafous S, Louvet A, Lafdil F, et al. M2 Kupffer cells promote M1 Kupffer cell apoptosis: A protective mechanism against alcoholic and non-alcoholic fatty liver disease. *Hepatology*. 2013 Jul 6. PubMed PMID: 23832548.
66. Mokarram N, Merchant A, Mukhatyar V, Patel G, Bellamkonda RV. Effect of modulating macrophage phenotype on peripheral nerve repair. *Biomaterials*. 2012 Dec;33(34):8793-801. PubMed PMID: 22979988. Pubmed Central PMCID: 3483037.
67. Gordon S, Martinez FO. Alternative activation of macrophages: mechanism and functions. *Immunity*. 2010 May 28;32(5):593-604. PubMed PMID: 20510870.
68. Biswas SK, Mantovani A. Macrophage plasticity and interaction with lymphocyte subsets: cancer as a paradigm. *Nature immunology*. 2010 Oct;11(10):889-96. PubMed PMID: 20856220.
69. Martinez FO, Helming L, Gordon S. Alternative activation of macrophages: an immunologic functional perspective. *Annual review of immunology*. 2009;27:451-83. PubMed PMID: 19105661.
70. Shaughnessy LM, Swanson JA. The role of the activated macrophage in clearing *Listeria monocytogenes* infection. *Frontiers in bioscience : a journal and virtual library*. 2007;12:2683-92. PubMed PMID: 17127272. Pubmed Central PMCID: 2851543.
71. Murphy JT, Sommer S, Kabara EA, Verman N, Kuelbs MA, Saama P, et al. Gene expression profiling of monocyte-derived macrophages following infection with *Mycobacterium avium* subspecies *avium* and *Mycobacterium avium* subspecies *paratuberculosis*. *Physiological genomics*. 2006 Dec 13;28(1):67-75. PubMed PMID: 17062651.
72. Filardy AA, Pires DR, Nunes MP, Takiya CM, Freire-de-Lima CG, Ribeiro-Gomes FL, et al. Proinflammatory clearance of apoptotic neutrophils induces an IL-12(low)IL-10(high) regulatory phenotype in macrophages. *Journal of immunology*. 2010 Aug 15;185(4):2044-50. PubMed PMID: 20660352.
73. Brown BN, Valentin JE, Stewart-Akers AM, McCabe GP, Badylak SF. Macrophage phenotype and remodeling outcomes in response to biologic scaffolds with and without a cellular component. *Biomaterials*. 2009 Mar;30(8):1482-91. PubMed PMID: 19121538. Pubmed Central PMCID: 2805023.

74. Badylak SF, Valentin JE, Ravindra AK, McCabe GP, Stewart-Akers AM. Macrophage phenotype as a determinant of biologic scaffold remodeling. *Tissue engineering Part A*. 2008 Nov;14(11):1835-42. PubMed PMID: 18950271.
75. Shechter R, Schwartz M. Harnessing monocyte-derived macrophages to control central nervous system pathologies: No longer 'if' but 'how'. *The Journal of pathology*. 2012 Sep 24. PubMed PMID: 23007711.
76. Schwartz M. "Tissue-repairing" blood-derived macrophages are essential for healing of the injured spinal cord: from skin-activated macrophages to infiltrating blood-derived cells? *Brain, behavior, and immunity*. 2010 Oct;24(7):1054-7. PubMed PMID: 20149864.
77. Bomstein Y, Marder JB, Vitner K, Smirnov I, Lisaey G, Butovsky O, et al. Features of skin-coincubated macrophages that promote recovery from spinal cord injury. *Journal of neuroimmunology*. 2003 Sep;142(1-2):10-6. PubMed PMID: 14512160.
78. Rapalino O, Lazarov-Spiegler O, Agranov E, Velan GJ, Yoles E, Fraidakis M, et al. Implantation of stimulated homologous macrophages results in partial recovery of paraplegic rats. *Nature medicine*. 1998 Jul;4(7):814-21. PubMed PMID: 9662373.
79. Durafourt BA, Moore CS, Zammit DA, Johnson TA, Zaguia F, Guiot MC, et al. Comparison of polarization properties of human adult microglia and blood-derived macrophages. *Glia*. 2012 May;60(5):717-27. PubMed PMID: 22290798.
80. Popovich PG, Jones TB. Manipulating neuroinflammatory reactions in the injured spinal cord: back to basics. *Trends in pharmacological sciences*. 2003 Jan;24(1):13-7. PubMed PMID: 12498725.
81. Butovsky O, Ziv Y, Schwartz A, Landa G, Talpalar AE, Pluchino S, et al. Microglia activated by IL-4 or IFN-gamma differentially induce neurogenesis and oligodendrogenesis from adult stem/progenitor cells. *Molecular and cellular neurosciences*. 2006 Jan;31(1):149-60. PubMed PMID: 16297637.
82. Knoller N, Auerbach G, Fulga V, Zelig G, Attias J, Bakimer R, et al. Clinical experience using incubated autologous macrophages as a treatment for complete spinal cord injury: phase I study results. *Journal of neurosurgery Spine*. 2005 Sep;3(3):173-81. PubMed PMID: 16235699.

83. Mantovani A, Biswas SK, Galdiero MR, Sica A, Locati M. Macrophage plasticity and polarization in tissue repair and remodelling. *The Journal of pathology*. 2013 Jan;229(2):176-85. PubMed PMID: 23096265.
84. Mantovani A, Locati M. Tumor-associated macrophages as a paradigm of macrophage plasticity, diversity, and polarization: lessons and open questions. *Arteriosclerosis, thrombosis, and vascular biology*. 2013 Jul;33(7):1478-83. PubMed PMID: 23766387.
85. Miron VE, Boyd A, Zhao JW, Yuen TJ, Ruckh JM, Shadrach JL, et al. M2 microglia and macrophages drive oligodendrocyte differentiation during CNS remyelination. *Nature neuroscience*. 2013 Jul 21. PubMed PMID: 23872599.
86. McDonald JW, Sadowsky C. Spinal-cord injury. *Lancet*. 2002 Feb 2;359(9304):417-25. PubMed PMID: 11844532.
87. Stevens RD, Bhardwaj A, Kirsch JR, Mirski MA. Critical care and perioperative management in traumatic spinal cord injury. *Journal of neurosurgical anesthesiology*. 2003 Jul;15(3):215-29. PubMed PMID: 12826969.
88. Hugenholtz H, Cass DE, Dvorak MF, Fewer DH, Fox RJ, Izukawa DM, et al. High-dose methylprednisolone for acute closed spinal cord injury--only a treatment option. *Can J Neurol Sci*. 2002 Aug;29(3):227-35. PubMed PMID: 12195611. Epub 2002/08/28. eng.
89. Bracken MB, Shepard MJ, Collins WF, Holford TR, Young W, Baskin DS, et al. A randomized, controlled trial of methylprednisolone or naloxone in the treatment of acute spinal-cord injury. Results of the Second National Acute Spinal Cord Injury Study. *N Engl J Med*. 1990 May 17;322(20):1405-11. PubMed PMID: 2278545. Epub 1990/05/17. eng.
90. Young W, Bracken MB. The Second National Acute Spinal Cord Injury Study. *J Neurotrauma*. 1992 Mar;9 Suppl 1:S397-405. PubMed PMID: 1588630. Epub 1992/03/01. eng.
91. Pereira JE, Costa LM, Cabrita AM, Couto PA, Filipe VM, Magalhaes LG, et al. Methylprednisolone fails to improve functional and histological outcome following spinal cord injury in rats. *Exp Neurol*. 2009 Nov;220(1):71-81. PubMed PMID: 19665461. Epub 2009/08/12. eng.

92. Rabinowitz RS, Eck JC, Harper CM, Jr., Larson DR, Jimenez MA, Parisi JE, et al. Urgent surgical decompression compared to methylprednisolone for the treatment of acute spinal cord injury: a randomized prospective study in beagle dogs. *Spine (Phila Pa 1976)*. 2008 Oct 1;33(21):2260-8. PubMed PMID: 18827690. Epub 2008/10/02. eng.
93. Hurlbert RJ, Hamilton MG. Methylprednisolone for acute spinal cord injury: 5-year practice reversal. *Can J Neurol Sci*. 2008 Mar;35(1):41-5. PubMed PMID: 18380276. Epub 2008/04/03. eng.
94. Godwin JW, Pinto AR, Rosenthal NA. Macrophages are required for adult salamander limb regeneration. *Proceedings of the National Academy of Sciences of the United States of America*. 2013 Jun 4;110(23):9415-20. PubMed PMID: 23690624. Pubmed Central PMCID: 3677454.
95. Badylak SF, Vorp DA, Spievack AR, Simmons-Byrd A, Hanke J, Freytes DO, et al. Esophageal reconstruction with ECM and muscle tissue in a dog model. *J Surg Res*. 2005 Sep;128(1):87-97. PubMed PMID: 15922361. Epub 2005/06/01. eng.
96. Badylak SF, Hoppo T, Nieponice A, Gilbert TW, Davison JM, Jobe BA. Esophageal preservation in five male patients after endoscopic inner-layer circumferential resection in the setting of superficial cancer: a regenerative medicine approach with a biologic scaffold. *Tissue engineering Part A*. 2011 Jun;17(11-12):1643-50. PubMed PMID: 21306292. Pubmed Central PMCID: 3098955.
97. Wood JD, Simmons-Byrd A, Spievack AR, Badylak SF. Use of a particulate extracellular matrix bioscaffold for treatment of acquired urinary incontinence in dogs. *J Am Vet Med Assoc*. 2005 Apr 1;226(7):1095-7. PubMed PMID: 15825734. Epub 2005/04/14. eng.
98. Sutherland RS, Baskin LS, Hayward SW, Cunha GR. Regeneration of bladder urothelium, smooth muscle, blood vessels and nerves into an acellular tissue matrix. *J Urol*. 1996 Aug;156(2 Pt 2):571-7. PubMed PMID: 8683736. Epub 1996/08/01. eng.
99. Zantop T, Gilbert TW, Yoder MC, Badylak SF. Extracellular matrix scaffolds are repopulated by bone marrow-derived cells in a mouse model of achilles tendon reconstruction. *Journal of orthopaedic research : official publication of the Orthopaedic Research Society*. 2006 Jun;24(6):1299-309. PubMed PMID: 16649228.

100. Iannotti JP, Codsì MJ, Kwon YW, Derwin K, Ciccone J, Brems JJ. Porcine small intestine submucosa augmentation of surgical repair of chronic two-tendon rotator cuff tears. A randomized, controlled trial. *J Bone Joint Surg Am*. 2006 Jun;88(6):1238-44. PubMed PMID: 16757756. Epub 2006/06/08. eng.
101. Robinson KA, Li J, Mathison M, Redkar A, Cui J, Chronos NA, et al. Extracellular matrix scaffold for cardiac repair. *Circulation*. 2005 Aug 30;112(9 Suppl):I135-43. PubMed PMID: 16159805. Epub 2005/09/15. eng.
102. Ota T, Gilbert TW, Schwartzman D, McTiernan CF, Kitajima T, Ito Y, et al. A fusion protein of hepatocyte growth factor enhances reconstruction of myocardium in a cardiac patch derived from porcine urinary bladder matrix. *The Journal of thoracic and cardiovascular surgery*. 2008 Nov;136(5):1309-17. PubMed PMID: 19026821. Pubmed Central PMCID: 2723859.
103. Derwin KA, Badylak SF, Steinmann SP, Iannotti JP. Extracellular matrix scaffold devices for rotator cuff repair. *Journal of shoulder and elbow surgery / American Shoulder and Elbow Surgeons [et al]*. 2010 Apr;19(3):467-76. PubMed PMID: 20189415.
104. Brewer MB, Rada EM, Milburn ML, Goldberg NH, Singh DP, Cooper M, et al. Human acellular dermal matrix for ventral hernia repair reduces morbidity in transplant patients. *Hernia : the journal of hernias and abdominal wall surgery*. 2011 Apr;15(2):141-5. PubMed PMID: 21072551.
105. Reing JE, Brown BN, Daly KA, Freund JM, Gilbert TW, Hsiong SX, et al. The effects of processing methods upon mechanical and biologic properties of porcine dermal extracellular matrix scaffolds. *Biomaterials*. 2010 Nov;31(33):8626-33. PubMed PMID: 20728934. Pubmed Central PMCID: 2956268.
106. Crapo PM, Gilbert TW, Badylak SF. An overview of tissue and whole organ decellularization processes. *Biomaterials*. 2011 Apr;32(12):3233-43. PubMed PMID: 21296410. Pubmed Central PMCID: 3084613.
107. Keane TJ, Londono R, Turner NJ, Badylak SF. Consequences of ineffective decellularization of biologic scaffolds on the host response. *Biomaterials*. 2012 Feb;33(6):1771-81. PubMed PMID: 22137126.

108. Valentin JE, Badylak JS, McCabe GP, Badylak SF. Extracellular matrix bioscaffolds for orthopaedic applications. A comparative histologic study. *The Journal of bone and joint surgery American volume*. 2006 Dec;88(12):2673-86. PubMed PMID: 17142418.
109. Bonenfant NR, Sokocevic D, Wagner DE, Borg ZD, Lathrop MJ, Lam YW, et al. The effects of storage and sterilization on de-cellularized and re-cellularized whole lung. *Biomaterials*. 2013 Apr;34(13):3231-45. PubMed PMID: 23380353.
110. Tottey S, Corselli M, Jeffries EM, Londono R, Peault B, Badylak SF. Extracellular matrix degradation products and low-oxygen conditions enhance the regenerative potential of perivascular stem cells. *Tissue engineering Part A*. 2011 Jan;17(1-2):37-44. PubMed PMID: 20653348. Pubmed Central PMCID: 3011908.
111. Agrawal V, Kelly J, Tottey S, Daly KA, Johnson SA, Siu BF, et al. An isolated cryptic peptide influences osteogenesis and bone remodeling in an adult mammalian model of digit amputation. *Tissue engineering Part A*. 2011 Dec;17(23-24):3033-44. PubMed PMID: 21740273. Pubmed Central PMCID: 3226059.
112. Agrawal V, Tottey S, Johnson SA, Freund JM, Siu BF, Badylak SF. Recruitment of progenitor cells by an extracellular matrix cryptic peptide in a mouse model of digit amputation. *Tissue engineering Part A*. 2011 Oct;17(19-20):2435-43. PubMed PMID: 21563860. Pubmed Central PMCID: 3179613.
113. Sudhakar A, Sugimoto H, Yang C, Lively J, Zeisberg M, Kalluri R. Human tumstatin and human endostatin exhibit distinct antiangiogenic activities mediated by alpha v beta 3 and alpha 5 beta 1 integrins. *Proceedings of the National Academy of Sciences of the United States of America*. 2003 Apr 15;100(8):4766-71. PubMed PMID: 12682293. Pubmed Central PMCID: 153630.
114. Davis GE, Bayless KJ, Davis MJ, Meininger GA. Regulation of tissue injury responses by the exposure of matricryptic sites within extracellular matrix molecules. *The American journal of pathology*. 2000 May;156(5):1489-98. PubMed PMID: 10793060. Pubmed Central PMCID: 1876929.
115. Hodde JP, Record RD, Liang HA, Badylak SF. Vascular endothelial growth factor in porcine-derived extracellular matrix. *Endothelium : journal of endothelial cell research*. 2001;8(1):11-24. PubMed PMID: 11409848.

116. Voytik-Harbin SL, Brightman AO, Kraine MR, Waisner B, Badylak SF. Identification of extractable growth factors from small intestinal submucosa. *Journal of cellular biochemistry*. 1997 Dec 15;67(4):478-91. PubMed PMID: 9383707.
117. Boruch AV, Nieponice A, Qureshi IR, Gilbert TW, Badylak SF. Constructive remodeling of biologic scaffolds is dependent on early exposure to physiologic bladder filling in a canine partial cystectomy model. *The Journal of surgical research*. 2010 Jun 15;161(2):217-25. PubMed PMID: 19577253.
118. Hodde JP, Badylak SF, Shelbourne KD. The effect of range of motion on remodeling of small intestinal submucosa (SIS) when used as an Achilles tendon repair material in the rabbit. *Tissue engineering*. 1997;3(1).
119. Gavazzi I, Boyle KS, Cowen T. Extracellular matrix molecules influence innervation density in rat cerebral blood vessels. *Brain research*. 1996 Sep 23;734(1-2):167-74. PubMed PMID: 8896822.
120. Gavazzi I, Boyle KS, Edgar D, Cowen T. Reduced laminin immunoreactivity in the blood vessel wall of ageing rats correlates with reduced innervation in vivo and following transplantation. *Cell and tissue research*. 1995 Jul;281(1):23-32. PubMed PMID: 7621524.
121. Kumar A, Godwin JW, Gates PB, Garza-Garcia AA, Brockes JP. Molecular basis for the nerve dependence of limb regeneration in an adult vertebrate. *Science*. 2007 Nov 2;318(5851):772-7. PubMed PMID: 17975060. Pubmed Central PMCID: 2696928.
122. Agrawal V, Brown BN, Beattie AJ, Gilbert TW, Badylak SF. Evidence of innervation following extracellular matrix scaffold-mediated remodelling of muscular tissues. *J Tissue Eng Regen Med*. 2009 Dec;3(8):590-600. PubMed PMID: 19701935. Pubmed Central PMCID: 2787980. Epub 2009/08/25. eng.
123. Sicari BM, Agrawal V, Siu BF, Medberry CJ, Dearth CL, Turner NJ, et al. A murine model of volumetric muscle loss and a regenerative medicine approach for tissue replacement. *Tissue engineering Part A*. 2012 Oct;18(19-20):1941-8. PubMed PMID: 22906411. Pubmed Central PMCID: 3463275.
124. Turner NJ, Badylak JS, Weber DJ, Badylak SF. Biologic scaffold remodeling in a dog model of complex musculoskeletal injury. *The Journal of surgical research*. 2012 Aug;176(2):490-502. PubMed PMID: 22341350.

125. Valentin JE, Stewart-Akers AM, Gilbert TW, Badylak SF. Macrophage participation in the degradation and remodeling of extracellular matrix scaffolds. *Tissue engineering Part A*. 2009 Jul;15(7):1687-94. PubMed PMID: 19125644. Pubmed Central PMCID: 2792102.
126. Cobb MA, Badylak SF, Janas W, Simmons-Byrd A, Boop FA. Porcine small intestinal submucosa as a dural substitute. *Surgical neurology*. 1999 Jan;51(1):99-104. PubMed PMID: 9952131.
127. Bejjani GK, Zabramski J, Durasis Study G. Safety and efficacy of the porcine small intestinal submucosa dural substitute: results of a prospective multicenter study and literature review. *Journal of neurosurgery*. 2007 Jun;106(6):1028-33. PubMed PMID: 17564175.
128. Xue H, Zhang XY, Liu JM, Song Y, Li YF, Chen D. Development of a chemically extracted acellular muscle scaffold seeded with amniotic epithelial cells to promote spinal cord repair. *Journal of biomedical materials research Part A*. 2013 Jan;101(1):145-56. PubMed PMID: 22829497.
129. Li C, Zhang X, Cao R, Yu B, Liang H, Zhou M, et al. Allografts of the acellular sciatic nerve and brain-derived neurotrophic factor repair spinal cord injury in adult rats. *PloS one*. 2012;7(8):e42813. PubMed PMID: 22952613. Pubmed Central PMCID: 3429476.
130. Liu J, Chen J, Liu B, Yang C, Xie D, Zheng X, et al. Acellular spinal cord scaffold seeded with mesenchymal stem cells promotes long-distance axon regeneration and functional recovery in spinal cord injured rats. *Journal of the neurological sciences*. 2013 Feb 15;325(1-2):127-36. PubMed PMID: 23317924.
131. Allen RA, Seltz LM, Jiang H, Kasick RT, Sellaro TL, Badylak SF, et al. Adrenal extracellular matrix scaffolds support adrenocortical cell proliferation and function in vitro. *Tissue engineering Part A*. 2010 Nov;16(11):3363-74. PubMed PMID: 20528677.
132. Ott HC, Clippinger B, Conrad C, Schuetz C, Pomerantseva I, Ikonomou L, et al. Regeneration and orthotopic transplantation of a bioartificial lung. *Nature medicine*. 2010 Aug;16(8):927-33. PubMed PMID: 20628374.
133. Price AP, England KA, Matson AM, Blazar BR, Panoskaltsis-Mortari A. Development of a decellularized lung bioreactor system for bioengineering the lung: the matrix reloaded. *Tissue engineering Part A*. 2010 Aug;16(8):2581-91. PubMed PMID: 20297903. Pubmed Central PMCID: 2947435.

134. Sellaro TL, Ravindra AK, Stolz DB, Badylak SF. Maintenance of hepatic sinusoidal endothelial cell phenotype in vitro using organ-specific extracellular matrix scaffolds. *Tissue engineering*. 2007 Sep;13(9):2301-10. PubMed PMID: 17561801.
135. Soto-Gutierrez A, Zhang L, Medberry C, Fukumitsu K, Faulk D, Jiang H, et al. A whole-organ regenerative medicine approach for liver replacement. *Tissue engineering Part C, Methods*. 2011 Jun;17(6):677-86. PubMed PMID: 21375407. Pubmed Central PMCID: 3103054.
136. Cortiella J, Niles J, Cantu A, Brettler A, Pham A, Vargas G, et al. Influence of acellular natural lung matrix on murine embryonic stem cell differentiation and tissue formation. *Tissue Eng Part A*. 2010 Aug;16(8):2565-80. PubMed PMID: 20408765. Epub 2010/04/23. eng.
137. Zhang Y, He Y, Bharadwaj S, Hammam N, Carnagey K, Myers R, et al. Tissue-specific extracellular matrix coatings for the promotion of cell proliferation and maintenance of cell phenotype. *Biomaterials*. 2009 Aug;30(23-24):4021-8. PubMed PMID: 19410290.
138. Lin P, Chan WC, Badylak SF, Bhatia SN. Assessing porcine liver-derived biomatrix for hepatic tissue engineering. *Tissue engineering*. 2004 Jul-Aug;10(7-8):1046-53. PubMed PMID: 15363162.
139. Wicha MS, Lowrie G, Kohn E, Bagavandoss P, Mahn T. Extracellular matrix promotes mammary epithelial growth and differentiation in vitro. *Proceedings of the National Academy of Sciences of the United States of America*. 1982 May;79(10):3213-7. PubMed PMID: 6954472. Pubmed Central PMCID: 346385.
140. Stern MM, Myers RL, Hammam N, Stern KA, Eberli D, Kritchevsky SB, et al. The influence of extracellular matrix derived from skeletal muscle tissue on the proliferation and differentiation of myogenic progenitor cells ex vivo. *Biomaterials*. 2009 Apr;30(12):2393-9. PubMed PMID: 19168212.
141. Crisan M, Yap S, Casteilla L, Chen CW, Corselli M, Park TS, et al. A perivascular origin for mesenchymal stem cells in multiple human organs. *Cell Stem Cell*. 2008 Sep 11;3(3):301-13. PubMed PMID: 18786417. Epub 2008/09/13. eng.
142. Reing JE, Zhang L, Myers-Irvin J, Cordero KE, Freytes DO, Heber-Katz E, et al. Degradation products of extracellular matrix affect cell migration and proliferation. *Tissue engineering Part A*. 2009 Mar;15(3):605-14. PubMed PMID: 18652541.

143. Calve S, Odelberg SJ, Simon HG. A transitional extracellular matrix instructs cell behavior during muscle regeneration. *Developmental biology*. 2010 Aug 1;344(1):259-71. PubMed PMID: 20478295.
144. Vorotnikova E, McIntosh D, Dewilde A, Zhang J, Reing JE, Zhang L, et al. Extracellular matrix-derived products modulate endothelial and progenitor cell migration and proliferation in vitro and stimulate regenerative healing in vivo. *Matrix biology : journal of the International Society for Matrix Biology*. 2010 Oct;29(8):690-700. PubMed PMID: 20797438.
145. Nelson CM, Bissell MJ. Of extracellular matrix, scaffolds, and signaling: tissue architecture regulates development, homeostasis, and cancer. *Annual review of cell and developmental biology*. 2006;22:287-309. PubMed PMID: 16824016. Pubmed Central PMCID: 2933192.
146. Gassmann P, Enns A, Haier J. Role of tumor cell adhesion and migration in organ-specific metastasis formation. *Onkologie*. 2004 Dec;27(6):577-82. PubMed PMID: 15591720.
147. Bissell MJ, Radisky DC, Rizki A, Weaver VM, Petersen OW. The organizing principle: microenvironmental influences in the normal and malignant breast. *Differentiation; research in biological diversity*. 2002 Dec;70(9-10):537-46. PubMed PMID: 12492495. Pubmed Central PMCID: 2933198.
148. Barkan D, Liu Z, Sacchettini JC, Glickman MS. Mycolic acid cyclopropanation is essential for viability, drug resistance, and cell wall integrity of *Mycobacterium tuberculosis*. *Chemistry & biology*. 2009 May 29;16(5):499-509. PubMed PMID: 19477414. Pubmed Central PMCID: 2731493.
149. Bonneh-Barkay D, Wiley CA. Brain extracellular matrix in neurodegeneration. *Brain pathology*. 2009 Oct;19(4):573-85. PubMed PMID: 18662234. Pubmed Central PMCID: 2742568.
150. Wainwright JM, Hashizume R, Fujimoto KL, Remlinger NT, Pesyna C, Wagner WR, et al. Right ventricular outflow tract repair with a cardiac biologic scaffold. *Cells, tissues, organs*. 2012;195(1-2):159-70. PubMed PMID: 22025093. Pubmed Central PMCID: 3325605.
151. Quarti A, Nardone S, Colaneri M, Santoro G, Pozzi M. Preliminary experience in the use of an extracellular matrix to repair congenital heart diseases. *Interactive cardiovascular and thoracic surgery*. 2011 Dec;13(6):569-72. PubMed PMID: 21979987.

152. Singelyn JM, DeQuach JA, Seif-Naraghi SB, Littlefield RB, Schup-Magoffin PJ, Christman KL. Naturally derived myocardial matrix as an injectable scaffold for cardiac tissue engineering. *Biomaterials*. 2009 Oct;30(29):5409-16. PubMed PMID: 19608268. Pubmed Central PMCID: 2728782.
153. O'Connor R C, Harding JN, 3rd, Steinberg GD. Novel modification of partial nephrectomy technique using porcine small intestine submucosa. *Urology*. 2002 Nov;60(5):906-9. PubMed PMID: 12429327.
154. Palminteri E, Berdondini E, Colombo F, Austoni E. Small intestinal submucosa (SIS) graft urethroplasty: short-term results. *European urology*. 2007 Jun;51(6):1695-701; discussion 701. PubMed PMID: 17207913.
155. Badylak SF, Kropp B, McPherson T, Liang H, Snyder PW. Small intestinal submucosa: a rapidly resorbed bioscaffold for augmentation cystoplasty in a dog model. *Tissue engineering*. 1998 Winter;4(4):379-87. PubMed PMID: 9916170.
156. Butler CE, Langstein HN, Kronowitz SJ. Pelvic, abdominal, and chest wall reconstruction with AlloDerm in patients at increased risk for mesh-related complications. *Plastic and reconstructive surgery*. 2005 Oct;116(5):1263-75; discussion 76-7. PubMed PMID: 16217466.
157. Mase VJ, Jr., Hsu JR, Wolf SE, Wenke JC, Baer DG, Owens J, et al. Clinical application of an acellular biologic scaffold for surgical repair of a large, traumatic quadriceps femoris muscle defect. *Orthopedics*. 2010 Jul;33(7):511. PubMed PMID: 20608620.
158. Turner NJ, Yates AJ, Jr., Weber DJ, Qureshi IR, Stolz DB, Gilbert TW, et al. Xenogeneic extracellular matrix as an inductive scaffold for regeneration of a functioning musculotendinous junction. *Tissue engineering Part A*. 2010 Nov;16(11):3309-17. PubMed PMID: 20528669.
159. Karabekmez FE, Duymaz A, Moran SL. Early clinical outcomes with the use of decellularized nerve allograft for repair of sensory defects within the hand. *Hand*. 2009 Sep;4(3):245-9. PubMed PMID: 19412640. Pubmed Central PMCID: 2724628.

160. Haq I, Cruz-Almeida Y, Siqueira EB, Norenberg M, Green BA, Levi AD. Postoperative fibrosis after surgical treatment of the porcine spinal cord: a comparison of dural substitutes. Invited submission from the Joint Section Meeting on Disorders of the Spine and Peripheral Nerves, March 2004. *Journal of neurosurgery Spine*. 2005 Jan;2(1):50-4. PubMed PMID: 15658126.
161. Ribatti D, Conconi MT, Nico B, Baiguera S, Corsi P, Parnigotto PP, et al. Angiogenic response induced by acellular brain scaffolds grafted onto the chick embryo chorioallantoic membrane. *Brain research*. 2003 Oct 31;989(1):9-15. PubMed PMID: 14519506.
162. Guo SZ, Ren XJ, Wu B, Jiang T. Preparation of the acellular scaffold of the spinal cord and the study of biocompatibility. *Spinal cord*. 2010 Jul;48(7):576-81. PubMed PMID: 20065987.
163. DeQuach JA, Yuan SH, Goldstein LS, Christman KL. Decellularized porcine brain matrix for cell culture and tissue engineering scaffolds. *Tissue engineering Part A*. 2011 Nov;17(21-22):2583-92. PubMed PMID: 21883047. Pubmed Central PMCID: 3204197.
164. Freytes DO, Stoner RM, Badylak SF. Uniaxial and biaxial properties of terminally sterilized porcine urinary bladder matrix scaffolds. *Journal of biomedical materials research Part B, Applied biomaterials*. 2008 Feb;84(2):408-14. PubMed PMID: 17618508.
165. Freytes DO, Tullius RS, Valentin JE, Stewart-Akers AM, Badylak SF. Hydrated versus lyophilized forms of porcine extracellular matrix derived from the urinary bladder. *Journal of biomedical materials research Part A*. 2008 Dec 15;87(4):862-72. PubMed PMID: 18228251.
166. Freytes DO, Tullius RS, Badylak SF. Effect of storage upon material properties of lyophilized porcine extracellular matrix derived from the urinary bladder. *Journal of biomedical materials research Part B, Applied biomaterials*. 2006 Aug;78(2):327-33. PubMed PMID: 16365866.
167. Ishii KJ, Akira S. Innate immune recognition of, and regulation by, DNA. *Trends in immunology*. 2006 Nov;27(11):525-32. PubMed PMID: 16979939.
168. Gilbert TW, Freund JM, Badylak SF. Quantification of DNA in biologic scaffold materials. *The Journal of surgical research*. 2009 Mar;152(1):135-9. PubMed PMID: 18619621. Pubmed Central PMCID: 2783373.

169. Goto N. Discriminative staining methods for the nervous system: luxol fast blue--periodic acid-Schiff--hematoxylin triple stain and subsidiary staining methods. *Stain technology*. 1987 Sep;62(5):305-15. PubMed PMID: 2447684.
170. Greene LA, Tischler AS. Establishment of a noradrenergic clonal line of rat adrenal pheochromocytoma cells which respond to nerve growth factor. *Proceedings of the National Academy of Sciences of the United States of America*. 1976 Jul;73(7):2424-8. PubMed PMID: 1065897. Pubmed Central PMCID: 430592.
171. Rydel RE, Greene LA. Acidic and basic fibroblast growth factors promote stable neurite outgrowth and neuronal differentiation in cultures of PC12 cells. *The Journal of neuroscience : the official journal of the Society for Neuroscience*. 1987 Nov;7(11):3639-53. PubMed PMID: 3316527.
172. Santos SD, Verveer PJ, Bastiaens PI. Growth factor-induced MAPK network topology shapes Erk response determining PC-12 cell fate. *Nature cell biology*. 2007 Mar;9(3):324-30. PubMed PMID: 17310240.
173. Hall FL, Fernyhough P, Ishii DN, Vulliamy PR. Suppression of nerve growth factor-directed neurite outgrowth in PC12 cells by sphingosine, an inhibitor of protein kinase C. *The Journal of biological chemistry*. 1988 Mar 25;263(9):4460-6. PubMed PMID: 3162237.
174. Allan G, Krakowka S, Ellis J, Charreyre C. Discovery and evolving history of two genetically related but phenotypically different viruses, porcine circoviruses 1 and 2. *Virus research*. 2012 Mar;164(1-2):4-9. PubMed PMID: 21945213.
175. Mankertz A, Persson F, Mankertz J, Blaess G, Buhk HJ. Mapping and characterization of the origin of DNA replication of porcine circovirus. *Journal of virology*. 1997 Mar;71(3):2562-6. PubMed PMID: 9032401. Pubmed Central PMCID: 191374.
176. Paul PS, Halbur P, Janke B, Joo H, Nawagitgul P, Singh J, et al. Exogenous porcine viruses. *Current topics in microbiology and immunology*. 2003;278:125-83. PubMed PMID: 12934944.
177. Vijayraghavan S, Wang M, Birnbaum SG, Williams GV, Arnsten AF. Inverted-U dopamine D1 receptor actions on prefrontal neurons engaged in working memory. *Nature neuroscience*. 2007 Mar;10(3):376-84. PubMed PMID: 17277774.

178. Mendes FA, Onofre GR, Silva LC, Cavalcante LA, Garcia-Abreu J. Concentration-dependent actions of glial chondroitin sulfate on the neuritic growth of midbrain neurons. *Brain research Developmental brain research*. 2003 May 14;142(2):111-9. PubMed PMID: 12711362.
179. Endeman D, Kamermans M. Cones perform a non-linear transformation on natural stimuli. *The Journal of physiology*. 2010 Feb 1;588(Pt 3):435-46. PubMed PMID: 20008463. Pubmed Central PMCID: 2825609.
180. Freytes DO, Martin J, Velankar SS, Lee AS, Badylak SF. Preparation and rheological characterization of a gel form of the porcine urinary bladder matrix. *Biomaterials*. 2008 Apr;29(11):1630-7. PubMed PMID: 18201760. Epub 2008/01/19. eng.
181. Hong Y, Huber A, Takanari K, Amoroso NJ, Hashizume R, Badylak SF, et al. Mechanical properties and in vivo behavior of a biodegradable synthetic polymer microfiber-extracellular matrix hydrogel biohybrid scaffold. *Biomaterials*. 2011 May;32(13):3387-94. PubMed PMID: 21303718. Pubmed Central PMCID: 3184831.
182. Crapo PM, Medberry CJ, Reing JE, Tottey S, van der Merwe Y, Jones KE, et al. Biologic scaffolds composed of central nervous system extracellular matrix. *Biomaterials*. 2012 May;33(13):3539-47. PubMed PMID: 22341938. Pubmed Central PMCID: 3516286.
183. Tottey S, Johnson SA, Crapo PM, Reing JE, Zhang L, Jiang H, et al. The effect of source animal age upon extracellular matrix scaffold properties. *Biomaterials*. 2011 Jan;32(1):128-36. PubMed PMID: 20870285. Pubmed Central PMCID: 2987535.
184. Sicari BM, Johnson SA, Siu BF, Crapo PM, Daly KA, Jiang H, et al. The effect of source animal age upon the in vivo remodeling characteristics of an extracellular matrix scaffold. *Biomaterials*. 2012 Aug;33(22):5524-33. PubMed PMID: 22575834. Pubmed Central PMCID: 3569720.
185. Beattie AJ, Gilbert TW, Guyot JP, Yates AJ, Badylak SF. Chemoattraction of progenitor cells by remodeling extracellular matrix scaffolds. *Tissue engineering Part A*. 2009 May;15(5):1119-25. PubMed PMID: 18837648. Pubmed Central PMCID: 2789572.
186. Brennan EP, Tang XH, Stewart-Akers AM, Gudas LJ, Badylak SF. Chemoattractant activity of degradation products of fetal and adult skin extracellular matrix for keratinocyte progenitor cells. *Journal of tissue engineering and regenerative medicine*. 2008 Dec;2(8):491-8. PubMed PMID: 18956412. Pubmed Central PMCID: 2706581.

187. Crapo PM, Wang Y. Small intestinal submucosa gel as a potential scaffolding material for cardiac tissue engineering. *Acta biomaterialia*. 2010 Jun;6(6):2091-6. PubMed PMID: 19887120. Pubmed Central PMCID: 2862886.
188. Dequach JA, Lin JE, Cam C, Hu D, Salvatore MA, Sheikh F, et al. Injectable skeletal muscle matrix hydrogel promotes neovascularization and muscle cell infiltration in a hindlimb ischemia model. *Eur Cell Mater*. 2012;23:400-12. PubMed PMID: 22665162. Epub 2012/06/06. eng.
189. Seif-Naraghi SB, Salvatore MA, Schup-Magoffin PJ, Hu DP, Christman KL. Design and characterization of an injectable pericardial matrix gel: a potentially autologous scaffold for cardiac tissue engineering. *Tissue Eng Part A*. 2010 Jun;16(6):2017-27. PubMed PMID: 20100033. Pubmed Central PMCID: 2949214. Epub 2010/01/27. eng.
190. Sellaro TL, Ranade A, Faulk DM, McCabe GP, Dorko K, Badylak SF, et al. Maintenance of human hepatocyte function in vitro by liver-derived extracellular matrix gels. *Tissue engineering Part A*. 2010 Mar;16(3):1075-82. PubMed PMID: 19845461. Pubmed Central PMCID: 2863084.
191. Wolf MT, Daly KA, Brennan-Pierce EP, Johnson SA, Carruthers CA, D'Amore A, et al. A hydrogel derived from decellularized dermal extracellular matrix. *Biomaterials*. 2012 Oct;33(29):7028-38. PubMed PMID: 22789723. Pubmed Central PMCID: 3408574. Epub 2012/07/14. eng.
192. Bible E, Dell'Acqua F, Solanky B, Balducci A, Crapo PM, Badylak SF, et al. Non-invasive imaging of transplanted human neural stem cells and ECM scaffold remodeling in the stroke-damaged rat brain by (19)F- and diffusion-MRI. *Biomaterials*. 2012 Apr;33(10):2858-71. PubMed PMID: 22244696. Pubmed Central PMCID: 3268910.
193. Kumar A, Nevill G, Brockes JP, Forge A. A comparative study of gland cells implicated in the nerve dependence of salamander limb regeneration. *J Anat*. 2010 Jul;217(1):16-25. PubMed PMID: 20456522. Epub 2010/05/12. eng.
194. Brockes JP. The nerve dependence of amphibian limb regeneration. *J Exp Biol*. 1987 Sep;132:79-91. PubMed PMID: 3323408. Epub 1987/09/01. eng.
195. Tuttle JB, Richelson E. Ionic excitation of a clone of mouse neuroblastoma. *Brain Res*. 1975 Jan 24;84(1):129-35. PubMed PMID: 234272. Epub 1975/01/24. eng.

196. Dan C, Nath N, Liberto M, Minden A. PAK5, a new brain-specific kinase, promotes neurite outgrowth in N1E-115 cells. *Mol Cell Biol.* 2002 Jan;22(2):567-77. PubMed PMID: 11756552. Pubmed Central PMCID: 139731. Epub 2002/01/05. eng.
197. Freytes DO, Badylak SF, Webster TJ, Geddes LA, Rundell AE. Biaxial strength of multilaminated extracellular matrix scaffolds. *Biomaterials.* 2004 May;25(12):2353-61. PubMed PMID: 14741600. Epub 2004/01/27. eng.
198. Piper DW, Fenton BH. pH stability and activity curves of pepsin with special reference to their clinical importance. *Gut.* 1965 Oct;6(5):506-8. PubMed PMID: 4158734. Pubmed Central PMCID: 1552331. Epub 1965/10/01. eng.
199. Gelman RA, Williams BR, Piez KA. Collagen fibril formation. Evidence for a multistep process. *J Biol Chem.* 1979 Jan 10;254(1):180-6. PubMed PMID: 758319. Epub 1979/01/10. eng.
200. Engler AJ, Sen S, Sweeney HL, Discher DE. Matrix elasticity directs stem cell lineage specification. *Cell.* 2006 Aug 25;126(4):677-89. PubMed PMID: 16923388.
201. Aguado BA, Mulyasmita W, Su J, Lampe KJ, Heilshorn SC. Improving viability of stem cells during syringe needle flow through the design of hydrogel cell carriers. *Tissue Eng Part A.* 2012 Apr;18(7-8):806-15. PubMed PMID: 22011213. Pubmed Central PMCID: 3313609. Epub 2011/10/21. eng.
202. Hoffman AS. Hydrogels for biomedical applications. *Adv Drug Deliv Rev.* 2002 Jan 17;54(1):3-12. PubMed PMID: 11755703. Epub 2002/01/05. eng.
203. Agashi K, Chau DY, Shakesheff KM. The effect of delivery via narrow-bore needles on mesenchymal cells. *Regenerative medicine.* 2009 Jan;4(1):49-64. PubMed PMID: 19105616.
204. Pedersen JA, Swartz MA. Mechanobiology in the third dimension. *Ann Biomed Eng.* 2005 Nov;33(11):1469-90. PubMed PMID: 16341917. Epub 2005/12/13. eng.
205. Obrink B. The influence of glycosaminoglycans on the formation of fibers from monomeric tropocollagen in vitro. *Eur J Biochem.* 1973 Apr 2;34(1):129-37. PubMed PMID: 4267112. Epub 1973/04/02. eng.

206. Stuart K, Panitch A. Influence of chondroitin sulfate on collagen gel structure and mechanical properties at physiologically relevant levels. *Biopolymers*. 2008 Oct;89(10):841-51. PubMed PMID: 18488988. Epub 2008/05/21. eng.
207. Birk DE, Silver FH. Collagen fibrillogenesis in vitro: comparison of types I, II, and III. *Arch Biochem Biophys*. 1984 Nov 15;235(1):178-85. PubMed PMID: 6437334. Epub 1984/11/15. eng.
208. Stuart K, Panitch A. Characterization of gels composed of blends of collagen I, collagen III, and chondroitin sulfate. *Biomacromolecules*. 2009 Jan 12;10(1):25-31. PubMed PMID: 19053290. Epub 2008/12/05. eng.
209. Ruoslahti E. Brain extracellular matrix. *Glycobiology*. 1996 Jul;6(5):489-92. PubMed PMID: 8877368. Epub 1996/07/01. eng.
210. Daley WP, Peters SB, Larsen M. Extracellular matrix dynamics in development and regenerative medicine. *J Cell Sci*. 2008 Feb 1;121(Pt 3):255-64. PubMed PMID: 18216330. Epub 2008/01/25. eng.
211. Adams JC, Watt FM. Regulation of development and differentiation by the extracellular matrix. *Development*. 1993 Apr;117(4):1183-98. PubMed PMID: 8404525. Epub 1993/04/01. eng.
212. Amano T, Richelson E, Nirenberg M. Neurotransmitter synthesis by neuroblastoma clones (neuroblast differentiation-cell culture-choline acetyltransferase-acetylcholinesterase-tyrosine hydroxylase-axons-dendrites). *Proc Natl Acad Sci U S A*. 1972 Jan;69(1):258-63. PubMed PMID: 4400294. Pubmed Central PMCID: 427587. Epub 1972/01/01. eng.
213. Mahoney MJ, Anseth KS. Three-dimensional growth and function of neural tissue in degradable polyethylene glycol hydrogels. *Biomaterials*. 2006 Apr;27(10):2265-74. PubMed PMID: 16318872.
214. Owens DF, Boyce LH, Davis MB, Kriegstein AR. Excitatory GABA responses in embryonic and neonatal cortical slices demonstrated by gramicidin perforated-patch recordings and calcium imaging. *The Journal of neuroscience : the official journal of the Society for Neuroscience*. 1996 Oct 15;16(20):6414-23. PubMed PMID: 8815920.

215. Yang P, Yang Z. Enhancing intrinsic growth capacity promotes adult CNS regeneration. *Journal of the neurological sciences*. 2012 Jan 15;312(1-2):1-6. PubMed PMID: 21924742.
216. Anderson KD. Targeting recovery: priorities of the spinal cord-injured population. *Journal of neurotrauma*. 2004 Oct;21(10):1371-83. PubMed PMID: 15672628.
217. Kokaia Z, Martino G, Schwartz M, Lindvall O. Cross-talk between neural stem cells and immune cells: the key to better brain repair? *Nature neuroscience*. 2012 Aug;15(8):1078-87. PubMed PMID: 22837038.
218. Lu P, Jones LL, Snyder EY, Tuszynski MH. Neural stem cells constitutively secrete neurotrophic factors and promote extensive host axonal growth after spinal cord injury. *Experimental neurology*. 2003 Jun;181(2):115-29. PubMed PMID: 12781986.
219. Liu S, Qu Y, Stewart TJ, Howard MJ, Chakraborty S, Holekamp TF, et al. Embryonic stem cells differentiate into oligodendrocytes and myelinate in culture and after spinal cord transplantation. *Proceedings of the National Academy of Sciences of the United States of America*. 2000 May 23;97(11):6126-31. PubMed PMID: 10823956. Pubmed Central PMCID: 18569.
220. Martino G, Pluchino S, Bonfanti L, Schwartz M. Brain regeneration in physiology and pathology: the immune signature driving therapeutic plasticity of neural stem cells. *Physiological reviews*. 2011 Oct;91(4):1281-304. PubMed PMID: 22013212. Pubmed Central PMCID: 3552310.
221. Giulian D, Robertson C. Inhibition of mononuclear phagocytes reduces ischemic injury in the spinal cord. *Annals of neurology*. 1990 Jan;27(1):33-42. PubMed PMID: 2301926.
222. Brown BN, Londono R, Tottey S, Zhang L, Kukla KA, Wolf MT, et al. Macrophage phenotype as a predictor of constructive remodeling following the implantation of biologically derived surgical mesh materials. *Acta biomaterialia*. 2012 Mar;8(3):978-87. PubMed PMID: 22166681.
223. Gilbert TW, Stolz DB, Biancaniello F, Simmons-Byrd A, Badylak SF. Production and characterization of ECM powder: implications for tissue engineering applications. *Biomaterials*. 2005 Apr;26(12):1431-5. PubMed PMID: 15482831.

224. Brown B, Lindberg K, Reing J, Stolz DB, Badylak SF. The basement membrane component of biologic scaffolds derived from extracellular matrix. *Tissue engineering*. 2006 Mar;12(3):519-26. PubMed PMID: 16579685.
225. Corraliza IM, Soler G, Eichmann K, Modolell M. Arginase induction by suppressors of nitric oxide synthesis (IL-4, IL-10 and PGE2) in murine bone-marrow-derived macrophages. *Biochemical and biophysical research communications*. 1995 Jan 17;206(2):667-73. PubMed PMID: 7530004.
226. Austin PE, McCulloch EA, Till JE. Characterization of the factor in L-cell conditioned medium capable of stimulating colony formation by mouse marrow cells in culture. *Journal of cellular physiology*. 1971 Apr;77(2):121-34. PubMed PMID: 5572424.
227. Zhang X, Goncalves R, Mosser DM. The isolation and characterization of murine macrophages. *Current protocols in immunology* / edited by John E Coligan [et al]. 2008 Nov;Chapter 14:Unit 14 1. PubMed PMID: 19016445. Pubmed Central PMCID: 2834554.
228. Cocks G, Romanyuk N, Amemori T, Jendelova P, Forostyak O, Jeffries AR, et al. Conditionally immortalized stem cell lines from human spinal cord retain regional identity and generate functional V2a interneurons and motoneurons. *Stem cell research & therapy*. 2013 Jun 7;4(3):69. PubMed PMID: 23759128. Pubmed Central PMCID: 3706922.
229. Pollock K, Stroemer P, Patel S, Stevanato L, Hope A, Miljan E, et al. A conditionally immortal clonal stem cell line from human cortical neuroepithelium for the treatment of ischemic stroke. *Experimental neurology*. 2006 May;199(1):143-55. PubMed PMID: 16464451.
230. El-Akabawy G, Medina LM, Jeffries A, Price J, Mado M. Purmorphamine increases DARPP-32 differentiation in human striatal neural stem cells through the Hedgehog pathway. *Stem cells and development*. 2011 Nov;20(11):1873-87. PubMed PMID: 21345011.
231. Verreck FA, de Boer T, Langenberg DM, Hoeve MA, Kramer M, Vaisberg E, et al. Human IL-23-producing type 1 macrophages promote but IL-10-producing type 2 macrophages subvert immunity to (myco)bacteria. *Proceedings of the National Academy of Sciences of the United States of America*. 2004 Mar 30;101(13):4560-5. PubMed PMID: 15070757. Pubmed Central PMCID: 384786.

232. Tran EH, Hardin-Pouzet H, Verge G, Owens T. Astrocytes and microglia express inducible nitric oxide synthase in mice with experimental allergic encephalomyelitis. *Journal of neuroimmunology*. 1997 Apr;74(1-2):121-9. PubMed PMID: 9119964.
233. Johansson CB, Momma S, Clarke DL, Risling M, Lendahl U, Frisen J. Identification of a neural stem cell in the adult mammalian central nervous system. *Cell*. 1999 Jan 8;96(1):25-34. PubMed PMID: 9989494.
234. Dromard C, Guillon H, Rigau V, Ripoll C, Sabourin JC, Perrin FE, et al. Adult human spinal cord harbors neural precursor cells that generate neurons and glial cells in vitro. *Journal of neuroscience research*. 2008 Jul;86(9):1916-26. PubMed PMID: 18335522.
235. Kelley JL, Rozek MM, Suenram CA, Schwartz CJ. Activation of human blood monocytes by adherence to tissue culture plastic surfaces. *Experimental and molecular pathology*. 1987 Jun;46(3):266-78. PubMed PMID: 3036568.
236. Gordon S. Alternative activation of macrophages. *Nature reviews Immunology*. 2003 Jan;3(1):23-35. PubMed PMID: 12511873.
237. Shechter R, Miller O, Yovel G, Rosenzweig N, London A, Ruckh J, et al. Recruitment of beneficial M2 macrophages to injured spinal cord is orchestrated by remote brain choroid plexus. *Immunity*. 2013 Mar 21;38(3):555-69. PubMed PMID: 23477737.
238. Bernhard M, Hilger T, Sikinger M, Hainer C, Haag S, Streitberger K, et al. [Spectrum of patients in prehospital emergency services. What has changed over the last 20 years?]. *Der Anaesthetist*. 2006 Nov;55(11):1157-65. PubMed PMID: 17063342. Patientenspektrum im Notarztdienst. Was hat sich in den letzten 20 Jahren geandert?
239. Siddall PJ, Loeser JD. Pain following spinal cord injury. *Spinal cord*. 2001 Feb;39(2):63-73. PubMed PMID: 11402361.
240. Bombardier CH, Richards JS, Krause JS, Tulskey D, Tate DG. Symptoms of major depression in people with spinal cord injury: implications for screening. *Archives of physical medicine and rehabilitation*. 2004 Nov;85(11):1749-56. PubMed PMID: 15520969.

241. Benevento BT, Sipski ML. Neurogenic bladder, neurogenic bowel, and sexual dysfunction in people with spinal cord injury. *Physical therapy*. 2002 Jun;82(6):601-12. PubMed PMID: 12036401.
242. Hicken BL, Putzke JD, Richards JS. Bladder management and quality of life after spinal cord injury. *American journal of physical medicine & rehabilitation / Association of Academic Physiatrists*. 2001 Dec;80(12):916-22. PubMed PMID: 11821674.
243. Burns AS, Rivas DA, Ditunno JF. The management of neurogenic bladder and sexual dysfunction after spinal cord injury. *Spine*. 2001 Dec 15;26(24 Suppl):S129-36. PubMed PMID: 11805620.
244. Tator CH, Fehlings MG. Review of the secondary injury theory of acute spinal cord trauma with emphasis on vascular mechanisms. *Journal of neurosurgery*. 1991 Jul;75(1):15-26. PubMed PMID: 2045903.
245. Kato H, Kanellopoulos GK, Matsuo S, Wu YJ, Jacquin MF, Hsu CY, et al. Neuronal apoptosis and necrosis following spinal cord ischemia in the rat. *Experimental neurology*. 1997 Dec;148(2):464-74. PubMed PMID: 9417826.
246. Choo AM, Liu J, Lam CK, Dvorak M, Tetzlaff W, Oxland TR. Contusion, dislocation, and distraction: primary hemorrhage and membrane permeability in distinct mechanisms of spinal cord injury. *Journal of neurosurgery Spine*. 2007 Mar;6(3):255-66. PubMed PMID: 17355025.
247. Warden P, Bamber NI, Li H, Esposito A, Ahmad KA, Hsu CY, et al. Delayed glial cell death following wallerian degeneration in white matter tracts after spinal cord dorsal column cordotomy in adult rats. *Experimental neurology*. 2001 Apr;168(2):213-24. PubMed PMID: 11259109.
248. Klekamp J, Batzdorf U, Samii M, Bothe HW. Treatment of syringomyelia associated with arachnoid scarring caused by arachnoiditis or trauma. *Journal of neurosurgery*. 1997 Feb;86(2):233-40. PubMed PMID: 9010425.
249. Basso DM, Beattie MS, Bresnahan JC. A sensitive and reliable locomotor rating scale for open field testing in rats. *Journal of neurotrauma*. 1995 Feb;12(1):1-21. PubMed PMID: 7783230.

250. Kunkel-Bagden E, Dai HN, Bregman BS. Recovery of function after spinal cord hemisection in newborn and adult rats: differential effects on reflex and locomotor function. *Experimental neurology*. 1992 Apr;116(1):40-51. PubMed PMID: 1559563.
251. de Medinaceli L, Freed WJ, Wyatt RJ. An index of the functional condition of rat sciatic nerve based on measurements made from walking tracks. *Experimental neurology*. 1982 Sep;77(3):634-43. PubMed PMID: 7117467.
252. Zhang L, Zhang F, Weng Z, Brown BN, Yan H, Ma XM, et al. Effect of an inductive hydrogel composed of urinary bladder matrix upon functional recovery following traumatic brain injury. *Tissue engineering Part A*. 2013 Sep;19(17-18):1909-18. PubMed PMID: 23596981. Pubmed Central PMCID: 3726021.
253. Wang JY, Liou AK, Ren ZH, Zhang L, Brown BN, Cui XT, et al. Neurorestorative effect of urinary bladder matrix-mediated neural stem cell transplantation following traumatic brain injury in rats. *CNS & neurological disorders drug targets*. 2013 May 1;12(3):413-25. PubMed PMID: 23469853.
254. Rolls A, Shechter R, London A, Segev Y, Jacob-Hirsch J, Amariglio N, et al. Two faces of chondroitin sulfate proteoglycan in spinal cord repair: a role in microglia/macrophage activation. *PLoS medicine*. 2008 Aug 19;5(8):e171. PubMed PMID: 18715114. Pubmed Central PMCID: 2517615.
255. Rolls A, Schwartz M. Chondroitin sulfate proteoglycan and its degradation products in CNS repair. *Advances in pharmacology*. 2006;53:357-74. PubMed PMID: 17239775.
256. Rolls A, Cahalon L, Bakalash S, Avidan H, Lider O, Schwartz M. A sulfated disaccharide derived from chondroitin sulfate proteoglycan protects against inflammation-associated neurodegeneration. *FASEB journal : official publication of the Federation of American Societies for Experimental Biology*. 2006 Mar;20(3):547-9. PubMed PMID: 16396993.
257. Cusimano M, Biziato D, Brambilla E, Donega M, Alfaro-Cervello C, Snider S, et al. Transplanted neural stem/precursor cells instruct phagocytes and reduce secondary tissue damage in the injured spinal cord. *Brain : a journal of neurology*. 2012 Feb;135(Pt 2):447-60. PubMed PMID: 22271661. Pubmed Central PMCID: 3558737.